PV Inverter Based Volt/Var Control of Active Distribution Networks with Inverter Reliability Assessment and Enhancement

Author:
Chai, Qingmian

Publication Date:
2023

DOI:
https://doi.org/10.26190/unsworks/24607

PV INVERTER BASED VOLT/VAR CONTROL OF ACTIVE DISTRIBUTION NETWORKS WITH INVERTER RELIABILITY ASSESSMENT AND ENHANCEMENT

QINGMIAN CHAI

B.Sc. and M.Sc. of Electrical Engineering

A thesis submitted in partial fulfilment

of the requirements for the degree of

Doctor of Philosophy

School of Electrical Engineering and Telecommunications

Faculty of Engineering

September 2022

Thesis Title and Abstract | **Declarations** | Inclusion of Publications Statement | Corrected Thesis and Responses

ORIGINALITY STATEMENT

☑ I hereby declare that this submission is my own work and to the best of my knowledge it contains no materials previously published or written by another person, or substantial proportions of material which have been accepted for the award of any other degree or diploma at UNSW or any other educational institution, except where due acknowledgement is made in the thesis. Any contribution made to the research by others, with whom I have worked at UNSW or elsewhere, is explicitly acknowledged in the thesis. I also declare that the intellectual content of this thesis is the product of my own work, except to the extent that assistance from others in the project's design and conception or in style, presentation and linguistic expression is acknowledged.

COPYRIGHT STATEMENT

AUTHENTICITY STATEMENT

☑ I certify that the Library deposit digital copy is a direct equivalent of the final officially approved version of my thesis.

UNSW is supportive of candidates publishing their research results during their candidature as detailed in the UNSW Thesis Examination Procedure.

Publications can be used in the candidate's thesis in lieu of a Chapter provided:

- The candidate contributed **greater than 50%** of the content in the publication and are the "primary author", i.e. they were responsible primarily for the planning, execution and preparation of the work for publication.
- The candidate has obtained approval to include the publication in their thesis in lieu of a Chapter from their Supervisor and Postgraduate Coordinator.
- The publication is not subject to any obligations or contractual agreements with a third party that would constrain its inclusion in the thesis.

☑ The candidate has declared that **their thesis has publications - either published or submitted for publication - incorporated into it in lieu of a Chapter/s. Details of these publications are provided below.**.

Publication Details #1

Full Title:	Operational reliability assessment of photovoltaic inverters considering voltage/VAR control function
Authors:	Qingmian Chai, Cuo Zhang, Zhao Yang Dong, and Yan Xu
Journal or Book Name:	Electric Power Systems Research
Volume/Page Numbers:	vol. 190, 106706
Date Accepted/Published:	Published in January 2021
Status:	published
The Candidate's Contribution to the Work:	The Candidate is the primary author of this article and contributed greater than 50% of the content in the publication.
Location of the work in the thesis and/or how the work is incorporated in the thesis:	The work forms Chapter 2 of this thesis.

Publication Details #2

Full Title:	PV Inverter Reliability-Constrained Volt/Var Control of Distribution Networks
Authors:	Qingmian Chai, Cuo Zhang, Yan Xu, and Zhao Yang Dong
Journal or Book Name:	IEEE Transactions on Sustainable Energy
Volume/Page Numbers:	vol. 12, no. 3, pp. 1788-1800
Date Accepted/Published:	Published in July 2021
Status:	published
The Candidate's Contribution to the Work:	The Candidate is the primary author of this article and contributed greater than 50% of the content in the publication.
Location of the work in the thesis and/or how the work is incorporated in the thesis:	The work forms Chapter 3 of this thesis.

Publication Details #3

Full Title:	PV Inverter Reliability Constrained Volt/Var Control with Power Smoothing via A Convex-Concave Programming Method
Authors:	Qingmian Chai, Cuo Zhang, Ziyuan Tong, Shuai Lu, Wen Chen, and Zhao Yang Dong
Journal or Book Name:	IEEE Transactions on Industrial Informatics
Volume/Page Numbers:	
Date Accepted/Published:	Accepted in March 2022
Status:	accepted
The Candidate's Contribution to the Work:	The Candidate is the primary author of this article and contributed greater than 50% of the content in the publication.
Location of the work in the thesis and/or how the work is incorporated in the thesis:	The work forms Chapter 4 of this thesis.

Publication Details #4

Full Title:	A Pareto Front Analysis Method for PV Inverter Based Volt/Var Control Considering Inverter Lifetime
Authors:	Qingmian Chai, Cuo Zhang, Yan Xu, Zhao Yang Dong, and Rui Zhang
Journal or Book Name:	CSEE Journal of Power and Energy Systems
Volume/Page Numbers:	
Date Accepted/Published:	Accepted in June 2022
Status:	accepted
The Candidate's Contribution to the Work:	The Candidate is the primary author of this article and contributed greater than 50% of the content in the publication.
Location of the work in the thesis and/or how the work is incorporated in the thesis:	The work forms Chapter 5 of this thesis.

Candidate's Declaration

I confirm that where I have used a publication in lieu of a chapter, the listed publication(s) above meet(s) the requirements to be included in the thesis. I also declare that I have complied with the Thesis Examination Procedure.

ABSTRACT

Traditional passive distribution networks can not sufficiently handle the voltage regulation issues brought by the increasingly integrated photovoltaic (PV) systems, while an active distribution network, which features active management of distributed energy resources, can flexibly utilise PV inverters to provide a volt/var control (VVC) function to regulate the network voltage. However, PV inverters are vulnerable power electronics devices and utilising them for additional VVC support can further degrade their reliability, leading to shortened inverter lifetime and impaired economic benefits. In this regard, the thesis focuses on addressing the PV inverter reliability issues in VVC methods, via assessing the PV inverter reliability in VVC and proposing advanced PV inverter based VVC methods considering inverter reliability enhancement.

The thesis consists of four stages of my research. Firstly, a comprehensive PV inverter reliability assessment approach is developed to evaluate inverter lifetime when used for VVC functions, and the impacts of the PV inverter based VVC on inverter lifetime are successfully quantified. Secondly, a PV inverter reliability constrained VVC method is proposed in which the constraints to enhance inverter reliability are developed with a restriction factor to regulate inverter apparent power outputs. This method can efficiently minimise network power loss and curtailed PV power, while guaranteeing long inverter lifetime. Thirdly, a PV inverter reliability constrained VVC approach with power smoothing is proposed, in which an inverter power smoothing scheme with high control flexibility is developed by utilising a power smoothing factor to constrict variations of inverter apparent power outputs. Additionally, a penalty convex-concave procedure (CCP) solution method is developed to solve the non-convex optimisation problem with high computing efficiency. Fourthly, a multi-objective PV inverter based VVC method is proposed to simultaneously minimise network power loss and inverter apparent power output, and a Pareto front analysis method is developed to select a solution to achieve efficient power loss reduction with expected inverter lifetime. All the proposed methods apply advanced network

operating models and optimisation methods to address uncertainties.

These methods have been successfully demonstrated and tested through comprehensive case studies, and numerical simulation results verified the feasibility and high efficiency of the proposed methods.

Dedicated To

My Beloved Family

ACKNOWLEDGEMENTS

I would like to express my deepest appreciation to my supervisor, Prof. ZhaoYang Dong, for his guidance, encouragement, and unlimited support during my Ph.D. journey. His character, vision, and attitude towards research have deeply inspired me and will continue motivating me to progress in my future career. I would like to deeply thank Dr. Cuo Zhang for his co-supervision during my Ph.D. research, who gave me valuable advice on my research direction and provided genuine, prompt and outstanding feedback on my research progress. I would like to express my sincere gratitude to Dr. Chaojie Li, Dr. Ziyuan Tong, and Dr. Rui Zhang in my supervisory team, for always being supportive to me, reviewing my progress constantly, and providing professional advice on my candidature. I would like to sincerely thank Dr. Ke Meng for his direction and kind support in the research projects I participated in during my Ph.D. candidature.

My sincere thanks also go to my progress review panel, Prof. Iain MacGill, Dr. Georgios Konstantinou, and Dr. Daming Zhang for their recognition of my research, to Prof. Yan Xu from Nanyang Technological University, Prof. Xiangjing Su from Shanghai University of Electric Power, Dr. Guo Chen, and my colleagues Dr. Bo Wang, Dr. Xuan Liu, Dr. Jiajia Yang, Mr. Hangyue Liu, Mr. Weiwei Zhou, Ms. Qijun Liang, Mr. Hossein Saberi, and Mr. Ruipeng Xu, for their help and advice, and the valuable discussions we had along the way.

I am also grateful to the Australian Government for their support through Research Training Program Scholarship, and to the ARC Research Hub for Integrated Energy Storage Solutions, the UNSW Digital Grid Futures Institute, and the School of Electrical Engineering and Telecommunications for their substantial support through research fundings.

Last but not least, I would like to genuinely thank my wife, Ms. Wen Chen, for her company and unconditional support to the family throughout this journey, and our beloved little angel, Yimeng Chai, for bringing so much joy and happiness that made this part of my life so bright and wonderful. I owe my deepest thanks to my parents, Mr. Shihe Chai and Ms. Fengxia Yan, for the sacrifices they made for my benefits and their endless love and care. Their love and support is a solid base for me to accomplish my study.

LIST OF PUBLICATIONS

The following publications as the major Ph.D. research results of this candidate are included as parts of this thesis.

- **Q. Chai**, C. Zhang, Z. Y. Dong, and Y. Xu, “Operational reliability assessment of photovoltaic inverters considering voltage/VAR control function,” ***Electric Power Systems Research***, vol. 190, Jan. 2021, 106706. (**Chapter 2** of this thesis)

- **Q. Chai**, C. Zhang, Y. Xu and Z. Y. Dong, "PV Inverter Reliability-Constrained Volt/Var Control of Distribution Networks," ***IEEE Transactions on Sustainable Energy***, vol. 12, no. 3, pp. 1788-1800, July 2021. (**Chapter 3** of this thesis)

- **Q. Chai**, C. Zhang, Z. Tong, S. Lu, W. Chen and Z. Y. Dong, "PV Inverter Reliability Constrained Volt/Var Control with Power Smoothing via A Convex-Concave Programming Method," ***IEEE Transactions on Industrial Informatics***, vol. 19, no. 1, pp. 109-120, Jan. 2023. (**Chapter 4** of this thesis)

- **Q. Chai**, C. Zhang, Y. Xu, Z. Y. Dong and R. Zhang, “A Pareto Front Analysis Method for PV Inverter Based Volt/Var Control Considering Inverter Lifetime,” ***CSEE Journal of Power and Energy Systems***, in press. (Accepted in June 2022) (**Chapter 5** of this thesis)

The following publications as part of the Ph.D. research results of this candidate are not included in this thesis.

- **Q. Chai**, C. Zhang, Z. Dong and W. Chen, "Optimal Daily Scheduling of Distributed Battery Energy Storage Systems Considering Battery Degradation Cost," ***2021 IEEE Power & Energy Society General Meeting (PESGM)***, Washington, DC, USA, 2021, pp. 1-5.

- W. Chen, J. Qiu, J. Zhao, **Q. Chai** and Z. Y. Dong, "Bargaining Game-Based Profit Allocation of Virtual Power Plant in Frequency Regulation Market Considering Battery Cycle Life," ***IEEE Transactions on Smart Grid***, vol. 12, no. 4, pp. 2913-2928, July 2021.

- W. Chen, J. Qiu and **Q. Chai**, "Customized Critical Peak Rebate Pricing Mechanism for Virtual Power Plants," ***IEEE Transactions on Sustainable Energy***, vol. 12, no. 4, pp. 2169-2183, Oct. 2021.

- H. Liu, C. Zhang, **Q. Chai**, K. Meng, Q. Guo and Z. Y. Dong, "Robust Regional Coordination of Inverter-Based Volt/Var Control via Multi-Agent Deep Reinforcement Learning," ***IEEE Transactions on Smart Grid***, vol. 12, no. 6, pp. 5420-5433, Nov. 2021.

- W. Chen, J. Qiu, J. Zhao, **Q. Chai** and Z. Y. Dong, "Customized Rebate Pricing Mechanism for Virtual Power Plants Using a Hierarchical Game and Reinforcement Learning Approach," ***IEEE Transactions on Smart Grid***, vol. 14, no. 1, pp. 424-439, Jan. 2023.

CONTENTS

LIST OF ABBREVIATIONS

AC	Alternating current
ADN	Active distribution network
CB	Capacitor bank
CCP	Convex-concave procedure
DC	Direct current
DER	Distributed energy resource
DoC	Difference of convex
DPV	Distributed photovoltaic
DSO	Distribution system operator
ESR	Equivalent series resistance
IGBT	Insulated gate bipolar transistor
IPOPT	Interior Point Optimizer
IRENA	International Renewable Energy Agency
MCS	Monte Carlo sampling
MOSFET	Metal-oxide-semiconductor field-effect transistor
MPPT	Maximum power point tracking
NREL	National Renewable Energy Laboratory
OLTC	On-load tap changer
PDF	Probability density function
PiReCon	PV inverter reliability constrained
PV	Photovoltaic
RMS	Root mean square
RTS	Reliability test system
SDP	Semidefinite programming

SOCP	Second-order cone programming
SVC	Static var compensator
VPP	Virtual power plant
VR	Voltage regulator
VVC	Volt/var control
WT	Wind turbine

LIST OF FIGURES

List of Tables

Chapter 1 INTRODUCTION

Rapid proliferation of solar photovoltaic (PV) systems in distribution networks brings about great challenges to network stability, especially the network voltage control. In an active distribution network (ADN), PV inverters can be utilised to provide reactive power support for voltage regulation, forming a PV inverter based volt/var control (VVC) method. This method is highly promising to defer investments of additional voltage regulation equipment such as capacitor banks, as well as to enhance the networks' capability in hosting more DERs.

However, with the implementation of PV inverter based VVC, a very practical concern emerges, i.e., PV inverter reliability. PV inverters are power electronics devices with high susceptibility to their working conditions and thus relatively short lifespan. The use of PV inverters for additional VVC support can further degrade their reliability, leading to much shortened inverter lifetime and impaired economic benefits. To this end, it is imperative to address the PV inverter reliability issues when applying PV inverter based VVC methods.

This chapter provides background information about distributed PVs and ADNs and a detailed review of state-of-the-art VVC methods, investigates the PV inverter reliability, identifies the research gaps, and summarises the main contributions of this thesis.

1.1 Distributed Photovoltaics

Current energy system is undergoing a rapid and profound transition from a system dominated by traditional fossil-based generation to a system penetrated with various clean energy resources such as solar, wind and hydro. A report by International Renewable Energy Agency (IRENA) indicates that the share of renewable energy in the global generation capacity expansion of 2021 has hit a new record of 81%, with solar and wind accounting for around 88% of the new renewable energy capacity [1]. Distributed photovoltaics (DPVs) generally refer to the small-scale solar PV systems located near sites of electricity use, for example, residential rooftop PV systems. Some small-scale PV systems installed on commercial & industrial sites can also be seen as DPVs.

DPVs are now quickly penetrating the distribution networks. Australia has the highest penetration rate of rooftop PVs in the world. By the end of 2021, the number of rooftop solar PV installations in Australia has crossed the line of 3 million, meaning that almost 1 in 3 households have installed rooftop PV systems, and the number is still growing rapidly with unbeatable momentum [2]. In 2021, the DPV generation took nearly a quarter of Australia's renewable generation and 8.1% of total generation [3]. In some regions such as South Australia, the share of DPV generation was significantly higher than the country's average. Among all types of distributed energy resources (DERs), the DPV is seen as a core game player that contributes the most to the Australia's ambitious energy transition.

A typical DPV system consists of solar PV panels, a PV inverter, and associated auxiliary devices. A PV panel is a collection of PV modules which generate direct current (DC) electricity from sunlight. The PV inverter is responsible for converting the DC power generated from the PV panels to alternating current (AC) power which can be consumed by electrical loads or fed into the grid. Auxiliary devices include micro-controllers, switches, as well as related telecommunication, metering, and protection devices. Batteries can also be connected to a DPV system with an alternative hybrid PV inverter or an additional battery bidirectional converter, forming a distributed PV-BESS system [4] [5].

PV inverter acts as the heart of a DPV system. Apart from power conversion from DC to AC, PV inverters utilise a DC/DC converter to perform maximum power point tracking (MPPT) to ensure maximum power output from PV panels in real time. Furthermore, PV inverters are highly controllable and can be embedded with various advanced functionalities such as PV output curtailment, reactive power support, low voltage ride through, grid forming, and frequency control services [6] [7] [8].

By taking off the loads from the grid and feeding back with excessive solar energy, DPVs contribute significantly to the decarbonisation of power systems. It is reported that the rooftop PVs installed across Australia have reduced over 17.7 million tonnes of CO2 in 2021 [9]. Moreover, DPVs can bring enormous benefits to the end-users by substantially reducing their electricity usage from the grid and thus cutting their electricity bills. It is approximated that every kW installation of a PV system can help reduce a household's electricity bill by around A$400 annually [10]. In some states of Australia, the Governments are supporting installations of DPVs via substantial subsidies, rebates or interest-free loans. The DPVs will continue contributing to the households' energy saving as well as the energy transition of the entire industry.

However, the rapid proliferation of DPVs in distribution networks also comes with great challenges. One of the most significant challenges is associated with the intermittency and volatility of power generation. The power generation of PV panels is highly dependent on the sunlight and can be significantly affected by the stochastic cloud movement, which causes a very high ramp rate and dynamic PV output profile [11]. Moreover, vast integration of DPVs into the network can cause transient network power flow variations and significant voltage fluctuations, impairing the power quality [12]. The work [13] also indicates that the undesired reverse power flow and voltage rise can often be seen in distribution networks with a high PV penetration level, due to the excessive PV output at midday when the load is relatively low.

Another great challenge is associated with the DPV management. Unlike large-scale renewable generation such as solar farms which can be easily scheduled and managed, DPVs are usually "behind-the-meter" resources that are invisible and non-controllable to the network operators [14]. In Australia, the AS/NZS 4777.2:2020 standard [15] has been released to specify a local control mode for the DPVs, but local control would be insufficient to ensure the non-violation of network constraints when large amounts of DPVs are integrated into the networks. Thus, an effective DPV management scheme featuring visibility of system-wide information and dispatchability of the DPVs would be highly essential for future PV penetrated networks.

On the customer side, their benefits are challenged by the mismatch of the peak-valley characteristics of PV outputs and loads, which leads to affected PV energy utilisation efficiency [16]. Moreover, the burdens on the network can be imposed on the end-users in return. For example, the AS/NZS 4777.2:2020 standard requires the DPV generation to be curtailed in response to the voltage rise of the network. The feed-in tariffs have been dropping all these years, and in some regions it is even not allowed to export any PV power into the grid due to network constraints [17].

Additionally, the network itself can be seen as a challenge. Traditional distribution networks are designed for large, centralised generators and operated with a single-direction power flow from upstream transmission networks to end-users. These traditional network infrastructures are passive, and insufficient to handle the bidirectional power flow and transient network voltage/current fluctuations brought by the DPVs. Some of the networks are facing ageing problems or having a much lower rating, and the network constraints can be easily violated with the integration of DPVs.

All these challenges urge the grid to upgrade with new infrastructure and technologies to efficiently manage the penetrating DPVs in a way that not only system stability can be securely maintained but also more DERs can be accommodated into the grid.

1.2 Active Distribution Networks

Traditional distribution networks focus on passive control of large-scale generation and load to maintain network stability, making them insufficient to accommodate the penetrating DERs and tackle the emerging challenges such as reverse power flow and voltage fluctuation. It is essential to change the way in which DERs are managed. An active distribution network (ADN), which features active management of DERs, is proposed in recent years as a direction for future network development. The CIGRE Working Group C6.11 gives a globally shared definition of ADNs as follows [18]:

"Active distribution networks have systems in place to control a combination of distributed energy resources, defined as generators, loads and storage. Distribution system operators have the possibility of managing the electricity flows using a flexible network topology. Distributed energy resources take some degree of responsibility for system support, which will depend on a suitable regulatory environment and connection agreement."

ADNs give distribution system operators (DSOs) access to the DERs, improving the flexibility in managing network power flow to cope with various system dynamic issues. For example, an ADN penetrated with DPVs can enable the DSO to actively control the active/reactive power outputs of selected PV systems to address the network voltage issues. The Government of South Australia is considering making the dynamic export function mandatory for all PV system installations, which allows the DSO to flexibly adjust the PV system exports in real time via remote dispatch signals [19]. Western Australia is also conducting an Emergency Solar

Management program which requires all rooftop PV installations to be capable of being switched off remotely by DSOs in emergency situations [20].

ADNs enable DSOs to further enhance the network hosting capacity of variable renewables without reinforcement on network infrastructure so that more DERs can be efficiently accommodated into the current network. It is proved in [21] and [22] that, an optimised DER allocation/operation under the ADN framework, especially when associated with battery energy storage systems, can help significantly improve the network hosting capacity of DERs. Moreover, flexible network reconfiguration approaches in either planning stage or real-time controlling stage can be utilised in ADNs to greatly enhance the network hosting capacity of DERs without extra augmentation of grid physical structure [23].

Moreover, ADNs help further explore the potentials of DERs in benefiting the end-users. A highly dispatchable and coordinative ADN penetrated with DERs can create significant value streams from arbitrage. For example, facilitated by an ADN framework, various DERs can be aggregated as virtual power plants (VPPs) to participate in electricity markets or ancillary service markets for arbitrage and the benefits can be spread to participant end-users across the network [24] [25] [26] [27]. Moreover, DPVs aggregated in an ADN have the potential to cooperate with large renewable generators such as wind farms to participate in frequency control markets and the benefit from arbitrage is proved to be larger than the case where they work separately [28].

With the growing penetration of DERs, ADNs stand out as a promising solution to tackle the associated network challenges as well as to bring significant benefits to network operators and end-users.

On the other hand, in terms of practicality, a well-established ADN would require supports from the following key aspects.

- Support of grid infrastructure. A supportive grid infrastructure such as distribution lines, network switches, smart metering equipment and associated telecommunication facilities would lay the foundation of an effective ADN.
- An intelligent control centre. A powerful control centre or platform with advanced control logics or optimisation algorithms is required to monitor the system-wide

information, calculate optimal network flow and provide instant operating decisions.

- Accessibility and compatibility of DERs. DSOs need to seek approval from DER owners to access their devices, and work with various industry parties including retailers, original equipment manufacturers and third-party aggregators to guarantee the DER devices are compatible and dispatchable with the DSO control platform.
- Incentive mechanisms. A well-developed incentive mechanism is needed to spread the benefit of ADNs to DER end-users and encourage broader DER participation in the ADN.

The following table summarises the key advantages and challenges of ADNs with high penetration of DPVs.

Table 1-I Advantages and Challenges of ADNs Penetrated with DPVs

Advantages	**Challenges**
Enhance visibility and controllability of DPVs to network operators	• Compatibility of various DPV systems to ADN operating platform. • Privacy issues from end-users and mutual agreements with different parties. • Network infrastructure support.
Address network operation issues with optimal decisions based on system-wide information	• Intelligent ADN control platform and advanced solution algorithms. • Device reliability issues under excessive usage. • Network infrastructure especially metering and telecommunication devices.
Improve network hosting capacity of DERs without augmentation on network physical structure.	• Advanced optimisation methods and economic modelling approaches. • PV and load forecasting and uncertainty modelling. • Distribution network unbalance issues.
Create additional value streams from arbitrage.	• DPV dispatchability and responsiveness. • Control platform support with advanced bidding and operating strategies. • Reasonable profit allocation approaches to incentivise participation.

1.3 Volt/Var Control

Penetration of DPVs in distribution networks poses huge threat on the network operation, especially the network voltage control. A network with significantly high PV penetration can have serious voltage rise issues during peak generation hours [29]. In South Australia, the voltage soaring caused by the DPV proliferation has made the DSO to start implementing flexible solar export with an option of limiting the maximum output of rooftop PV systems to only 1.5kW per phase in some overloaded areas, at the cost of compromising the solar energy utilisation and customers' benefits [30]. Additionally, the uncertainty and intermittency of PV power generation leads to dynamic power flows and voltage fluctuations, impairing power quality.

Volt/var control (VVC) generally refers to a control function that optimally manages the operation of voltage regulating devices and the network reactive power flows to achieve predefined objectives such as minimising voltage deviations or reducing network power losses [31]. In this subchapter, conventional VVC methods using mechanically voltage regulating devices, as well as the emerging inverter-based VVC method, are introduced.

1.3.1 Conventional VVC Methods

Conventional VVC methods utilise traditional voltage regulating or reactive power compensation devices such as on-load tap changers (OLTCs), capacitor banks (CBs), and voltage regulators (VRs), to maintain the network voltage level within an allowed range [32].

OLTCs help regulate the network voltage level via altering the tap positions on network transformers, which leads to different transformer ratios and thus stepped voltage output levels. In distribution networks, OLTCs are usually operated by DSOs in a mechanical manner. OLTC is considered as one of the critical network operational devices for high DER integration. In the work [33], a coordinatively operating scheme of OLTCs along with static var compensators (SVCs) is proposed to optimally regulate the bus voltages in distribution networks. Other optimal control strategies of OLTCs for tackling issues associated with high DER integration can be found in the works [34] and [35].

CBs are another type of conventional VVC device commonly used in distribution networks. They are one of the main reactive power resources for power factor correction which compensates the broadly existing inductive loads with capacitance for network voltage regulation. CBs are usually operated by DSOs as well. CBs can be used to switch in/out to provide adjustable reactive power support that efficiently addresses the bidirectional power flow and rectifies the fluctuant voltages caused by DER integration. By deploying CBs, additional loads and DERs can be added to the network without enhancing the network line capacity. A two-stage hybrid voltage control approach for optimal sizing and location of CBs in distribution networks is developed in [36]. The work [37] develops an optimal placement/operation scheme of CBs for transformers power loss reduction and voltage regulation, while another online determination method for optimal location of CBs in distribution networks is proposed in [38].

Voltage regulators are also commonly used across the distribution networks. VRs are auto-transformers located at distribution feeders for voltage management, which use a VR tap changer to adjust the voltage ratios of the auto-transformer and thus maintain the network voltage level. VRs are usually mechanically operated by DSOs, and can be coordinatively operated with OLTCs and CBs. The work [39] proposes a multistage optimal operation of cascaded OLTCs, CBs and VRs for voltage regulation of distribution networks.

Conventional VVC devices are relatively low-cost and easy to operate. However, these devices are usually mechanically operated and may not respond swiftly enough to tackle the dynamic voltage changes [40]. Moreover, the increasing penetration of variable renewables such as DPVs in distribution networks has added to the voltage fluctuation issues, making it more imperative to develop and apply advanced fast-response VVC devices.

1.3.2 Inverter-Based VVC Methods

Compared with conventional VVC devices, power electronic devices have been proved to have fast and flexible response with the ability to provide VVC in terms of addressing the dynamic voltage fluctuations [41]. SVCs and STATCOMs are typical VVC devices using power electronic components. However, these devices are relatively expensive and mainly aimed for transmission networks, and wide deployment in distribution networks would be uneconomical [42]. On the other hand, PV inverters are smart power electronic devices which can provide fast and flexible reactive power support. More importantly, as heart of the DPVs, PV inverters are on-the-spot reactive power resources that broadly penetrate the distribution networks. Utilising the inverters of DPVs to provide VVC functions can be highly promising.

As an emerging VVC method, PV inverter based VVC is broadly suggested due to its high efficiency, scalability, flexibility, and practicability [43] [44]. The National Renewable Energy Laboratory (NREL) assesses the impact of PV inverter based VVC on distribution networks and demonstrates its high effectiveness in saving energy and improving power quality [45]. The work [46] proves that a properly oversized PV inverter can significantly enhance its reactive power availability for VVC, and the associated costs of oversizing can be offset by avoiding investment of conventional VVC devices such as CBs. The IEEE 1547.8 working group has been promoting the use of PV inverters for VVC support in distribution networks [47]. Electric Power Research Institute is also updating protocols of operating PV inverters for reactive power support [48]. In Australia, it is required that all the rooftop PV inverters should have the capability of providing var support and adjusting their var outputs in response to the local voltage levels [15].

Moreover, different advanced PV inverter based VVC models have been proposed in literature. The work [49] develops a two-stage centralised VVC model which optimally chooses PV inverters for var support and determines the var amount for voltage regulation. A hierarchically coordinated inverter based VVC method is proposed in [42] which coordinatively optimises both the var dispatch set points and droop control functions of the PV inverters in distribution networks. A distributed online VVC method for ADNs is proposed in [50] to achieve efficient voltage regulation and network power loss minimisation. In [51], a robust VVC method with PV inverters via a two-step calculation approach for inverter droop decisions is proposed. Ref [52] proposes a three-stage robust VVC model that coordinates various VVC devices including inverters from both local and central control perspectives. In the work [53], an inter-phase coordinative VVC method considering the imbalance of PV integration in distribution networks is developed. A bi-level VVC optimisation model coordinating both mechanical devices and smart PV inverters is proposed in [54], and a two-level distributed VVC scheme utilising aggregated PV inverters via consensus algorithm and droop controller is developed in [55]. Ref [56] develops a real-time central and local combined PV inverter based VVC method for both voltage regulation and power loss minimisation. An affinely adjustable robust VVC method for high PV penetrating distribution network is proposed in [57]. The work [58] develops a robust regionally coordinated inverter-based VVC method based on a multi-agent deep reinforcement learning approach. A multi-objective VVC model which hierarchically coordinates and optimises the PV inverter droop functions in the network is proposed in [59]. In [60], a multi-objective adaptive inverter based VVC method is developed to simultaneously minimise both the network power loss and bus voltage deviation.

PV inverter based VVC is proved as an outstanding solution to tackle the voltage regulation issues caused by the integration of renewables such as PVs. Moreover, it can effectively defer investments of additional voltage regulating equipment such as CBs and VRs, and enhance the networks' capability in hosting more DERs. With the growing penetration of PVs in distribution networks, network voltage management is facing significant challenges. At the same time, great potential lies inside this trend as more PV inverters can be aggregated and utilised for inverter-based VVC functions, to maintain network voltage security in an efficient, economical and renewable-friendly way.

The characteristics of the above VVC devices are summarised in Table 1-II.

Table 1-II Comparison of Characteristics of Common VVC Devices

VVC Device	Mechanism	Operation	Voltage Regulation Variability	Var Capability	Responsive-ness	Cost
OLTC	Transformer Tap Changing	Mechanical	Step Change	N/A	Slow	Low
CB	Var Compensation	Mechanical	Step Change	Medium	Medium	Low
VR	Transformer Tap Changing	Mechanical	Step Change	N/A	Medium	Medium
SVC	Var Compensation	Power Electronics Based	Continuously Variable	Large	Fast	High
STATCOM	Var Compensation	Power Electronics Based	Continuously Variable	Large	Very Fast	Very High
PV Inverter Based VVC	Var Compensation	Power Electronics Based	Continuously Variable	Flexible	Very Fast	Low with Existing Inverters

1.4 PV Inverter Reliability

Utilising PV inverters to provide VVC functions for network voltage regulation is theoretically proved to be highly promising. However, in regards of VVC implementation, a very practical concern emerges, i.e., PV inverter reliability.

PV inverters are power electronics devices that convert direct current originated from solar panels into alternating current so that the solar energy can be utilised by loads or the grid. The schematic diagram of a single phase two-stage PV inverter is demonstrated in Figure 1.1.

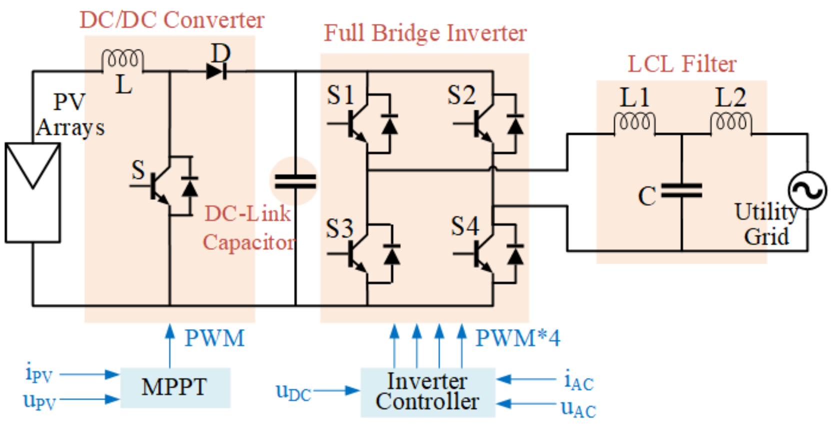

Figure 1.1 Schematic of a Single-Phase Two-Stage PV Inverter

At the first stage, a DC/DC converter is connected to the PV panels to perform maximum power point tracking (MPPT). The second stage utilises a full bridge inverter to perform power conversion from DC to AC, where 4 power devices (S1-S4) are placed at the 4 arms of the full bridge inverter for pulse width modulation (PWM) control. A DC-link capacitor is paralleled in between the two stages to stabalise DC link voltage and arrest current harmonics. An LCL filter is usually used before connecting to the grid for voltage and current filtering purpose.

PV inverter is the core device of a solar PV system, but also the most fragile one. A PV inverter contains vulnerable power electronic components, which makes it less reliable than any other components of a PV system. Compared to solar panels which can last for about 20 to 30 years, the associated PV inverters usually have a lifespan of less than 15 years [61]. In Australia, most of the rooftop PV inverters in market only have a warranty period of 5 to 10 years, which is much shorter than that of associated solar panels and battery modules. A study points out that the PV inverter is the most vulnerable PV subsystem due to its physical complexity and high susceptibility to the working conditions [62]. Moreover, Figure 1.2 demonstrates the analysis results of PV subsystem reliability for a PV generation plant over a 5-year operation period [63]. It can be seen that the cost related to unscheduled PV inverter maintenance takes 59% of the total maintenance cost, while the number of unscheduled maintenance events for PV inverters takes 37% of the total events, and both figures are much higher than those of other PV subsystems.

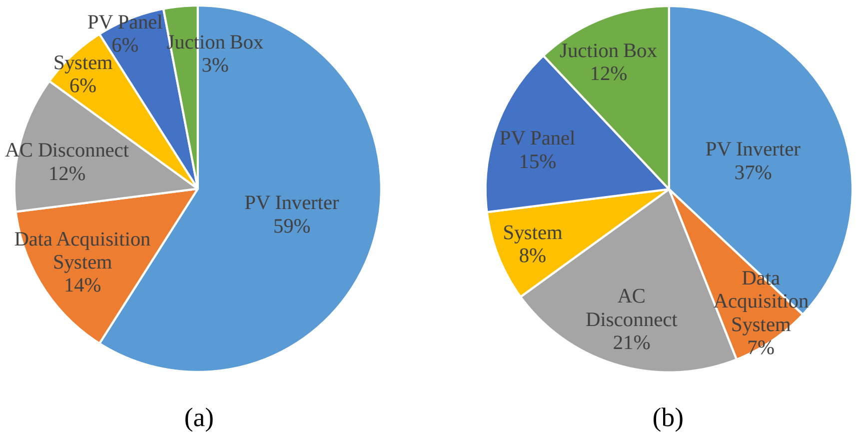

Figure 1.2 Analysis Results of a 3.5MW PV Plant under 5 Years' Field Experience. (a) Unscheduled Maintenance Costs by Subsystem. (b) Unscheduled Maintenance Events by Subsystem.

To analyse PV inverter reliability, it is essential to understand the inverter failure mechanism. As in Figure 1.1, the power switches S1-S4, typically insulated gate bipolar transistors (IGBTs), and the DC-link capacitor, are the two most critical power electronic components inside a PV inverter, and their lifetimes are usually considered as determinants for inverter reliability assessment [64] [65]. Meanwhile, thermal loading is considered as one of the most significant factors that contribute to the failure of the power electronic components [66]. For power devices, it is the loading of junction temperature, while for the DC-link capacitor, it is the core temperature. To obtain the thermal loading of power devices and the DC-link capacitor, their power loss models and thermal models are needed to interpret their operational conditions into temperature statuses [67] [68]. Then a cycle counting methodology such as Rainflow counting [69] may be needed to analyse the thermal loading for lifetime evaluation. Based on the thermal loading analysis results, their lifetime models can be utilised to calculate their lifetime, and different lifetime models can be found in [70] [71] [72] for power devices, and [73] [74] for DC-link capacitors. Moreover, PV inverters' operational conditions are also the key factors affecting their reliability, which include the inverter control strategies such as MPPT and droop control, as well as the inverter external conditions such as solar irradiance and ambient temperature. Significant impacts of inverter control strategies and external conditions on inverter lifetime have been analysed in literature [75] [76].

Utilising PV inverters to provide reactive power support can further degrade the inverter reliability. The work [77] indicates a negative impact of non-unity power factor operation on PV inverter reliability. In [67], the reliability of PV inverters used for reactive power compensation during none feed-in hours is analysed, and significant lifetime degradation is identified compared to inverters at normal working conditions.

As an active inverter control strategy for network voltage regulation, PV inverter based VVC aims at optimising and dispatching the var support of PV inverters across the network. Given the vulnerability of PV inverters as well as the potential negative impact of reactive power support on PV inverter reliability, this leads to a significant thought that whether the use of PV inverters for VVC is economically efficient in the long run. However, none of the VVC works in literature have discussed PV inverter reliability issues, and the long-term impact of VVC on PV inverter reliability remains to be investigated, leaving a research gap.

1.5 Addressing PV Inverter Reliability in VVC

PV inverter based VVC utilises PV inverters to provide additional reactive power support, which may pose extra burden on PV inverters, causing increased thermal load, and thus affected inverter reliability. On the other hand, existing VVC models mainly focus on network voltage regulation and power loss reduction, and none of them have ever considered PV inverter reliability which is crucial for both sustainable PV energy utilisation and reliable VVC support. To this end, this subsection focuses on assessing PV inverter reliability under the VVC function, and investigating how to involve PV inverter reliability in VVC models.

1.5.1 PV Inverter Reliability Assessment under VVC

The work [67] analysed the impact of reactive power compensation on PV inverter reliability, where a localised var control method is applied. However, for VVC models, the inverter reactive power support is determined by various factors, including the solar irradiance across the network, the network topology and parameters, the PV inverter location in the network, as well as the customers' load demand profiles. All the system-wide information is embedded into the VVC optimisation model to obtain the inverter reactive power output decisions. With the inverter reactive power output details, the inverter reliability analysis models discussed in Chapter 1.4 can be applied to analyse the inverter thermal loading and lifetime. Figure 1.3 visualises the inverter reliability analysis process based on lifetime evaluation of critical IGBTs under the VVC function.

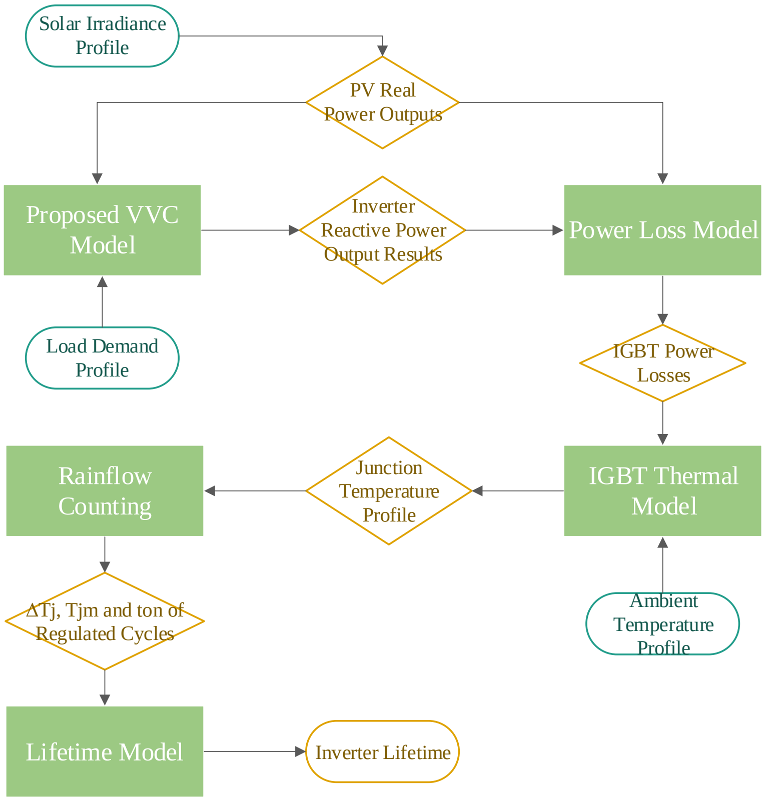

Figure 1.3 Inverter Reliability Analysis Procedure Based on IGBT Lifetime Evaluation.

In Figure 1.3, the blue capsules are the external mission profiles which create direct impacts on PV active power outputs, network power flow, and inverter thermal loading. The green rectangles are the key IGBT reliability models for power loss and junction temperature calculation, and lifetime evaluation. The orange diamonds indicate the critical electrical/thermal parameters obtained from or applied to the reliability models for thermal/lifetime assessment. Application of the inverter reliability analysis process and detailed analysis results can be found in Chapter 2. It is worth noting that other components especially DC-link capacitors, may fail before IGBTs, thus determining the inverter lifetime. The DC-link capacitor reliability models and the reliability assessment procedure are discussed in detail in Chapter 3.

1.5.2 VVC Considering PV Inverter Reliability

The potential negative impact of VVC on PV inverter reliability also points to another direction, i.e., whether PV inverter reliability can be involved into the VVC models, to proactively prevent the reliability degradation or even enhance the inverter reliability with VVC applications. This direction is meaningful as the device reliability is arising as a major concern for inverter based ADN operation [78]. Considering PV inverter reliability in VVC schemes contributes to both the ADN voltage security and operational reliability.

As is discussed in Chapter 1.3, typical PV inverter based VVC methods mainly consider network voltage regulation and power loss reduction. For power loss reduction, majority of the VVC works in literature put the network power loss into the objective function for minimisation. For voltage regulation, it can be put into the objective function to minimise voltage deviations, or be directly involved into constraints via setting upper/lower bounds. The network power loss expression is a convex model while the voltage model is linear, both of which can be directly incorporated into VVC optimisation models.

To consider PV inverter reliability in VVC, it is essential to effectively incorporate PV inverter reliability models into VVC optimisation model. However, as indicated in [67] and [68], the PV inverter power loss models and lifetime models are complex non-convex models that contain exponential and high-dimensional terms, which are intractable and hard to be incorporated into optimisation models. Furthermore, as part of the inverter reliability analysis process for thermal load interpretation, the Rainflow counting technique is a logic based algorithm, which is completely intractable for mathematical programming optimisation.

Considering the difficulties of involving PV inverter reliability models in VVC optimisation, this thesis innovatively bypasses the complex reliability models and directly incorporates the inverter apparent power in VVC modelling, based on the proof that the inverter apparent power outputs have indirect impact on PV inverter lifetime [79]. On the other hand, the inverter apparent power has a quadratic equality relationship with inverter active and reactive power, which is non-convex and hard to be solved. Conventional convex programming methods such as semidefinite programming (SDP) [80] and second-order cone programming (SOCP) [81] can be used to solve the non-convex quadratic optimisation problems. However, these methods are not universal for use and only apply to certain conditions, and the exactness of these relaxation methods can be challenged by various factors such as network topologies and formulation of objective functions [82]. A practicable and efficient solution method is required to address the non-convexity issue when incorporating inverter apparent power into VVC models.

Different schemes of VVC modelling with inverter apparent power regulation to address PV inverter reliability are discussed in Chapters 3, 4 and 5. Especially, an efficient solution method is developed in Chapter 4 to tackle the non-convexity of the proposed VVC optimisation model.

1.6 Research Gaps and Significance

Based on the above discussions, the following major research gaps can be identified.

- PV inverter based VVC is theoretically proved to be highly efficient for network voltage management, but its potential negative effect on inverter reliability has never been revealed.
- Current inverter reliability analysis methods mainly focus on single independent devices, while a comprehensive reliability assessment procedure compatible with VVC and associated PV inverters in the network level is absent.
- Current advanced VVC methods in literature mainly focus on network voltage regulation and power loss reduction, but none of the works ever considers the PV inverter reliability in VVC modelling.
- PV inverter reliability analysis models contain intractable nonlinear terms, which are hard to be incorporated into the VVC optimisation model.
- The potential positive impacts of properly designed VVC on PV inverter reliability have never been investigated, and enhancing PV inverter reliability via incorporating inverter reliability models into the constraints or objective function of a VVC optimisation model remains totally untapped.

This research focuses on addressing the above research gaps. Firstly, the research proposes an entire PV inverter reliability assessment process under the VVC function to address the first two gaps. The proposed reliability assessment process successfully reveals the impact of VVC on PV inverter reliability and effectively estimates the inverters' lifetime when used for a centralised VVC method. Then, for the first time the research develops three advanced PV inverter based VVC methods considering inverter reliability to address the following three gaps. These methods develop solvable convex PV inverter reliability models and effectively incorporate them into the constraints or objective function of the VVC optimisation model, to realise efficient network voltage regulation, power loss reduction, and inverter reliability enhancement.

1.7 Research Contributions

This research mainly focuses on assessing the PV inverter reliability under the VVC function and developing advanced PV inverter based VVC methods considering PV inverter reliability enhancement. In this research, a series of advanced PV inverter based VVC optimisation models are developed, a complete PV inverter reliability assessment procedure compatible with VVC operation is proposed, and efficient solution algorithms addressing the non-convexity and uncertainty problems of VVC optimisation models are developed. The major contributions of this research are summarised as follows.

Contributions to Inverter Reliability Constrained VVC Modelling.

- New inverter reliability constraints for power restriction are developed, which are used to ensure inverter lifetime commitment by utilising a proposed restriction factor to regulate the amplitude of inverter apparent power output.
- A multi-objective PV inverter reliability constrained VVC optimisation model with the developed inverter power restriction constraints and a PV curtailment scheme is proposed, to minimise network power loss and curtailed PV output under uncertainties, while guaranteeing long inverter lifetime. It is the first time to incorporate PV inverter reliability into an inverter-based VVC model.
- New inverter reliability constraints for power smoothing are further developed, which utilise a proposed smoothing factor to constrict the variation of inverter apparent power output.
- A PV inverter reliability constrained VVC method is proposed with the developed power smoothing constraints and formulated as an optimisation problem with system-

wide information. It is the first time to address the inverter junction temperature variation in a VVC model to enhance inverter reliability.

- A multi-objective PV inverter based VVC optimisation model is developed with a proposed slack variable and a weighting factor to simultaneously minimise both the network power loss and inverter apparent power output. It is the first time to address inverter reliability in the objective function of a VVC optimisation model.

Contributions to Methodology of Inverter Reliability Assessment and Enhancement.

- A complete PV inverter reliability assessment approach is developed to evaluate the reliability of PV inverters when used for the VVC function. This approach is the first time to successfully quantifies the impact of inverter-based VVC on the lifetime of associated PV inverters in the network.

- An inverter power smoothing scheme with high control flexibility is developed, which utilises VVC reactive power support and PV power curtailment to ensure that the inverter apparent power output is efficiently smoothed and the variation is confined within a prespecified percentage of inverter apparent power capacity.

- A Pareto front analysis method is proposed to select a proper value for the weighting factor, through numerical simulations of long-term VVC operation. With the selected weighting factor, the proposed VVC optimisation model can achieve the most efficient network power loss reduction with guaranteed inverter lifetime.

Contributions to Optimisation Method and Solution Algorithm.

- A scenario-based stochastic optimisation method is developed to solve the uncertainty problems of PV power generation and loads in VVC optimisation models, where a slack variable is introduced to guarantee a feasible region for the optimised reactive power results under PV generation uncertainties.

- A penalty convex-concave procedure (CCP) programming method is developed to solve the non-convexity problem of the proposed PV inverter reliability constrained VVC optimisation model, and the computing efficiency is proved to be outstanding in comparison with the off-the-shelf solvers.

The proposed models, methodologies, and solution algorithms, in comparison with the existing proposals in literature, have been successfully demonstrated in case studies, and the simulation results have verified their high efficiency.

1.8 Thesis Outline

The thesis outline is described as follows.

Chapter 1 gives the introduction of this research, in which the background information about DPVs, ADNs and inverter-based VVC is introduced, the challenges to PV inverter reliability are analysed, the research gaps are identified, and the research contributions are summarised.

Chapter 2 develops a complete PV inverter reliability assessment approach to analyse the impact of inverter-based VVC functions on PV inverter reliability. This approach is the first time to successfully quantifies the impact of VVC on the lifetime of associated PV inverters, providing insights on enhancing PV inverter reliability via properly designed VVC models.

Chapter 3 proposes a PV inverter reliability constrained VVC method for distribution networks. New inverter reliability constraints are proposed with a restriction factor to limit the inverter apparent power amplitude. With the reliability constraints, a multi-objective PV inverter reliability constrained VVC optimisation model is developed to simultaneously minimise the network power loss and curtailed PV power, while guaranteeing enhanced inverter lifetime. It is the first time to consider PV inverter reliability in an inverter-based VVC model.

Chapter 4 proposes a PV inverter reliability constrained VVC method with power smoothing to enhance inverter reliability. Compared to the proposed method in Chapter 3, this method develops a highly flexible inverter power smoothing scheme utilising a smoothing factor to constrict the inverter apparent power variation instead of compromising the apparent power capability. Besides, a penalty CCP solution method is developed to tackle the proposed non-convex VVC optimisation problem with high computing efficiency.

Chapter 5 proposes a novel Pareto front analysis method for PV inverter based VVC methods to achieve guaranteed inverter lifetime. In this Chapter, a multi-objective PV inverter based VVC model is developed with a weighting factor to simultaneously minimise the network power loss and inverter apparent power output. With the proposed Pareto front analysis method, a proper weighting factor for the VVC model is obtained to achieve the most efficient network power loss reduction while guaranteeing expected inverter lifetime.

Chapter 6 concludes the research and suggests directions of future work.

The framework of this thesis is illustrated in Figure 1.4.

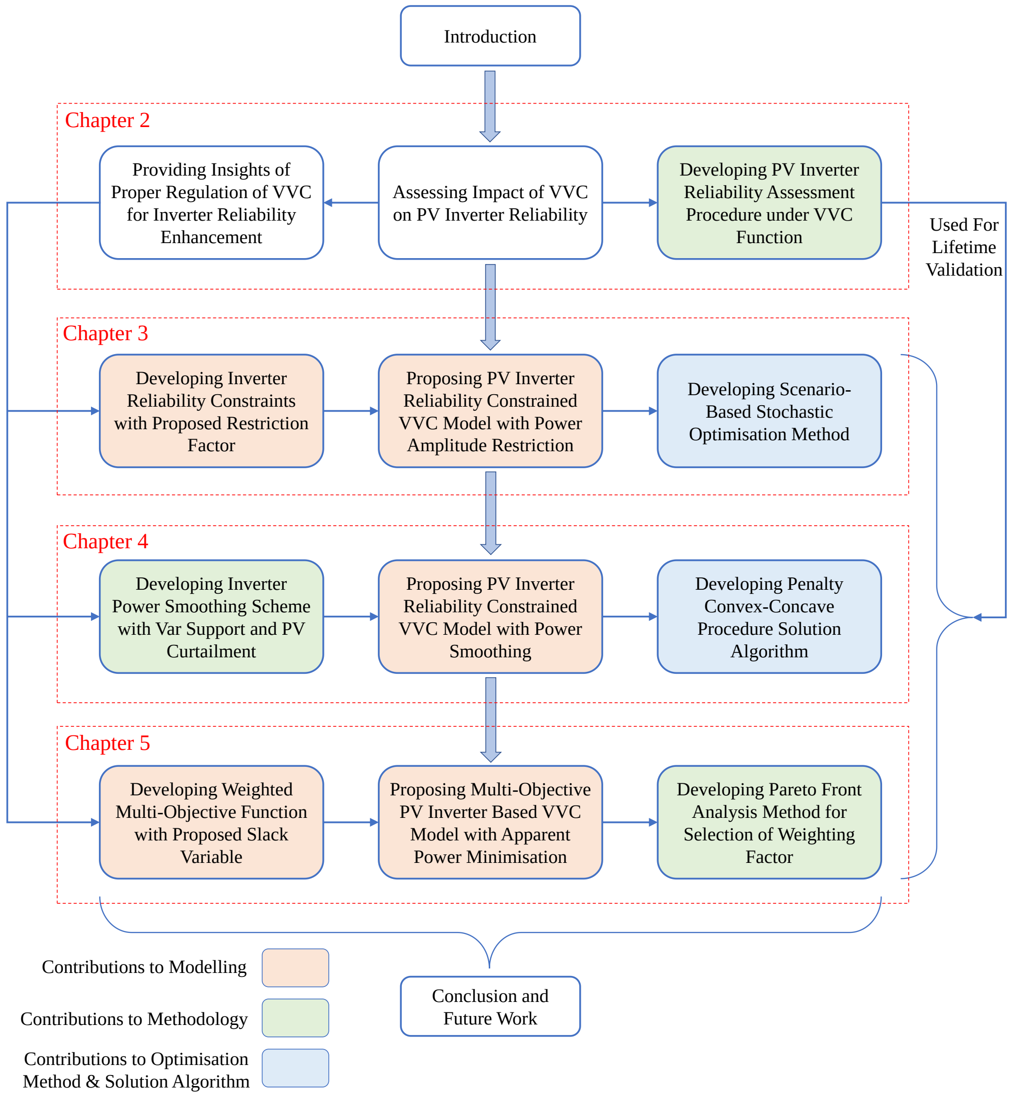

Figure 1.4 Thesis Framework

Chapter 2 OPERATIONAL RELIABILITY ASSESSMENT OF PHOTOVOLTAIC INVERTERS CONSIDERING VOLT/VAR CONTROL FUNCTION

In this chapter, the long-term operational reliability of PV inverters when used for the VVC function is analysed. A complete operational reliability assessment approach is developed to efficiently quantify the impact of VVC functions on PV inverter lifetime. Firstly, an inverter based VVC model considering uncertainties of PV power generation and loads is developed and it is solved by a stochastic optimisation method. Then, a long-term reliability assessment procedure for the PV inverters utilised in the VVC model is proposed. To assess the reliability, a power loss model considering the VVC results is developed and a modified lifetime model based on Coffin-Manson model and manufacturing information is proposed. The proposed VVC model and the inverter reliability assessment approach are verified on a 33-bus distribution network. The simulation results successfully reveal and quantify the long-term impacts of additional VVC utilisation on the operational reliability and lifetime of PV inverters.

2.0 Nomenclature

A. Sets and Indices

i	Index of IGBT thermal cycles.
$K,\ k$	Set and index of network buses.
$SC,\ sc$	Set and index of uncertainty scenarios.
$T,\ t$	Set and index of operating time intervals.

B. Parameters

1) PV Inverter Parameters

$E_{on,nom}$,$E_{off,nom}$	Nominal single-pulse turn-on and turn-off energy loss of IGBT unit (J).
$E_{rec,nom}$	Nominal single-pulse reverse recovery energy loss of diode unit (J).

f_{sw}	Switching frequency (Hz).
i_P, u_P	Output sinusoidal current and voltage amplitude (A,V).
I_{nom},V_{nom}	Nominal current and voltage of IGBT module (A,V).
m	PWM modulation rate.
P_{IG}^{loss}	Power loss on IGBT unit (W).
P_{D}^{loss}	Power loss on reverse recovery diode unit (W).
T_a	Ambient temperature (K).
T_j, T_c, T_h	Junction, case and heatsink temperature (K).
V_{AC}	AC voltage RMS value (V).
V_{DC}	Applied DC-link voltage (V).
V_{CE0},r_{CE}	Zero-current on-state collector-emitter voltage and on-state collector-emitter resistance of IGBT unit (V, Ω).
V_{D0},r_D	Zero-current on-state voltage drop and on-state resistance of diode unit (V, Ω).
$Z_{th(j-c)}$	Thermal impedance from junction to case (K/W).
$Z_{th(c-h)}$	Thermal impedance from case to heatsink (K/W).
$Z_{th(h-a)}$	Thermal impedance from heatsink to ambient (K/W).
φ	Phase difference between PWM modulation signal and inverter current (rad).

2) Network Parameters

$P^{net,loss}$	Network power loss on the branch lines (W).
r_k, x_k	Resistance/Reactance of the branch line from bus k to bus $k+1$ (Ω).
S_k^{cap}	Inverter apparent power capacity at bus k (VA).
$\underline{V}_k$, $\overline{V}_k$	Lower and upper limits of voltage at bus k (p.u.).
V_0	Voltage at the substation (p.u.).

C. Variables

$P_{k,t}$,$Q_{k,t}$	Active/Reactive power through the branch line from bus k to bus $k+1$ at time t (W,var).
$P_{k,t}^L$, $Q_{k,t}^L$	Uncertain active/reactive load at bus k at time t (W,var).

$P_{i,t}^{PV}$, $Q_{k,t}^{inv}$	PV inverter active/reactive power output at bus k at time t (W,var).
$Q_{k,t}^{max}$	Maximum inverter reactive power capacity at bus k at time t (var).
$V_{k,t}$	Voltage of bus k at time t (p.u.).
ρ	Occurrence probability of uncertainty scenarios.

2.1 Introduction

2.1.1 Photovoltaic Development and Ancillary Services

Solar energy is considered as a primary alternative energy resource to reduce the reliance on traditional fossil energy. With the advance of modern technologies, the utilisation of photovoltaics (PVs) has been in a rapid growth in the power systems. It is reported by [2] that there are over 3 million distributed rooftop PV systems installed in Australia. The distributed PVs that significantly penetrate in distribution networks can be aggregated as virtual power plants (VPPs), which can provide reliable management support for the power systems. Moreover, the PV based VPPs have the potential to support ancillary services such as voltage/VAR control (VVC) functions. IEEE 1547.8 working group has been revising relevant standards to allow PV inverters to participate in network voltage regulation [47]. Electric Power Research Institute [48] has recently given protocols for inverter based reactive power compensation methods, including various control modes. Furthermore, it is suggested that PV inverters can be oversized to allow more reactive power compensation capacity and the additional cost can be offset by the reduction of capacitor banks' investment [46]. The optimal energy management ability and the ancillary services supported by the PV based VPPs provide a potential to construct active distribution networks. Particularly, in short future, utilising the PV based VPPs to support the VVC functions in the active distribution networks, improving power quality and reducing power losses, is inevitable.

2.1.2 Photovoltaic Inverter Reliability

With the rapid proliferation of PV systems in distribution networks, operational reliability issues come into the picture. The warranted lifetime of PV modules is about 20-30 years, whereas the lifetime of associated inverters is usually less than 15 years, and the number analysed in 2012 was only around 5 years on average for PV inverters [61]. According to a study on the 5-year operating experience of a PV generation plant [63], the cost associated with PV inverter malfunctions takes 59% of the total system maintenance cost. Thus, the operational reliability of PV inverters is becoming one of the most crucial factors for the performance of the whole PV systems.

Power devices, e.g., insulated gate bipolar transistors (IGBTs) or metal-oxide-semiconductor field-effect transistors (MOSFETs) are the key power electronic components inside inverters. According to an industry-based survey [64], power devices are considered as one of the significantly fragile parts of inverters. Understanding failure mechanisms of power devices would be essential for the inverter reliability analysis. In addition, it is observed that the thermal cycling, i.e., the swings of junction temperature, is one of the most critical failure reasons for the power devices [83].

For the PV inverters, the lifetime of power devices is significantly affected by their operational conditions, which include control strategies, e.g., maximum power point tracking (MPPT) and reactive power compensation, as well as mission profiles including solar irradiance and ambient temperature. The reliability of PV systems under a MPPT algorithm is analysed in [75] and an improved algorithm that can achieve a tradeoff between energy harvesting and lifetime consumption is proposed. Besides, the study in [76] indicates that both the PV active power outputs which are directly affected by solar irradiance and the ambient temperature have tremendous impacts on the lifetime of PV inverters. Thus, in order to predict the lifetime of PV inverters, both the control strategies and the mission profiles are expected to be taken into consideration. However, operational reliability of the PV inverters which are utilised for the VVC function has not been studied, leaving a research gap.

2.1.3 VVC and Reliability Analysis

As PV inverters can provide fast and flexible reactive power support with the marginal operating cost, the VVC based on the PV inverters is highly promising. To achieve a VVC function, the inverters in the VPPs can be dispatched to support the optimal reactive power injection to the active distribution networks, aiming to minimise network power losses while keeping bus voltages within operating limits. It is worth noting that the reactive power compensation imposes additional operating burdens on the PV inverters, which have negative impacts on the inverter operational reliability in a long term. Thus, this issue leads to a significant thought whether the use of the inverters for the VVC function is economically efficient in the long run. In [77], the reliability of PV inverters under non-unity power factor operation and low-voltage ride-through is studied, but the reliability degradation rate and estimated lifetime of inverters are not specified. The operational reliability of PV inverters is analysed in [67] and heavy lifetime degradation is identified due to reactive power compensation outside day-time feed-in hours. However, the analysis is conducted on a device level and only the functionality outside the feed-in hours is considered. In [84], a reactive power control scheme is proposed to stabilise the thermal fluctuation of power devices in wind farm, which indicates the potential positive impacts of reactive power on inverter reliability. Thus, it is imperative to further investigate the operational reliability of inverters which are coordinated for the VVC function on a system level.

In summary, utilisation of PV inverters in VPPs to support the VVC function is highly promising for the stability and sustainability of modern power systems. However, the impacts of the additional VVC function on the inverter operational reliability have not been studied and addressed. Thus, this chapter develops an inverter based VVC model considering uncertainties, a power loss model of the switch module considering the VVC results and a modified lifetime model based on Coffin-Manson model and manufacturing information. Last, with these models, this chapter proposes an operational reliability assessment approach of PV inverters considering the VVC function. In case study, this approach is validated on a 33-bus distribution network, indicating the impacts of the additional VVC function on the inverter operational reliability and suggesting potential solutions.

2.2 Inverter Based VVC Under Uncertainties

In order to analyse the inverter operational reliability considering the VVC function, firstly, an inverter based VVC optimisation model under uncertainties such as PV power generation and load demand is developed in this subchapter.

2.2.1 Inverter Based VVC Optimisation Model

The inverter based VVC optimisation model aims to minimise the total network power losses while keeping bus voltages within allowed range, by optimising the inverter reactive power outputs. The inverter based VVC optimisation model is formulated as follows:

$$\min_{Q_{k,t}^{inv}} \sum_{t\in T}\sum_{k\in K} P_{k,t}^{net,loss} \tag{2.1}$$

$$\text{s.t.} \quad P_{k+1,t} = P_{k,t} + P_{k+1,t}^{PV} - P_{k+1,t}^{L}, \forall k,t \tag{2.2}$$

$$Q_{k+1,t} = Q_{k,t} + Q_{k+1,t}^{inv} - Q_{k+1,t}^{L}, \forall k,t \tag{2.3}$$

$$V_{k+1,t} = V_{k,t} - \frac{\left(r_k P_{k,t} + x_k Q_{k,t}\right)}{V_0}, \forall k,t \tag{2.4}$$

$$P_{k,t}^{net,loss} = r_k \frac{P_{k,t}^2 + Q_{k,t}^2}{V_0^2}, \forall k,t \tag{2.5}$$

$$\underline{V}_k \leq V_{k,t} \leq \overline{V}_k, \forall k,t \tag{2.6}$$

$$-Q_{k,t}^{max} \leq Q_{k,t}^{inv} \leq Q_{k,t}^{max}, \forall k,t \tag{2.7}$$

$$(Q_{k,t}^{max})^2 = (S_k^{cap})^2 - (P_{k,t}^{PV})^2, \forall k,t \tag{2.8}$$

Objective function (2.1) aims to minimise the total network power loss over a given dispatch period T by optimising control variables, i.e., the inverter reactive power outputs $Q_{k,t}^{inv}$. Note that index t denotes each operation time interval in T and index k denotes the bus number in the bus set K. Equations (2.2)-(2.4) are the linearised DistFlow equations given by [52]. Herein, P_k and Q_k are active and reactive power flowing from bus k to $k+1$, P_k^L and Q_k^L are active and reactive power demand at bus k, P_k^{PV} represents active power generation of the PV systems at bus k, r_k and x_k represent resistance and reactance of the branch line between bus k and $k+1$, V_k is voltage magnitude of bus k and V_0 denotes voltage magnitude at the substation. Eq. (2.5) calculates power loss of each branch line. Constraints (2.6) and (2.7) ensure that bus voltage magnitude and inverter reactive power output of each bus are limited within the allowed ranges. Eq. (2.8) calculates real-time reactive power capacity of the inverters at each bus, where S_k^{cap} denotes total apparent power capacity of the inverters at bus k.

The proposed VVC model (2.1)-(2.8) forms a quadratic programming problem containing uncertainty variables such as PV active power generation (P^{PV}) and load demand (P^L and Q^L).

2.2.2 Stochastic Optimisation Method

To solve the VVC model that contains uncertainty variables, i.e., P^{PV}, P^{L} and Q^{L}, this chapter applies a scenario-based stochastic optimisation method.

The objective function of a scenario-based stochastic optimisation model can be written as:

$$\min_{x} \sum_{sc\in SC} \rho_{sc} G(x, \xi_{sc}) \tag{2.9}$$

where x stands for the control variables, ξ_{sc} denotes the uncertainty realisation in scenario sc, ρ_{sc} represents the corresponding occurrence probability of scenario sc and $G(x, \xi_{sc})$ is the objective function with the realised ξ_{sc}.

Thus, the proposed VVC model can be converted as:

$$\min_{Q_{k,t}^{inv}} \sum_{sc\in SC} \rho_{sc} \sum_{k\in K} P_{k,sc}^{net,loss} \tag{2.10}$$

$$\text{s.t.} \quad (2.2)\text{-}(2.8), \forall k, sc$$

$$\left\{(P_{k,sc}^{PV}, P_{k,sc}^{L}, Q_{k,sc}^{L}), \rho_{sc}\right\} \in \Psi_k, \forall k \tag{2.11}$$

where $P_{k,sc}^{PV}$, $P_{k,sc}^{L}$ and $Q_{k,sc}^{L}$ represent the PV active power generation, active and reactive power demand in scenario sc, and Ψ_k denotes the scenario set.

In this chapter, Monte Carlo sampling (MCS) is used to generate the uncertainty realisation scenarios with given probability density functions (PDFs) which can characterise realisation probability distribution. For example, Gaussian PDF, which can efficiently represent the uncertainty realisation of PV outputs and loads, is applied in the MCS to construct the scenarios.

The proposed stochastic optimisation problem of the VVC model can be solved by commercial solvers such as the GUROBI solver [85].

2.3 Inverter Reliability Assessment

With the VVC optimisation model, the long-term inverter reactive power outputs can be simulated and obtained. Then the long-term operational reliability of the inverters considering the VVC function and the mission profiles (solar irradiance and ambient temperature) can be assessed.

Firstly, a power loss model based on inverter active and reactive power outputs is developed to calculate the power losses dissipated in power devices inside the inverters. Herein, the active power outputs are affected by the solar irradiance and the reactive power outputs are optimised by the proposed VVC model under the uncertainties. Secondly, with the power losses, this chapter applies the thermal model and one-year real-field data of ambient temperature to obtain the junction temperature profiles of the power devices. Then, a Rainflow counting technique [69] is used to interpret the randomly varying junction temperature profiles into regulated thermal cycles. Last, this chapter modifies the Coffin-Manson model to estimate the lifetime of the power devices in the inverters with consideration of practical concerns.

2.3.1 Power Loss Model

In this chapter, a single-phase PV inverter using IGBTs as power devices is used for operational reliability analysis. Since an IGBT module contains two parts, an IGBT unit and a diode unit, the power losses dissipated in these units are calculated separately.

2.3.1.1 IGBT Power Loss Calculation

The power loss of the IGBT unit (P_{IG}^{loss}) during one certain period can be expressed as:

$$P_{IG}^{loss} = P_{IG,con}^{loss} + P_{IG,sw}^{loss} \tag{2.12}$$

where $P_{IG,con}^{loss}$ and $P_{IG,sw}^{loss}$ denote the conduction and switching losses of the IGBT unit, respectively. $P_{IG,con}^{loss}$ and $P_{IG,sw}^{loss}$ can be calculated by the following equations:

$$P_{IG,con}^{loss} = \left(\frac{1}{2\pi} + \frac{m \times \cos\varphi}{8}\right) \times V_{CE0} \times i_P + \left(\frac{1}{8} + \frac{m \times \cos\varphi}{3\pi}\right) \times r_{CE} \times {i_P}^2 \tag{2.13}$$

$$P_{IG,sw}^{loss} = \frac{f_{sw}}{\pi} \times \left(E_{on,nom} + E_{off,nom}\right) \times \frac{i_P \times V_{DC}}{I_{nom} \times V_{nom}} \tag{2.14}$$

where i_P denotes the inverter sinusoidal output current amplitude, V_{CE0} denotes the IGBT on-state zero-current collector-emitter voltage, r_{CE} denotes the IGBT on-state collector-emitter resistance, I_{nom}, V_{nom}, $E_{on,nom}$ and $E_{off,nom}$ denote the nominal current/voltage and the corresponding nominal single-pulse turn-on/off energy losses respectively, m denotes the PWM modulation rate, φ denotes the phase difference between modulation signal and inverter current,

f_{sw} represents the switching frequency and V_{DC} denotes the applied DC link voltage.

2.3.1.2 Diode Power Loss Calculation

The power loss dissipated on the diode unit can be calculated by:

$$P_D^{loss} = P_{D,con}^{loss} + P_{D,sw}^{loss} \tag{2.15}$$

$$P_{D,con}^{loss} = \left(\frac{1}{2\pi} - \frac{m \times \cos\varphi}{8}\right) \times V_{D0} \times i_P + \left(\frac{1}{8} - \frac{m \times \cos\varphi}{3\pi}\right) \times r_D \times {i_P}^2 \tag{2.16}$$

$$P_{D,sw}^{loss} = \frac{f_{sw}}{\pi} \times E_{rec,nom} \times \frac{i_P \times V_{DC}}{I_{nom} \times V_{nom}} \tag{2.17}$$

where P_D^{loss} denotes the power loss of the diode unit during one period, $P_{D,con}^{loss}$ and $P_{D,sw}^{loss}$ represent the conduction and switching power losses of the diode unit respectively, V_{D0} denotes the on-state zero-current voltage drop on the diode, r_D denotes the diode on-state resistance and $E_{rec,nom}$ represents the nominal value of single-pulse reverse recovery energy of the diode.

It is worth noting that generally, V_{CE0}, r_{CE}, V_{D0}, r_D, $E_{on,nom}$, $E_{off,nom}$, I_{nom}, V_{nom} and $E_{rec,nom}$ can be directly obtained from the IGBT manufacturer's datasheet. Thus, given the PWM modulation pulse patterns and the inverter DC link voltage, the total power loss of an IGBT module is a quadratic function of i_P.

2.3.1.3 Power Loss Calculation Considering VVC Function

As mentioned, the total power loss of an IGBT module has a close relationship with the sinusoidal output current amplitude i_P. For an inverter used to support the VVC function, i_P and $\cos\varphi$ can be calculated as follows:

$$i_P = \sqrt{2} \times \frac{\sqrt{(P^{PV})^2 + (Q^{inv})^2}}{V_{AC}} \tag{2.18}$$

$$\cos\varphi = \frac{P^{PV}}{\sqrt{(P^{PV})^2 + (Q^{inv})^2}} \tag{2.19}$$

where P^{PV} denotes the PV active power output affected by the solar irradiance, Q^{inv} represents the inverter reactive power output determined by the VVC model, and V_{AC} denotes the inverter AC root mean square voltage. By substituting (2.18) and (2.19) into (2.12)-(2.17), the power loss model of an IGBT module considering inverter active and reactive power outputs can be obtained.

2.3.2 Thermal Loading

2.3.2.1 Thermal Model

The power losses dissipated in the power devices lead to junction temperature rise. Thus, an accurate thermal model of the IGBT module is required to transfer power losses into junction temperature fluctuations. In this chapter, an IGBT thermal model based on Foster RC model as shown in Figure 2.1 is developed. The junction temperature of the IGBT unit $T_{j,IG}$ can be calculated as follows:

$$T_{j,IG} = Z_{th,IG(j-c)} \times P_{IG}^{loss} + T_c \tag{2.20}$$

$$T_c = Z_{th(c-h)} \times (P_{IG}^{loss} + P_D^{loss}) + T_h \tag{2.21}$$

$$T_h = Z_{th(h-a)} \times (P_{IG}^{loss} + P_D^{loss}) + T_a \tag{2.22}$$

where T_c and T_h denote the temperatures of the case and heatsink of the IGBT module, respectively, and T_a denotes the ambient temperature, $Z_{th(j-c)}$, $Z_{th(c-h)}$ and $Z_{th(h-a)}$ are the thermal impedances from junction to case, from case to heatsink and from heatsink to ambient, respectively. The junction temperature of the IGBT unit can be obtained by:

$$T_{j,IG} = Z_{th,IG(j-c)} \times P_{IG}^{loss} + \left(Z_{th(c-h)} + Z_{th(h-a)}\right) \times \left(P_{IG}^{loss} + P_D^{loss}\right) + T_a. \tag{2.23}$$

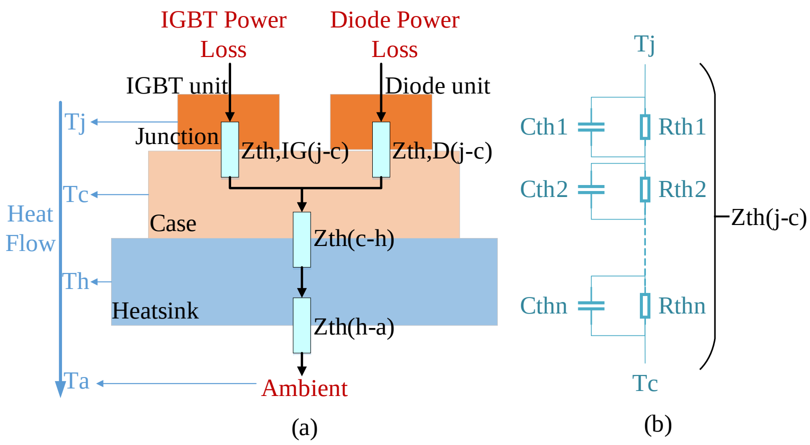

Figure 2.1 IGBT thermal model. (a) Thermal structure of an IGBT module. (b) Foster RC thermal model.

Similarly, the junction temperature of the diode unit $T_{j,D}$ can be calculated as:

$$T_{j,D} = Z_{th,D(j-c)} \times P_D^{loss} + \left(Z_{th(c-h)} + Z_{th(h-a)}\right) \times \left(P_{IG}^{loss} + P_D^{loss}\right) + T_a. \tag{2.24}$$

Note that the thermal capacitances in the applied thermal model only lead to fast thermal changes in time constants of milliseconds to seconds. For the long-term thermal analysis, the thermal capacitances can be ignored, and only the thermal resistances are taken into consideration [72].

2.3.2.2 Ambient Temperature Profile

Conventional reliability analysis usually focuses on the thermal loading and lifetime assessment under simple external conditions where the ambient temperature is assumed constant, which is not practical. Besides, it can be seen from (2.23) and (2.24) that the ambient temperature directly impacts on the IGBT and diode junction temperature. Thus, it is essential to have an accurate mission profile of ambient temperature for thermal loading analysis. Mission profiles of real-field ambient temperature are representative and often used for thermal loading analysis [86]. This chapter applies an extensive real-field ambient temperature data for the long-term thermal loading analysis.

2.3.2.3 Thermal Cycling Interpretation

Due to irregular characteristics of the mission profiles, i.e., long-term PV outputs and ambient temperature, the obtained junction temperature profiles cannot follow repetitive patterns in terms of amplitude and duration. Thus, this chapter applies a Rainflow counting method [69], which is a widely used cycle counting technique for stress analysis, to interpret the irregularly varying thermal loading into regulated thermal cycles. As a result, junction temperature variation ΔT_j, mean junction temperature T_{jm} and cycle heating period t_{on} of each regulated thermal cycle can be extracted for further lifetime estimation.

2.3.2.4 Lifetime Estimation

Coffin-Manson model can be used for lifetime estimation of the power devices inside the inverters [70]. This model mainly describes the impact of the junction temperature variation ΔT_j on the lifetime, and it can be expressed as follows:

$$N_f = A \times (\Delta T_j)^{\alpha} \tag{2.25}$$

where N_f denotes the number of cycles to failure under the given ΔT_j, and A and α are constant coefficients.

The Coffin-Manson model is modified in [71] by adding the impact of the mean junction temperature T_{jm}, as:

$$N_f = A \times (\Delta T_j)^{\alpha} \times \exp\left(\frac{E_a}{k_B \times T_{jm}}\right) \tag{2.26}$$

where k_B is Boltzmann constant ($8.617 \times 10^{-5} eV \cdot K^{-1}$), and E_a denotes the activation energy, which is derived from extensive accelerated lifetime tests [87].

Furthermore, it is indicated in [88] that the thermal cycle heating period t_{on} can also significantly impact on the lifetime of the power devices.

On the other hand, lifetime models which are built on extensive lifetime test results done by the device manufacturers, are also widely adopted for lifetime estimation [72]. Thus, to consider the impacts of ΔT_j, T_{jm} as well as t_{on}, this chapter proposes a modified lifetime model, combining the modified Coffin-Manson model in (2.26) and the manufacturer's application model in [89], as:

$$N_f = A \times (\Delta T_j)^{\alpha} \times \exp\left(\frac{E_a}{k_B \times T_{jm}}\right) \times \left(\frac{t_{on}}{t_{nom}}\right)^{-0.3} \tag{2.27}$$

where t_{nom} denotes the nominal cycle heating period, which is equal to 1.5 s. It is worth noting that the typical range of t_{on} adopted in [89] is from 0.1 s to 60 s. If used for longer cycles, the approximation can be applied based on the assumption that viscoplastic deformation saturates for time larger than 60 s.

Thus, N_f regarding certain ΔT_j, T_{jm} and t_{on} of each regulated cycle through the Rainflow counting is calculated by using (2.27). With the obtained N_f at each regulated cycle, Miner's rule [90] is applied to calculate the accumulated lifetime consumption LF_C of one mission profile duration T_{mp}, as:

$$LF_C = \sum_i \frac{n_i}{N_{fi}} \tag{2.28}$$

where i denotes the cycle number, n_i denotes the number of cycles accumulated for a certain ΔT_j, T_{jm} and t_{on}, and N_{fi} denotes the corresponding number of cycles to failure for the certain ΔT_j, T_{jm} and t_{on}. Thus, the final estimated lifetime of the IGBT modules can be obtained as:

$$LF = \frac{T_{mp}}{LF_C}. \tag{2.29}$$

2.4 Case Study

2.4.1 Test System and Parameter Settings

In this chapter, a 33-bus radial distribution network [91] is used to verify the proposed operational reliability assessment approach. This chapter considers a high PV penetration case where 10 PV based VPPs are allocated at buses 6, 10, 13, 16, 17, 18, 21, 22, 25 and 30. Each VPP contains 100 individual PV systems of 5 kW and has the total PV power generation capacity of 500 kW. It is assumed that the inverter of each individual PV system is oversized by 10% to 5.5 kVA so as to provide more available reactive power compensation. The network topology with the VPPs is shown in Figure 2.2. In this test, $V_0 = 1\mathrm{p.u.}$, and the allowed bus voltage range $[\underline{V}_i, \overline{V}_i] = [0.95, 1.05]\mathrm{p.u.}$, the VVC dispatch interval is set at 1 hour, and the mission profile duration T_{mp} is one year. This chapter assumes that all the inverters in a VPP share the same reactive power output amounts during each dispatch interval. It is also assumed that the network covers a relatively small area where the solar irradiance and the ambient temperature are identical at all the buses.

In this test, a 650-V/75-A IGBT module is used as the power device of the PV inverters. Parameters of this IGBT module can be found in [92]. PWM modulation rate m is set as 0.8, and switching frequency f_{sw} is 20 kHz. In this chapter, according to [71], [89] and [93], the activation energy E_a is set as $0.8eV$, and A and α are set as 4400 and –6.68, respectively.

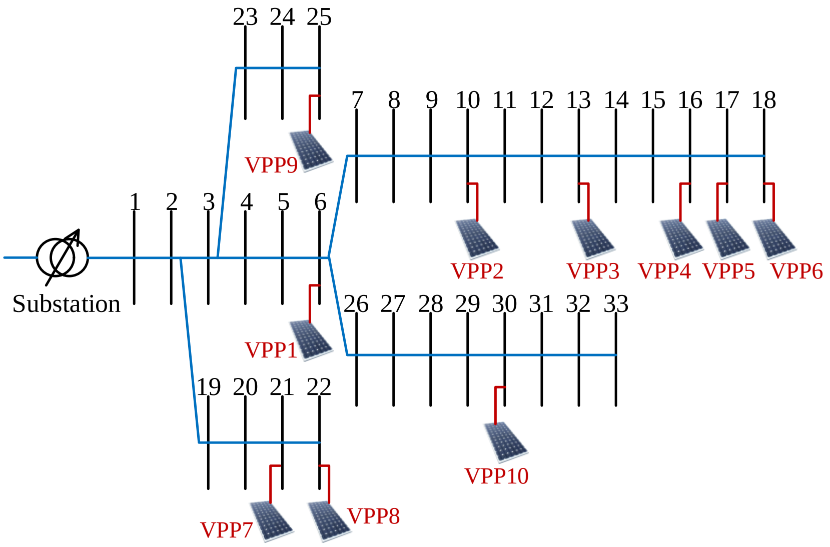

Figure 2.2 Network topology of the test system.

Note that other systems, inverters and power devices can also be used without affecting the efficiency of the proposed operational reliability assessment approach.

2.4.2 VVC Model Simulation

In this chapter, firstly, the PV power generation scenarios are constructed by the MCS with the Gaussian PDF based on historical solar irradiance profiles and the load scenarios are based on data of the IEEE Reliability Test System-1996 [94]. Then, the proposed inverter based VVC problem is solved by the stochastic optimisation method (objective (2.10) subject to (2.2)-(2.8), (2.11)). The hourly dispatch results of each VPP for the whole year can be obtained. The inverter reactive power outputs of the VPPs 1, 4 and 10 are shown in Figure 2.3. It is worth noting that positive values mean the VPP is injecting reactive power into the network while negative values for absorbing reactive power.

It can be seen that VPPs 1 and 10 are injecting reactive power the whole year, while VPP 4 is reducing reactive power injection and even absorbing reactive power during the midday peak PV generation periods.

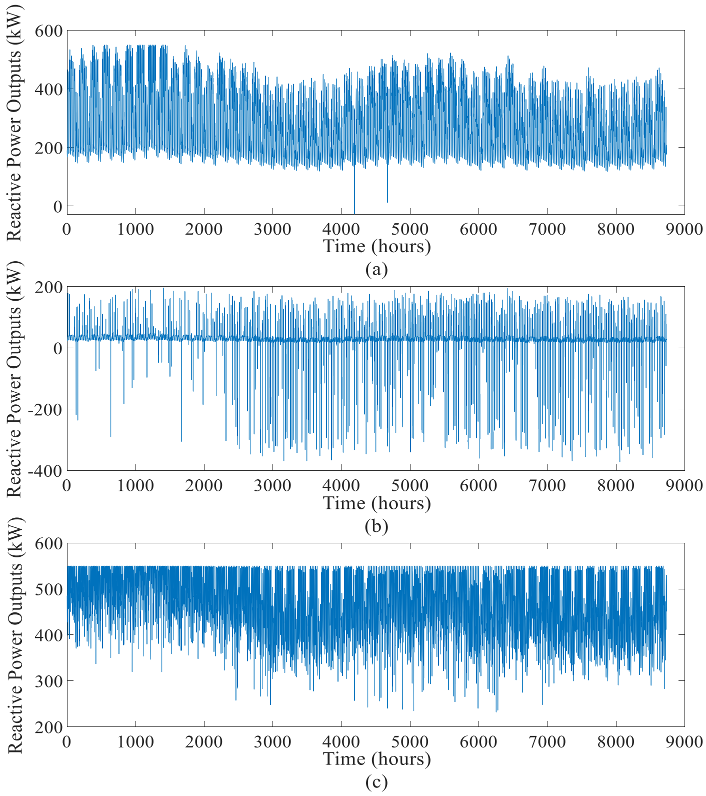

Figure 2.3 One-year reactive power outputs of (a) VPP 1; (b) VPP 4; (c) VPP 10.

2.4.3 Thermal Loading and Cycling Results

To conduct the thermal loading analysis of inverters, a one-year mission profile of PV power generation and ambient temperature is needed. It is worth noting that the PV active power generation is based on the constructed PV output scenarios in the VVC model and the ambient temperature is based on the one-year hourly real-field data of Los Angeles from December 2016 to November 2017 [95].

With the mission profile, by applying the thermal model developed in Chapter 2.3.2, the IGBT junction temperature profiles of the VPPs can be obtained, which are shown in Figure 2.4. Junction temperature profiles without the VVC function are also obtained and shown for comparison in this figure. It can be seen that the junction temperatures of the IGBT modules increase due to the implementation of the VVC function. Moreover, VPP 10 has the largest temperature rise, but its temperature variation is smaller than that without the VVC function.

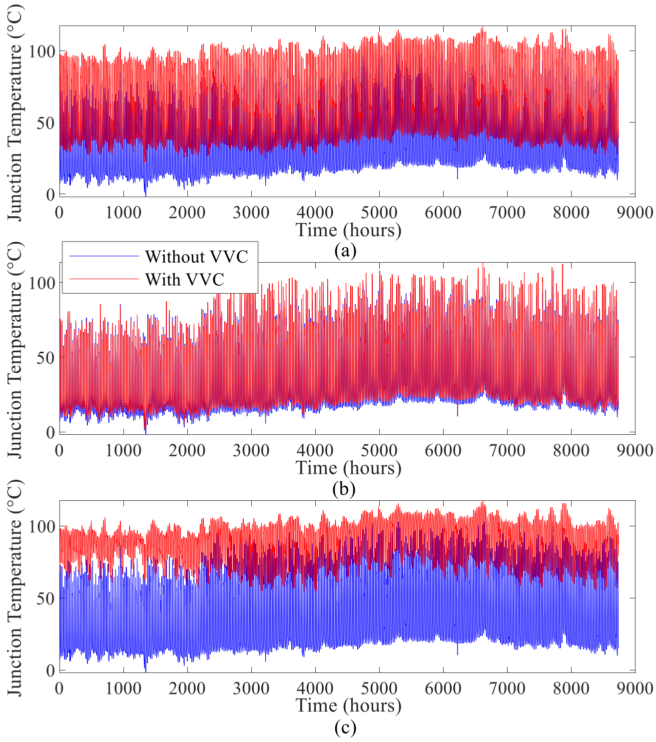

Figure 2.4 One-year junction temperature profiles of the IGBT modules of (a) VPP 1; (b) VPP 4; (c) VPP 10.

These junction temperature profiles can be further interpreted by the Rainflow counting method. It is worth noting that the junction temperature Rainflow counting results of all the VPPs are identical when not used for VVC function, due to the same mission profiles of PV power generation and ambient temperature at all buses. Taking the thermal loading of the IGBT modules in VPP 4 as an example, a total number of 4632 regulated thermal cycles are identified when used for the VVC function, and the corresponding ΔT_j, T_{jm} and t_{on} of each regulated cycle are obtained. Figure 2.5 gives the Rainflow counting results of VPPs 1, 4 and 10 with and without the VVC function, which indicate the variations of ΔT_j and T_{jm} under the VVC case.

Figure 2.6 gives a two-dementional demonstration of ΔT_j and T_{jm} to represent the difference between cases with and without VVC function. It can be seen that the implementation of VVC increases the mean junction temperature of VPPs 4 and 10, as well as the junction temperature variation of VPP 4. However, the jucntion temperature variation of VPP 10 is decreased.

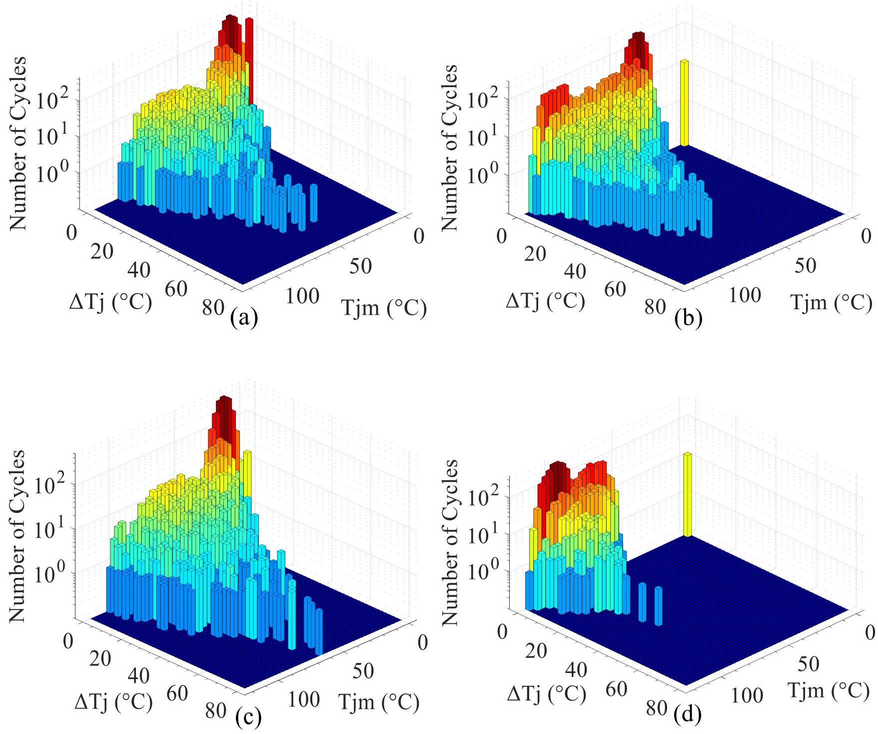

Figure 2.5 Rainflow counting results of (a) VPPs without VVC; (b) VPP 1 with VVC; (c) VPP 4 with VVC; (d) VPP 10 with VVC.

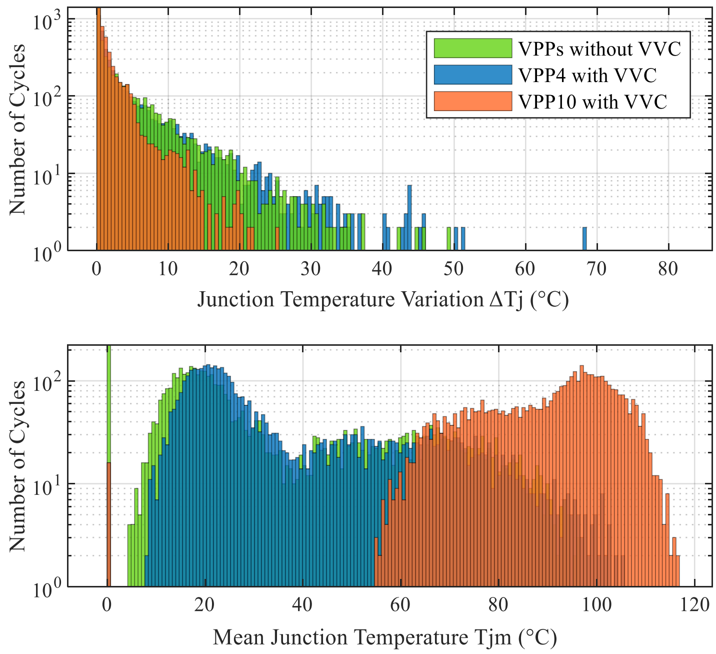

Figure 2.6 Comparison of results of VPPs 4 and 10 under VVC case.

2.4.4 Lifetime Estimation Results

With the Rainflow counting results, the estimated lifetime of the IGBT modules inside the PV inverters can be obtained by (2.27)-(2.29). Without the VVC function, the lifetime of all the inverters is calculated as a uniform 40.8 years, due to the identical mission profiles of PV active power outputs and ambient temperature. The estimated lifetime of all the inverters when used for the VVC function has been given in Table 2-I. Furthermore, the lifetime reduction percentages are also calculated and shown in the table. The negative percentages mean the lifetime increment rates.

Table 2-I Estimated Lifetime of Inverters

VPP No.	**1**	**2**	**3**	**4**	**5**
Lifetime (years)	21.3	50.5	12.1	7.1	10.2
Reduction Percentage	47.8%	-23.8%	70.3%	82.6%	75%

VPP No.	**6**	**7**	**8**	**9**	**10**
Lifetime (years)	9.6	47.2	33.5	21	296.1
Reduction Percentage	76.5%	-15.7%	17.9%	48.5%	-625.7%

The implementation of the inverter based VVC model reduces the lifetime of the inverters in VPPs 1, 3, 4, 5, 6, 8 and 9, whereas the other inverters have longer lifetime than that without the VVC function. It is worth noting that the inverters in VPP 4 have largest lifetime reduction, about 82.6% lifetime degradation, but the lifetime of the inverters in VPP 10 increases by about 6.3 times when used for the VVC function.

The Rainflow counting results of VPP 4 indicate larger mean junction temperature and junction temperature variation when used for the VVC function, which leads to significantly shortened lifetime. However, as for VPP 10, the junction temperature profile and the Rainflow counting results show that the implementation of the VVC function raises the mean junction temperature but reduces the junction temperature variation. This leads to the longer lifetime, indicating that in this simulation case, the lifetime degradation caused by junction temperature variation is larger than that by mean junction temperature.

In this test, the VVC reactive power output results are mainly impacted by the settings of network topology as well as the locations of VPPs. As for VPPs 4, 5 and 6, they have short lifetime. This is because they are densely located at the feeder end, and they need to absorb reactive power at peak power generation hours, which leads to significantly varying junction temperature. For VPP 10, it is the only VPP at its own feeder, so that it needs to constantly provide reactive power injection to the network. This leads to high mean junction temperature with low temperature variation, and then eventually leads to the extended lifetime. Thus, the simulation results provide useful insights on the impacts of VPP location on the inverter lifetime.

2.4.5 Reliability Assessment with Different Oversizing Rates

This subchapter aims to explore the impacts of inverter oversizing rate on the inverter lifetime when used for the VVC function. Herein, the 5% and 20% inverter oversizing rates are also applied in the proposed VVC model. Note that other parameter settings are kept the same during the VVC optimisation and reliability assessment processes. The simulation results regarding the different oversizing rates are given in Table 2-II.

Table 2-II Inverter Lifetime (Years) With Different Oversizing Rates

Oversizing Rate	VPP No.				
	1	2	3	4	5
5%	48.2	25.8	12.8	13.1	15.2
10%	21.3	50.5	12.1	7.1	10.2
20%	3.4	56.8	7.4	3.6	5.2
Oversizing Rate	**VPP No.**				
	6	**7**	**8**	**9**	**10**
5%	9.6	43.9	35.6	17.4	656.2
10%	9.6	47.2	33.5	21	296.1
20%	9.8	48.1	33.5	16.8	97.4

It can be seen that the inverters' lifetime has high correlation with the oversizing rate. The lifetime of inverters in VPPs 1, 3, 4, 5 and 10 is decreased with the increasing oversizing rate. This indicates the oversizing of inverters at these buses has direct impacts on their reactive power output results during VVC process, which leads to high junction temperature variation or high mean junction temperature. Lifetime of inverters in VPPs 6, 7, 8 and 9 has minor changes, indicating the oversizing has less impacts on their VVC results. It is worth noting that there is a notable increase of inverter lifetime in VPP 2. Through analysis of the VVC simulation results, it is found that the reactive power outputs in VPP 2 are actually reduced due to the increased outputs of the oversized inverters at other buses.

It can be concluded that during VVC implementation, the inverter oversizing rate can have significant impacts on the inverter reliability and lifetime. The inverter oversizing is expected to be optimised considering the inverter reliability assessment in future works.

2.5 Conclusion

This chapter proposes an operational reliability assessment approach of PV inverters considering the VVC function. In this approach, with inverter based VVC results under the uncertainties, a power loss model and a thermal loading model of the inverter power devices are developed. Then, a modified lifetime estimation method based on the Coffin-Manson model is proposed. This approach is verified on a 33-bus radial distribution network.

The simulation results indicate that the implementation of the VVC function increases mean junction temperature but may decrease junction temperature variation, which may lead to positive or negative impacts on the lifetime of the power devices. Moreover, reliability assessment considering different inverter oversizing rates is conducted, which demonstrates high correlation between the inverter oversizing and its reliability. Thus, impacts of the VVC function on the inverter lifetime are expected to be considered with additional reliability constraints in the VVC optimisation model, aiming to achieve a trade-off between VVC performance and inverter long-term reliability.

Chapter 3 PV INVERTER RELIABILITY-CONSTRAINED VOLT/VAR CONTROL OF DISTRIBUTION NETWORKS WITH INVERTER APPARENT POWER RESTRICTION

Chapter 2 develops a PV inverter reliability assessment approach under the VVC function, reveals the close relationship between VVC functions and associated inverter lifetime, and provides insights that a properly designed VVC function can have positive impacts on PV inverter reliability via successfully containing the thermal stress of PV inverters. Following this thread, this chapter proposes a PV inverter reliability-constrained VVC method of distribution networks under uncertainties. Firstly, compared to Chapter 2, a more comprehensive reliability analysis procedure for PV inverters is developed to estimate the lifetimes of both the power device and the DC-link capacitor inside inverters. Secondly, considering the impacts of VVC on PV inverter reliability, reliability constraints are proposed based on regulation of inverter apparent power and application of a PV curtailment scheme, and a restriction factor is proposed to realise different restriction levels for analysis. Thirdly, a multi-objective PV inverter reliability-constrained VVC optimisation model is proposed, which aims to minimise the network power loss and PV curtailed power, simultaneously. Accordingly, the nonconvex model is relaxed by a second-order cone programming method, and the uncertainties such as PV power generation and loads are addressed by a scenario-based stochastic optimisation method. The proposed VVC method is tested on the 33-bus and 69-bus distribution networks, and the simulation results verify high efficiency of the proposed method in network energy loss reduction and inverter reliability enhancement.

3.0 Nomenclature

A. Sets and Indices

B	Set of network branches.
i	Index of IGBT thermal cycles.
$j,\ k,\ l$	Index of network buses.

$J(k)$	Set of parent buses of bus k.
K	Set of network buses.
$L(k)$	Set of child buses of bus k.
n	Index of capacitor ripple current frequencies.
SC, sc	Set and index of uncertainty scenarios.
T, t	Set and index of operating time intervals.

B. Parameters

1) PV Inverter Parameters

$E_{on,nom}$,$E_{off,nom}$	Nominal single-pulse turn-on and turn-off energy loss of IGBT unit (J).
$E_{rec,nom}$	Nominal single-pulse reverse recovery energy loss of diode unit (J).
$ESR(f_n)$	Equivalent series resistance of capacitor under frequency f_n (Ω).
f_{sw}	Switching frequency (Hz).
H_b	Base lifetime of capacitor (hours).
i_P, u_P	Output sinusoidal current and voltage amplitude (A,V).
I_{nom},V_{nom}	Nominal current and voltage of IGBT module (A,V).
m	PWM modulation rate.
P_{IG}^{loss}	Power loss on IGBT unit (W).
P_{D}^{loss}	Power loss on reverse recovery diode unit (W).
P_{CA}^{loss}	Power loss on DC-link capacitor (W).
$R_{th(co-a)}$	Capacitor thermal resistance from core to ambient (K/W).
T_a	Ambient temperature (K).
T_{co}	Capacitor core temperature (K).
T_j, T_c, T_h	IGBT junction, case and heatsink temperature (K).
T_m	Maximum rated core temperature of capacitor (K).
V_{AC}	AC voltage RMS value (V).
V_{DC}	Applied DC-link voltage (V).
V_{CE0},r_{CE}	Zero-current on-state collector-emitter voltage and on-state collector-emitter

resistance of IGBT unit (V, Ω).

V_{D0},r_D Zero-current on-state voltage drop and on-state resistance of diode unit (V, Ω).

V_{DCr} Rated DC voltage of capacitor (V).

$Z_{th(j-c)}$ IGBT thermal impedance from junction to case (K/W).

$Z_{th(c-h)}$ IGBT thermal impedance from case to heatsink (K/W).

$Z_{th(h-a)}$ IGBT thermal impedance from heatsink to ambient (K/W).

φ Phase difference between PWM modulation signal and inverter current (rad).

2) Network Parameters

I_{jk}^{cap} Current capacity of the branch line from bus j to bus k (A).

$P^{net,loss}$ Network power loss on branch lines (W).

$P^{curt,loss}$ Power loss on PV curtailment (W).

r_{jk}, x_{jk} Resistance/Reactance of the branch line from bus j to bus k (Ω).

S_k^{cap} Inverter apparent power capacity at bus k (VA).

$\underline{V}_k$, $\overline{V}_k$ Lower and upper limits of voltage at bus k (p.u.).

δ Restriction factor for inverter apparent power.

C. Variables

$I_{jk,t}$, $i_{jk,t}$ Current and its square value of the branch line from bus j to bus k at time t (A,A^2).

$P_{jk,t}$,$Q_{jk,t}$ Active/Reactive power through the branch line from bus j to bus k at time t (W,var).

$P_{k,t}^L$, $Q_{k,t}^L$ Uncertain active/reactive load at bus k at time t (W,var).

$P_{k,t}^{PV}$, $Q_{k,t}^{inv}$ Scheduled inverter active/reactive power output at bus k at time t (W,var).

$P_{k,t}^{PV,a}$ Actual PV active power output at bus k at time t (W).

$P_{k,t}^{PV,c}$ PV curtailed active power at bus k at time t (W).

$P_{k,t}^{PV,m}$ Uncertain PV MPPT power generation at bus k at time t (W).

$S_{k,t}$ Inverter apparent power output at bus k at time t (VA).

$V_{k,t}$, $v_{k,t}$ Voltage and its square value of bus k at time t(p.u.).

ρ Occurrence probability of uncertainty scenarios.

3.1 Introduction

In recent years, with the advance of photovoltaic (PV) technologies, the penetration of PV systems is having an unprecedentedly fast growth. It is reported by [2] that by the end of 2021, there are over 3 million rooftop PV systems installed in Australia. The wide utilisation of PV energy is beneficial to the construction of a cost-efficient, low-carbon and sustainable power system. However, it also brings about challenges, especially to the voltage regulation and control in distribution networks. The work [96] points out that the main challenge of renewable energy integration is associated with the power generation intermittency and volatility. It is indicated in [41] that the stochastic characteristics of PV power generation can lead to fast and dramatic voltage fluctuations. Moreover, the voltages at the buses with high PV levels tend to rise beyond the limit during peak power generation hours, impairing the power quality [13].

To address these issues, volt/var control (VVC) acts as an effective method for voltage regulation and power loss minimisation in distribution networks. Conventionally, on-load tap changers (OLTCs) and capacitor banks (CBs) are utilised in the VVC methods, to provide adjustable and reliable voltage regulation and reactive power compensation support. The work [33] proposes a coordinative approach of OLTCs and static var compensators for optimal voltage regulation in distribution networks. A two-loop hybrid method for optimal sizing and placement of CBs in distribution networks is proposed in [36]. However, these conventional devices are mechanically operated and cannot respond fast enough to address rapid voltage variations due to the uncertain and intermittent PV power generation [43].

On the other hand, PV inverters are power electronic devices which can provide fast and flexible reactive power support. Besides, PV inverters can be controlled to curtail the PV power generation to further mitigate the voltage rise when necessary. IEEE 1547.8 working group has advocated the utilisation of PV inverters for VVC implementation [47]. Electric Power Research Institute has also been updating protocols of PV inverter operating modes for network voltage regulation [48]. Furthermore, according to [46], a properly oversized PV inverter can efficiently increase its reactive power capacity, and the additional costs can be offset by reducing the investment of traditional CBs. With the advantages of PV inverters for reactive power compensation and PV curtailment in distribution networks, advanced inverter-based VVC schemes considering uncertainties have been proposed. A two-stage centralised VVC model is proposed in [49], which optimally selects PV inverters for VVC function and then dispatches reactive power in active distribution networks. Considering real-time uncertain network operating conditions, ref. [42] proposes a hierarchically coordinated VVC model, which coordinatively optimises central dispatch setpoints of PV inverters for network power loss minimisation and local droop control functions for real-time voltage regulation. In [97], a two-stage robust reactive power optimisation method against uncertainty of renewable power generation is proposed. The work [53] proposes a distributed inter-phase coordinative VVC method considering unbalanced PV integration in three-phase distribution networks. A local two-layer real-time adaptive VVC method is proposed in [98], which can dynamically adapt its droop control function to enhance performance under system disturbances. In addition, a three-stage robust inverter-based VVC model is developed in [52], which coordinates three different control stages of slow scheduling of OLTCs and CBs, fast dispatching of inverter base outputs and local control on inverters. In [60], a multi-objective adaptive VVC model is proposed to minimise both network power loss and bus voltage deviations. Furthermore, a distributed online VVC method coordinating PV curtailment to achieve efficient voltage regulation and power loss reduction is proposed in [50]. Different control methods are presented in the above literature to highlight the advantages and remarkable potentials of utilising PV inverters for system voltage regulation. However, there is still one practical concern for the implementation of inverter-based VVC functions, i.e., the reliability of PV inverters.

PV inverters are the key devices for var compensation in inverter-based VVC methods. Besides, they are responsible for converting active power generated from PV panels, as a basic function. Thus, the operational reliability of PV inverters is a crucial factor to ensure both reliable VVC support and PV power generation. Ref. [62] indicates that PV inverters are the most vulnerable subsystems in PV systems due to their complexity in both the physical structure and operating conditions. Study in [61] indicates that compared to other components in PV systems, PV inverters have much shorter lifetime which is usually less than 15 years. Moreover, significant lifetime degradation is identified in [67], if a PV inverter is used to provide reactive power support at night. Thus, the additional utilisation of PV inverters for VVC functions may seriously affect the PV inverter reliability, leading to shortened lifetime and poor economic results. In this regard, it is imperative that the PV inverter reliability is systematically considered, analysed and modeled in VVC methods. However, in the existing literature, such a problem has not been investigated.

To conduct inverter reliability analysis, it is important to understand the inverter failure mechanisms. According to [65], the power devices, e.g., insulated gate bipolar transistors (IGBTs) and metal-oxide-semiconductor field-effect transistors (MOSFETs), as well as the DC-link capacitor, are the two most fragile components inside an inverter, and their lifetime is a predominant factor for inverter reliability. Besides, for both the power devices and DC-link capacitors, their lifetime is critically affected by their thermal status, i.e., the junction temperature cycling of power devices and the core temperature of DC-link capacitors [66]. The thermal status is subject to power losses dissipated on the devices. Thus, the power loss modeling and thermal analysis of the power devices and the DC-link capacitors play a key role in inverter lifetime estimation. Furthermore, lifetime models are required for lifetime estimation. Regarding the power devices, a Coffin-Manson model [70] which describes the impact of junction temperature variation on lifetime can be used; a modified Coffin-Manson model is proposed in [71], by adding the impact of junction temperature mean values; moreover, lifetime models provided by manufacturers, which are based on intensive power cycling tests, can also be used for lifetime estimation [72]. For DC-link capacitors, the lifetime models regarding different device types can be found in [73], and those from manufacturers [74] can also be used. Thus, with the above reliability analysis models, the inverter lifetime can be calculated. However, due to the complexity of the above models, the inverter reliability analysis methods cannot be directly involved in the VVC optimisation model.

According to the above literature review, two unsolved problems can be identified: 1) the existing inverter-based VVC methods do not consider the inverter reliability issues; 2) the existing inverter reliability analysis models cannot be directly used in VVC optimisation models for lifetime improvement purpose. To solve these problems, this chapter develops the inverter reliability constraints via a full inverter reliability analysis process, and further proposes a multi-objective PV inverter reliability-constrained VVC optimisation model which can guarantee improved inverter lifetime.

The main contributions of this chapter are as follows.

1) A full PV inverter reliability analysis procedure is developed to estimate the lifetime of power devices and DC-link capacitor inside inverters. With this procedure, the impacts of VVC on inverter lifetime can be quantified.

2) New constraints modeling inverter reliability are proposed, which are used to ensure inverter lifetime commitment by utilising a restriction factor to regulate inverter apparent power output.

3) A multi-objective PV inverter reliability-constrained VVC optimisation model with PV curtailment is proposed, to minimise the network power loss and PV curtailed power under uncertainties, while guaranteeing long inverter lifetime.

The rest of this chapter is organised as follows: Chapter 3.2 describes a PV inverter reliability analysis process and analyses the impact of VVC on the inverter lifetime; then, in Chapter 3.3, inverter reliability constraints are developed and a multi-objective reliability-constrained VVC optimisation model is proposed; case studies are conducted in Chapter 3.4 to validate the proposed reliability constraints and VVC method; last, conclusions and future works are given in Chapter 3.5.

3.2 Reliability Analysis of PV Inverters

3.2.1 Single-Phase Grid-Connected PV Inverter

Single-phase grid-connected PV inverters are widely used in small-scale PV systems, especially residential rooftop PVs. The schematic of a typical two-stage single-phase full-bridge grid-connected PV inverter is shown in Figure 3.1.

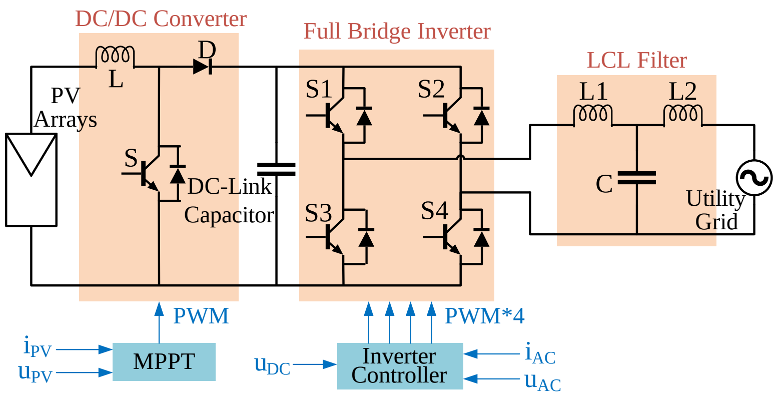

Figure 3.1 Schematic diagram of a single-phase two-stage full-bridge grid-connected PV inverter.

A DC/DC converter is applied at the first stage to conduct the maximum power point tracking (MPPT). Then, a full-bridge inverter is placed at the second stage to complete power conversion from DC to AC. A DC-link capacitor is paralleled between the converter and the inverter to efficiently arrest multi-frequency harmonics and stabilise DC-link voltage. The inductor-capacitor-inductor (LCL) filter is usually utilised before connection to the grid to reduce current harmonics and smooth voltage output.

3.2.2 Reliability Analysis Process

In this chapter, reliability analysis will be applied for the components in the inverter including the power devices (S1-S4) and the DC-link capacitor as shown in Figure 3.1. In addition, IGBTs and an aluminum electrolytic capacitor are used as the power devices and the DC-link capacitor, respectively.

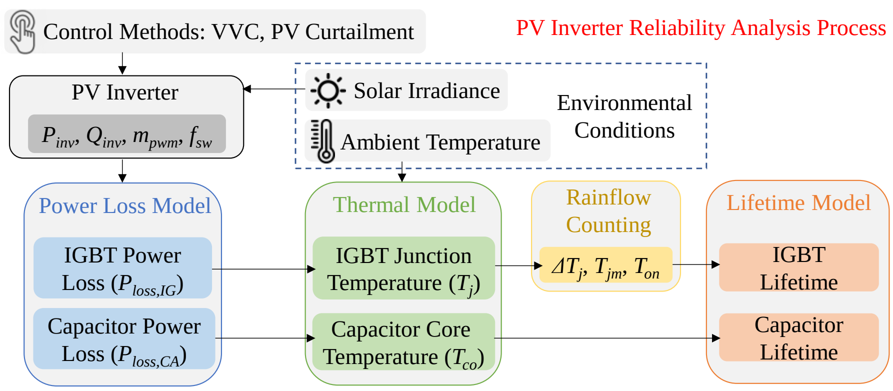

Figure 3.2 PV inverter reliability analysis process.

The reliability analysis process is demonstrated in Figure 3.2. Firstly, with the PV inverter power outputs (P_{inv}, Q_{inv}) and modulation parameters (m_{pwm}, f_{sw}), the power losses dissipated on the IGBTs ($P_{loss,IG}$) and the capacitor ($P_{loss,CA}$) are calculated by their power loss models. Secondly, the junction temperature of IGBTs (T_j) and the core temperature of capacitor (T_{co}) are computed by their thermal models with the obtained power losses. Then, a thermal cycle interpretation technique, i.e., the Rainflow counting technique, is used to transfer the irregular junction temperature profile into useful information (ΔT_j, T_{jm}, T_{on}). Last, the IGBT and capacitor lifetime models are applied to obtain their estimated lifetime.

3.2.3 Reliability Models of IGBT Module

3.2.3.1 Power Loss Model

An IGBT module consists of the IGBT unit and the reverse recovery diode unit. The power loss of IGBT unit P_{IG}^{loss} contains conduction loss $P_{IG,con}^{loss}$ and switching loss $P_{IG,sw}^{loss}$, which can be calculated by the following equations.

$$P_{IG}^{loss} = P_{IG,con}^{loss} + P_{IG,sw}^{loss} \tag{3.1}$$

$$P_{IG,con}^{loss} = \left(\frac{1}{2\pi} + \frac{m\cos\varphi}{8}\right) V_{CE0} i_P + \left(\frac{1}{8} + \frac{m\cos\varphi}{3\pi}\right) r_{CE} {i_P}^2 \tag{3.2}$$

$$P_{IG,sw}^{loss} = \frac{f_{sw}}{\pi}\left(E_{on,nom} + E_{off,nom}\right)\frac{i_P V_{DC}}{I_{nom} V_{nom}} \tag{3.3}$$

Here, i_P denotes the inverter output sinusoidal current amplitude, V_{CE0} denotes the IGBT zero-current on-state collector-emitter voltage and r_{CE} denotes the IGBT on-state collector-emitter resistance. m is the PWM modulation rate and φ is the phase difference between modulation signal and inverter output current. Moreover, f_{sw} is the switching frequency and V_{DC} is the applied DC-link voltage. $E_{on,nom}$ and $E_{off,nom}$ are the IGBT nominal single-pulse turn-on and turn-off energy losses under nominal current I_{nom} and nominal voltage V_{nom}.

The reverse recovery diode unit conducts on the other half cycle. With the diode zero-current on-state voltage drop V_{D0}, on-state resistance r_D and nominal single-pulse reverse recovery energy loss $E_{rec,nom}$, its power loss P_D^{loss} can also be obtained. Detailed diode power loss model can be found in [99].

3.2.3.2 Thermal Model

The thermal model of an IGBT module is shown in Figure 3.3. The power losses generated from the chips are dissipated through each layer into the ambient, causing different temperature levels. The temperature of each layer can be calculated as follows.

$$T_{j,IG} = Z_{th,IG(j-c)} P_{IG}^{loss} + T_c \tag{3.4}$$

$$T_c = Z_{th(c-h)} \left(P_{IG}^{loss} + P_D^{loss} \right) + T_h \tag{3.5}$$

$$T_h = Z_{th(h-a)} (P_{IG}^{loss} + P_D^{loss}) + T_a \tag{3.6}$$

Here, $T_{j,IG}$, T_c and T_h denote the junction temperature of the IGBT unit, case temperature and heatsink temperature of the IGBT module, T_a is ambient temperature. Besides, $Z_{th(j-c)}$, $Z_{th(c-h)}$ and $Z_{th(h-a)}$ are the thermal impedances from junction to case, from case to heatsink and from the heatsink to ambient, respectively. Note that the thermal capacitances C_{th} in Figure 3.3 (b) only account for transient thermal dynamics in terms of milliseconds to seconds. For long-term thermal analysis, only the thermal resistances R_{th} is considered in the thermal model [72].

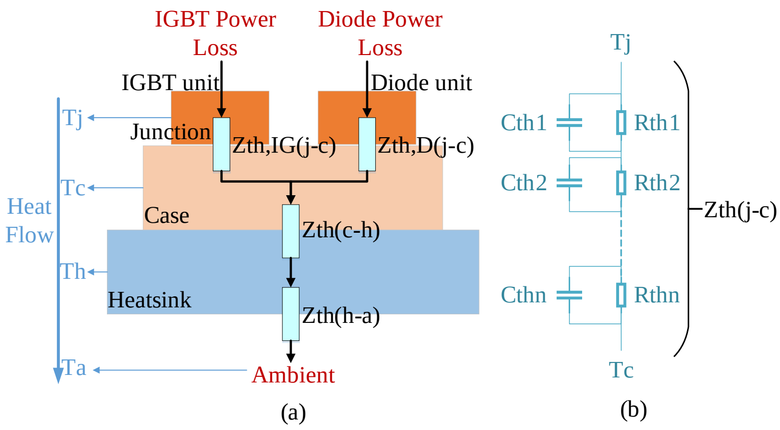

Figure 3.3 IGBT thermal model. (a) Thermal structure of an IGBT module. (b) Foster RC thermal model.

For an IGBT module working in the power inverting mode, the IGBT unit usually has dominant power loss and thus much severer thermal stress than the diode unit [100]. Therefore, in this chapter, it is assumed that the reliability of the IGBT module is mainly dependent on the thermal loading of the IGBT unit.

3.2.3.3 Thermal Cycle Interpretation Technique

Due to the irregular variations of power losses and ambient temperature, the IGBT junction temperature profile may not follow repetitive patterns regarding amplitude and duration. In this chapter, a Rainflow counting technique [69] is applied to transfer the irregularly varying junction temperature profile into regulated thermal cycles. By using this technique, key thermal parameters such as junction temperature variation ΔT_j, mean junction temperature T_{jm} and cycle heating time t_{on} of each cycle can be obtained for further lifetime estimation.

3.2.3.4 Lifetime Model

The extracted parameters from the Rainflow counting results can be utilised to calculate the lifetime of the IGBT module. This chapter applies a combined lifetime model based on the improved Coffin-Manson model in [71] and the manufacturing information in [89], as follows.

$$N_f = A \cdot (\Delta T_j)^{\alpha} \cdot \exp\left(\frac{E_a}{k_B \times T_{jm}}\right) \cdot \left(\frac{t_{on}}{t_{nom}}\right)^{-0.3} \tag{3.7}$$

Here, N_f denotes the number of thermal cycles until failure, E_a is activation energy and k_B is Boltzmann constant. In addition, t_{nom} denotes the nominal cycle heating time according to manufacturers' datasheet. A and α are constant coefficients.

Then, N_f of each regulated thermal cycle can be obtained by (3.7). Following the Miner's rule [90], the efforts of each thermal cycle to failure are accumulated linearly and independently. Then, the accumulated lifetime consumption C_{LF} during a specific time horizon TH can be obtained as below.

$$C_{LF} = \sum_{i \in TH} \frac{n_i}{N_{fi}} \tag{3.8}$$

Here, i is the index of thermal cycles in TH, n_i is the number of cycles accumulated for a certain stress level of ΔT_j, T_{jm}, and t_{on}. N_{fi} denotes corresponding cycling number to failure at the stress level. Thus, the final IGBT module lifetime can be computed as follows.

$$LF_{IG} = \frac{TH}{C_{LF}} \tag{3.9}$$

3.2.4 Reliability Models of DC-Link Capacitor

3.2.4.1 Power Loss Model and Thermal Model

The power loss of a DC-link capacitor is mainly affected by the ripple current flowing through the capacitor and its equivalent series resistance (ESR). The power loss can be calculated as follows.

$$P_{CA}^{loss} = \sum_{n} \{[I_{RP}(f_n)]^2 \cdot ESR(f_n)\} \tag{3.10}$$

Here, n is the index of harmonic frequencies of the ripple current on the capacitor. With frequency f_n, $I_{RP}(f_n)$ represents the capacitor ripple current root mean square (RMS) value and $ESR(f_n)$ denotes the capacitor ESR value. For a single-phase inverter, the two main ripple current frequency components on the DC side are twice the fundamental frequency and the switching frequency [101]. Thus, in this chapter, it is assumed that only the ripple currents at these two frequency levels contribute to the power loss.

The RMS value of ripple current with the frequency that is twice the fundamental frequency can be calculated as below.

$$I_{RP}(f_1) = \frac{u_P i_P}{2\sqrt{2}V_{DC}} \tag{3.11}$$

Here, u_P and i_P are the inverter output voltage and current amplitudes, respectively, and V_{DC} is the applied DC-link voltage. The ripple current with the switching frequency is subject to different modulation schemes, and the detailed calculation method can be found in [102]. The corresponding ESRs under the two frequencies are usually given by manufacturers. Thus, with these parameters, the capacitor power loss can be obtained.

The thermal stress of a capacitor is reflected by its core temperature. Similar to the IGBT thermal model, the core temperature T_{co} of the DC-link capacitor can be calculated as follows.

$$T_{co} = T_a + R_{th(co-a)} P_{CA}^{loss} \tag{3.12}$$

Here, $R_{th(co-a)}$ is the capacitor's thermal resistance from the core to the ambient.

3.2.4.2 Lifetime Model

The operational reliability of capacitors is mainly affected by the operating temperature and DC-link voltage. In this chapter, the lifetime model of the aluminum electrolytic capacitor from [74] is applied to calculate the lifetime of the DC-link capacitor.

$$H_f = H_b \cdot \left(4.3 - 3.3\frac{V_{DC}}{V_{DCr}}\right) \cdot 2^{((T_m - T_{co})/10)} \tag{3.13}$$

Here, H_f denotes the capacitor lifetime (in hours) to failure under the thermal stress level of T_{co} and V_{DC}. H_b is the base lifetime, V_{DCr} is the rated DC voltage and T_m denotes the maximum rated core temperature.

As H_f is calculated for each operation interval based on static thermal loading instead of thermal cycling stress, no cycle counting technique is required. The accumulated lifetime consumption and the final lifetime of the DC-link capacitor can be directly obtained by the Miner's rule, similar to (3.8) and (3.9).

3.2.5 Impacts of VVC on PV Inverter Reliability

The above reliability models indicate high correlation between the inverter thermal status and its output current amplitude i_P. Taking the IGBT module as an example, it can be seen from the power loss models (3.1)-(3.3) that the IGBT power loss presents a quadratic equation of i_P, which means that a higher inverter output current can increase the power loss. Moreover, the IGBT thermal models (3.4)-(3.6) demonstrate a linear relationship between the IGBT junction temperature and the power loss, such that the increased inverter output current can lead to raised junction temperature. Similarly, increment in the inverter output current can increase the DC-link capacitor core temperature. Therefore, it can be concluded that the inverter thermal states, i.e., the IGBT junction temperature and the DC-link capacitor core temperature, are mainly affected by the inverter output current amplitude i_P.

Without the VVC function, the PV inverter only delivers active power generated from PV panels, and i_P can be computed as follows.

$$i_P = \frac{\sqrt{2}P^{PV}}{V_{AC}} \tag{3.14}$$

Here, P^{PV} denotes the PV active power generation and V_{AC} is the inverter AC voltage RMS value.

With the VVC function, the inverter is controlled to provide a reactive power output Q^{inv}. Thus, i_P can be calculated below.

$$S = \sqrt{(P^{PV})^2 + (Q^{inv})^2} \tag{3.15}$$

$$i_P = \frac{\sqrt{2}S}{V_{AC}} \tag{3.16}$$

Here, S represents the apparent power through the inverter.

Therefore, the inverter-based VVC aims to utilise the PV inverters to provide reactive power compensation, which leads to increased inverter apparent power and output current. As a result, the IGBT junction temperature and the DC-link capacitor core temperature increase accordingly. Finally, based on the lifetime models (3.7) and (3.13), the inverter lifetime may be reduced.

Considering this issue, this chapter develops inverter reliability constraints which can keep or even enhance the lifetime of PV inverters, and applies them in the VVC optimisation model for high-PV penetrated distribution networks.

3.3 PV Inverter Reliability Constrained VVC

According to the reliability analysis of PV inverters, this chapter proposes inverter reliability constraints for a multi-objective VVC model. The proposed PV inverter reliability-constrained VVC model aims to guarantee both the inverter lifetime and the VVC performance for power loss reduction.

The PV inverter reliability-constrained VVC is formulated and solved by the following key steps. Firstly, reliability constraints are developed considering inverter apparent power output regulation and PV power generation curtailment. Secondly, a multi-objective PV inverter reliability-constrained VVC optimisation model is proposed to minimise network power losses and PV curtailment. Then, a second-order cone programming method is applied to reformulate the proposed VVC model into a convex optimisation problem. Last, a scenario-based stochastic optimisation method is used to address the uncertainty issues in the VVC optimisation problem.

3.3.1 Reliability Constraints

3.3.1.1 Regulation of Inverter Apparent Power

Chapter 3.2.5 indicates that the VVC function can increase the inverter apparent power output, leading to increased inverter output current, higher component temperature and eventually reduced lifetime. On the other hand, the inverter reliability models in Chapter 3.2, especially the power loss models and lifetime models, contain complex numbers and nonlinear terms. Furthermore, the applied Rainflow counting algorithm in Chapter 3.2.3.3 is a logic-based algorithm which is intractable for mathematical optimisation. Thus, it is difficult to directly incorporate the inverter lifetime or temperature variables into a VVC optimisation problem. Considering the potential impact of the increased inverter apparent power on the inverter lifetime, this chapter proposes a restriction factor δ (in percentage) and reliability constraints, in order to limit the inverter apparent power output $S_{k,t}$, as follows.

$$S_{k,t} \leq \delta \cdot S_k^{cap} \tag{3.17}$$

$$S_{k,t} = \sqrt{\left(P_{k,t}^{PV}\right)^2 + \left(Q_{k,t}^{inv}\right)^2} \tag{3.18}$$

Here, k is the index of network buses, and t is the index of operation time intervals. $P_{k,t}^{PV}$ is the PV active power output and $Q_{k,t}^{inv}$ is the inverter reactive power output. S_k^{cap} is the apparent power capacity of inverter at bus k.

The restriction factor δ can be set to different values to indicate different restriction levels. A high δ means the inverter allows more apparent power output, but it may impair the inverter reliability. On the other hand, a low δ can limit the apparent power output, and thus lead to improved inverter temperature profile for longer lifetime; however, it may affect the inverter VVC capability and the PV power generation.

3.3.1.2 PV Generation Curtailment

Normally, PV inverters operate in the MPPT mode to generate maximal active power. As the restriction factor δ is applied to limit the inverter apparent power output, the circumstance that the PV power output in the MPPT mode is larger than the restricted inverter apparent power level may occur. Under this circumstance, the proposed apparent power regulation method becomes invalid. Thus, to ensure the inverter apparent power output limited by δ, a PV curtailment scheme is applied in the VVC model as below.

$$0 \leq P_{k,t}^{PV} \leq P_{k,t}^{PV,m} \tag{3.19}$$

$$P_{k,t}^{PV,c} = P_{k,t}^{PV,m} - P_{k,t}^{PV} \tag{3.20}$$

Here, $P_{k,t}^{PV,m}$ denotes the MPPT active power output, $P_{k,t}^{PV}$ is the actual PV active power output and $P_{k,t}^{PV,c}$ is the curtailed active power. As a kind of power loss, the curtailed active power is expected to be minimised in the VVC method.

3.3.2 Multi-Objective VVC Optimisation Model

In this chapter, two conflicting VVC objectives are considered, i.e., reduction of power loss in the network and that in the PV curtailment. Thus, this chapter proposes a multi-objective VVC optimisation model with the reliability constraints as follows.

$$\min_{P_{k,t}^{PV}, Q_{k,t}^{inv}} \left(w_1 P^{net,loss} + w_2 P^{curt,loss} \right) \tag{3.21}$$

$$\text{s.t.} \quad P^{net,loss} = \sum_{t \in T} \sum_{j,k \in B} r_{jk} I_{jk,t}^2 \, , \forall jk, t \tag{3.22}$$

$$P^{curt,loss} = \sum_{t \in T} \sum_{k \in K} P_{k,t}^{PV,c} \, , \forall k, t \tag{3.23}$$

$$P_{k,t}^{PV} - P_{k,t}^{L} = \sum_{l \in L(k)} P_{kl,t} - \sum_{j \in J(k)} (P_{jk,t} - r_{jk} I_{jk,t}^2) \, , \forall k, t \tag{3.24}$$

$$Q_{k,t}^{inv} - Q_{k,t}^{L} = \sum_{l \in L(k)} Q_{kl,t} - \sum_{j \in J(k)} (Q_{jk,t} - x_{jk} I_{jk,t}^2) \, , \forall k, t \tag{3.25}$$

$$V_{k,t}^2 = V_{j,t}^2 - 2\left(r_{jk} P_{jk,t} + x_{jk} Q_{jk,t}\right) + (r_{jk}^2 + x_{jk}^2) I_{jk,t}^2, \forall jk, t \tag{3.26}$$

$$I_{jk,t}^2 = \frac{P_{jk,t}^2 + Q_{jk,t}^2}{V_{j,t}^2}, \forall jk, t \tag{3.27}$$

$$\underline{V}_k \leq V_{k,t} \leq \overline{V}_k, \forall k, t \tag{3.28}$$

$$0 \leq I_{jk,t} \leq I_{jk}^{cap}, \forall jk, t \tag{3.29}$$

$$\sqrt{\left(P_{k,t}^{PV}\right)^2 + \left(Q_{k,t}^{inv}\right)^2} \leq \delta \cdot S_k^{cap}, \forall k, t \tag{3.30}$$

$$0 \leq P_{k,t}^{PV} \leq P_{k,t}^{PV,m}, \forall k, t \tag{3.31}$$

$$P_{k,t}^{PV,c} = P_{k,t}^{PV,m} - P_{k,t}^{PV}, \forall k, t \tag{3.32}$$

The objective function (3.21) with weighting factors w_1 and w_2 minimises the total network power loss $P^{net,loss}$ and PV curtailment power loss $P^{curt,loss}$, by optimising $P_{k,t}^{PV}$ and $Q_{k,t}^{inv}$. The power losses in the objective function are calculated by (3.22) and (3.23). Equations (3.24)-(3.27) give the branch flow model which is well established and highly efficient. Herein, j, k and l are the indices of network buses, $J(k)$ and $L(k)$ are the set of parent and child buses of bus k, respectively. Besides, P_{jk}, Q_{jk}, r_{jk}, x_{jk} and I_{jk} denote the active power, reactive power, line resistance, line reactance and current through branch from bus j to bus k. Moreover, P_k^{PV}, Q_k^{inv}, P_k^L, Q_k^L and V_k denote the PV active power, inverter reactive power, active and reactive loads and voltage at bus k. Constraints (3.28) and (3.29) present the limits of bus voltage and branch current. Constraints (3.30)-(3.32) are the proposed reliability constraints for ensuring the lifetime of the inverters.

3.3.3 Second-Order Cone Programming

The proposed VVC optimisation model (3.21)-(3.32) is a non-convex model, and thus this chapter applies an SOCP method to reformulate it into a convex solvable optimisation problem.

Firstly, two variables are introduced to replace $I_{jk,t}^2$ and $V_{k,t}^2$.

$$i_{jk,t} = I_{jk,t}^2 \tag{3.33}$$

$$v_{k,t} = V_{k,t}^2 \tag{3.34}$$

Secondly, (3.24)-(3.26) can be rewritten as below.

$$P_{k,t}^{PV} - P_{k,t}^L = \sum_{l \in L(k)} P_{kl,t} - \sum_{j \in J(k)} (P_{jk,t} - r_{jk} i_{jk,t}), \forall k, t \tag{3.35}$$

$$Q_{k,t}^{inv} - Q_{k,t}^{L} = \sum_{l \in L(k)} Q_{kl,t} - \sum_{j \in J(k)} (Q_{jk,t} - x_{jk} i_{jk,t}), \forall k, t \tag{3.36}$$

$$v_{k,t} = v_{j,t} - 2\left(r_{jk} P_{jk,t} + x_{jk} Q_{jk,t}\right) + (r_{jk}^2 + x_{jk}^2) i_{jk,t}, \forall jk, t \tag{3.37}$$

For constraint (3.27), it can be relaxed into a second-order conic inequality constraint as (3.38) and be further formulated into a standard second-order cone form as (3.39).

$$P_{jk,t}^2 + Q_{jk,t}^2 \leq i_{jk,t} v_{j,t}, \forall jk, t \tag{3.38}$$

$$\left\| \begin{matrix} 2P_{jk,t} \\ 2Q_{jk,t} \\ i_{jk,t} - v_{j,t} \end{matrix} \right\|_2 \leq i_{jk,t} + v_{j,t}, \forall jk, t \tag{3.39}$$

Similarly, constraint (3.30) can also be formulated in a second-order cone form as below.

$$\left\| \begin{matrix} P_{k,t}^{PV} \\ Q_{k,t}^{inv} \end{matrix} \right\|_2 \leq \delta \cdot S_k^{cap}, \forall k, t \tag{3.40}$$

Last, constraints (3.22), (3.28) and (3.29) can be rewritten with $i_{jk,t}$ and $v_{k,t}$, as follows.

$$P^{net,loss} = \sum_{t \in T} \sum_{j,k \in B} r_{jk} i_{jk,t}, \forall jk, t \tag{3.41}$$

$$\left(\underline{V}_k\right)^2 \leq v_{k,t} \leq \left(\overline{V}_k\right)^2, \forall k, t \tag{3.42}$$

$$0 \leq i_{jk,t} \leq \left(I_{jk}^{cap}\right)^2, \forall jk, t \tag{3.43}$$

Since the VVC model minimises the network power loss with a function of $i_{jk,t}$, zero relaxation gap can be achieved for constraint (3.39). Thus, the VVC optimisation model formulated by (3.21), (3.23), (3.31)-(3.32), (3.35)-(3.37), (3.39)-(3.43) becomes a convex SOCP problem that can be efficiently solved.

3.3.4 Scenario-Based Stochastic Optimisation Method

Considering the uncertainty variables in the proposed VVC model, i.e., $P_{k,t}^{PV,m}$, $P_{k,t}^{L}$ and $Q_{k,t}^{L}$, this chapter utilises a scenario-based stochastic optimisation method to address the uncertainties.

According to [42], the objective function of a scenario-based stochastic optimisation model can be expressed as below.

$$\min_{x} \sum_{sc\in SC} \left(\rho_{sc} \cdot f(x, \lambda_{sc})\right) \tag{3.44}$$

Here, sc is the index of scenarios in a scenario set SC, ρ_{sc} is the scenario occurrence probability, x represents the control variables, and $f(x, \lambda_{sc})$ denotes the objective function with λ_{sc} which indicates the uncertainty parameters of scenario sc.

In the proposed VVC problem (31), the control variable $P_{k,t}^{PV}$ is limited by $P_{k,t}^{PV,m}$. However, with different scenarios that have different values of $P_{k,t}^{PV,m}$, the optimised control variable $P_{k,t}^{PV}$ is always confined by the scenario that has the least $P_{k,t}^{PV,m}$, which is not reasonable. To solve this issue, a slack variable $P_{k,t}^{PV,a}$, i.e., the actual PV power generation under different scenarios, is introduced to replace (3.31), (3.32) and (3.35) with the following constraints.

$$P_{k,t}^{PV,a} = \begin{cases} P_{k,t}^{PV,m}, & if\ P_{k,t}^{PV} \geq P_{k,t}^{PV,m} \\ P_{k,t}^{PV}, & if\ P_{k,t}^{PV} < P_{k,t}^{PV,m} \end{cases} \tag{3.45}$$

$$P_{k,t}^{PV,c} = P_{k,t}^{PV,m} - P_{k,t}^{PV,a} \tag{3.46}$$

$$P_{k,t}^{PV,a} - P_{k,t}^{L} = \sum\nolimits_{l\in L(k)} P_{kl,t} - \sum\nolimits_{j\in J(k)} (P_{jk,t} - r_{jk} i_{jk,t}), \forall k, t \tag{3.47}$$

Constraint (3.45) means that for a given inverter active power output result $P_{k,t}^{PV}$ and a specific scenario, if the MPPT power $P_{k,t}^{PV,m}$ is smaller than $P_{k,t}^{PV}$, the actual PV output will be $P_{k,t}^{PV,m}$; otherwise, the actual output will be curtailed to $P_{k,t}^{PV}$. As the objective function contains the minimisation of $P_{k,t}^{PV,c}$, which is equivalent to maximising $P_{k,t}^{PV,a}$, constraint (3.45) can be further linearised into the following two inequalities.

$$P_{k,t}^{PV,a} \leq P_{k,t}^{PV,m} \tag{3.48}$$

$$P_{k,t}^{PV,a} \leq P_{k,t}^{PV} \tag{3.49}$$

Finally, this chapter formulates a scenario-based stochastic multi-objective convex optimisation problem for the PV inverter reliability-constrained VVC model. Ψ denotes a scenario set.

$$\min_{P_{k,t}^{PV},Q_{k,t}^{inv}} \sum_{sc\in SC} \{\rho_{sc}(w_1 P^{net,loss} + w_2 P^{curt,loss})\} \tag{3.50}$$

s.t. (3.23), (3.36), (3.37), (3.39)-(3.43), (3.46)-(3.49), $\forall k,t,sc$

$$\{(P_{k,t,sc}^{PV,m}, P_{k,t,sc}^{L}, Q_{k,t,sc}^{L}), \rho_{sc}\} \in \Psi, \forall k,t,sc \tag{3.51}$$

In this chapter, Monte Carlo Sampling (MCS) is used to construct the scenarios of PV power generation and loads, based on the Gaussian distribution [103]. A backward scenario reduction method [104] is then applied to reduce the sampled scenarios into a proper scale for high stochastic programming efficiency.

3.4 Case Studies

3.4.1 Test System Description

In this chapter, a 33-bus distribution network is used to verify the proposed VVC model. The network topology is given in Figure 3.4, and the network parameters can be found in [91]. This chapter considers a case with high PV penetration, and the PV locations are shown in Figure 3.4. Each location has 100 individual PV systems with a total generation capacity of 500 kW. Besides, the associated inverters of the individual PV systems are all oversized by 10% to 5.5 kVA. In this test, the weighting factors w_1 and w_2 in (3.50) are set to be the same. The voltage at the root bus $V_1 = 1$ p.u., and voltage limits $[\underline{V}_k, \overline{V}_k] = [0.95, 1.05]$ p.u. The VVC dispatch time interval is set as one hour. To complete the inverter reliability analysis, the proposed VVC is implemented for one year. It is assumed that the test distribution network covers a relatively small area where solar irradiance and ambient temperature are the same for the whole network. Note that other system requirements such as communication and advanced metering infrastructure are essential for implementation but beyond the numerical simulations of this chapter. These system requirements can be found in [105] and [106] for practical implementation.

Regarding the inverter reliability analysis, a 650-V/75-A IGBT module and a 450-V/105-°C aluminum electrolytic capacitor are applied. Their parameters can be found in Table 3-I. The applied IGBT PWM is the sinusoidal bipolar PWM, the modulation rate m is set as 0.8, and the switching frequency f_{sw} is 20 kHz. The DC-link voltage V_{DC} is set as 450 V. In the lifetime model (3.7), according to [71] and [89], A and α are set as 4400 and −6.68, respectively, E_a is set as 0.8 eV, and t_{nom} is 1.5 s. The ambient temperature used in (3.6) and (3.12) is set as the historical one-year hourly temperature of Chicago from December 2016 to November 2017 [95].

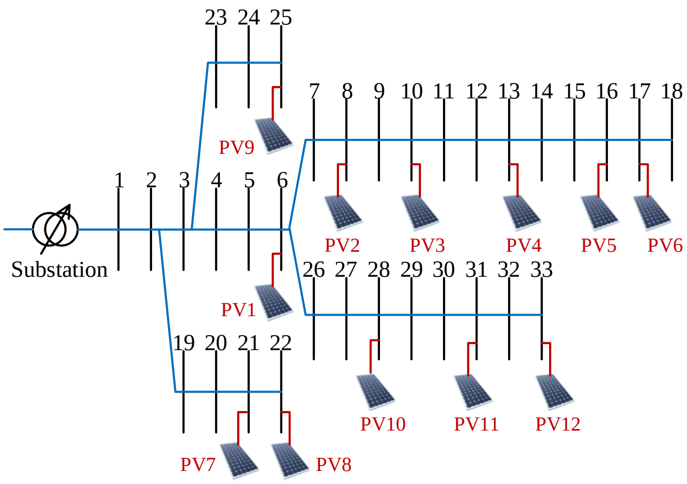

Figure 3.4 Network topology of the test system.

Table 3-I Parameters of IGBT Module and DC-Link Capacitor

IGBT Module				DC-link Capacitor	
V_{CE0}	1V	$R_{th,IG(j-c)}$	0.55K/W	V_{DCr}	450V
r_{CE}	9.3mΩ	$R_{th(c-h)}$	0.75K/W	ESR(100Hz)	52.1mΩ
V_{D0}	1.1V	$R_{th(h-a)}$	0.45K/W	ESR(20kHz)	35.6mΩ
r_D	9.3mΩ	$E_{on,nom}$	1.1mJ	$R_{th(co-a)}$	3.73K/W
I_{nom}	37.5A	$E_{off,nom}$	0.65mJ	H_b	2000h
V_{nom}	400V	$E_{rec,nom}$	0.5mJ	T_m	105°C

In this test, 2000 random scenarios are generated by MCS to represent uncertainties. The MCS of PV power generation is based on historical profiles from [107], and that of loads is based on the profile from IEEE Reliability Test System-1996 [94]. Gaussian distribution is applied for both PV power generation and loads. Then, the scenario reduction method is applied to reduce the initial 2000 scenarios to 50 representative scenarios with corresponding occurrence probabilities.

The 50 representative scenarios form the scenario set Ψ for the proposed scenario-based stochastic optimisation model.

The simulations are carried out on a 64-bit PC with 3.20-GHz CPU and 16-GB RAM by MATLAB platform. The proposed VVC optimisation problem, which is an SOCP problem, is solved by the barrier algorithm in the GUROBI solver [85].

3.4.2 VVC Optimisation Results

In this test, the apparent power restriction factor δ is set as different values including 100%, 90% and 80%, to verify the performance of the proposed PV inverter reliability-constrained VVC method.

Solving the VVC optimisation problem formulated in Chapter 3.3.4, the inverter active and reactive power outputs, i.e., $P_{k,t}^{PV}$ and $Q_{k,t}^{inv}$, are optimised. The optimisation results are significantly different with the different values of δ. Figure 3.5 presents the one-year reactive power output results of PV 5 with 100% and 80% as the δ values. Moreover, a zoomed-in portion of the reactive power profile of PV 5 is given in Figure 3.6 to demonstrate the reactive power output variations for two days. Note that positive outputs mean reactive power injection while negative ones mean absorption.

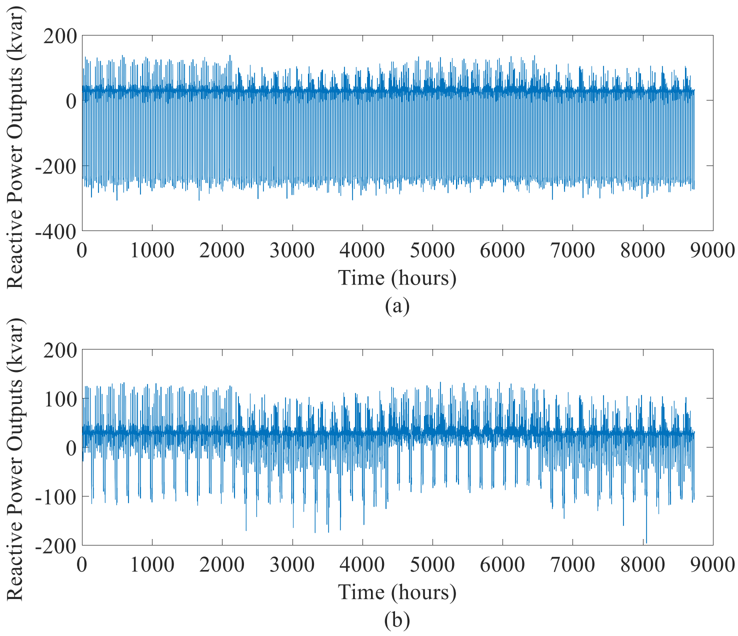

Figure 3.5 One-year reactive power outputs of PV 5 with (a) δ=100%; (b) δ=80%.

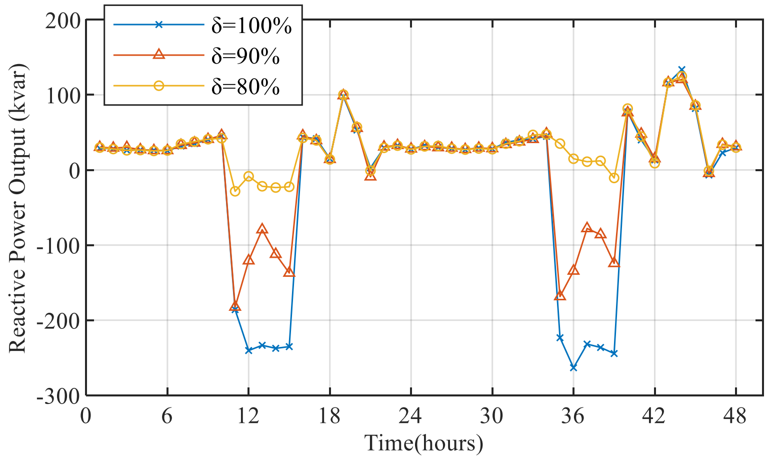

Figure 3.6 Zoomed-in reactive power profiles of PV 5 for Day 1 and Day 2.

It can be seen from Figure 3.5 that with no restriction of apparent power, i.e., δ=100%, PV 5 tends to absorb reactive power during peak PV generation hours over the whole year. On the other hand, when the restriction (δ=80%) is applied, its reactive power absorption is significantly reduced. Figure 3.6 also verifies the efficiency of the restriction factor in regulating the inverter reactive power. It can be seen that a lower restriction factor can result in greater reduction in the reactive power outputs.

Furthermore, taking the first day of this one-year profile as an example, daily profiles of the inverter apparent power of PV 5 with 100% and 80% as the δ values are shown in Figure 3.7. The proposed reliability constraints can effectively limit the inverter apparent power outputs during peak PV generation hours by significantly reducing the reactive power outputs.

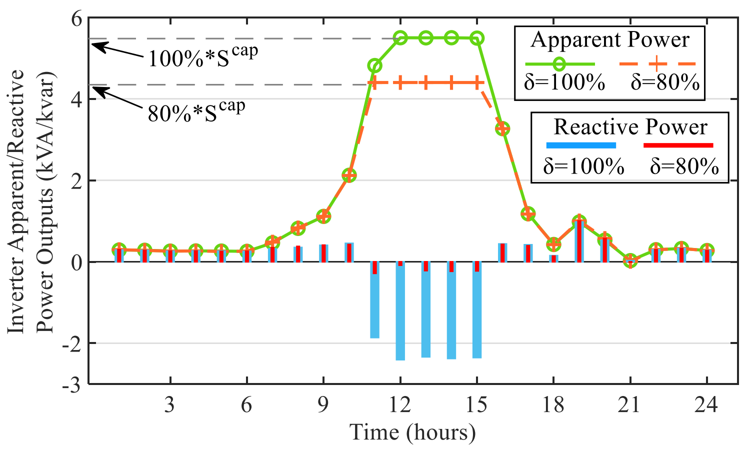

Figure 3.7 Daily profiles of inverter apparent power and reactive power of PV 5.

It is worth noting that with the reduced scenario set, the stochastic optimisation efficiency is significantly improved. The average solving time of the one-hour VVC optimisation problem is only 6 seconds which is fully compatible for online use.

3.4.3 Thermal Analysis of Inverters

With the VVC optimisation results of the whole year, the proposed inverter reliability analysis process in Chapter 3.2 is carried out. The inverter output current amplitude i_P is obtained by (3.15) and (3.16). With the ambient temperature and the device power loss, the IGBT junction temperature and the capacitor core temperature are calculated by (3.4)-(3.6) and (3.12). Furthermore, applying the Rainflow counting technique, the junction temperature variation ΔT_j and mean value T_{jm} of regulated cycles are obtained. Note that all the calculations are based on $P_{k,t}^{PV,a}$ of all the representative scenarios and their probabilities.

Figure 3.8 illustrates the inverter thermal analysis results at PV 5, including the Rainflow counting results of the IGBT junction temperature and the statistical results of the DC-link capacitor core temperature. The thermal analysis results without the VVC function are also included for comparison.

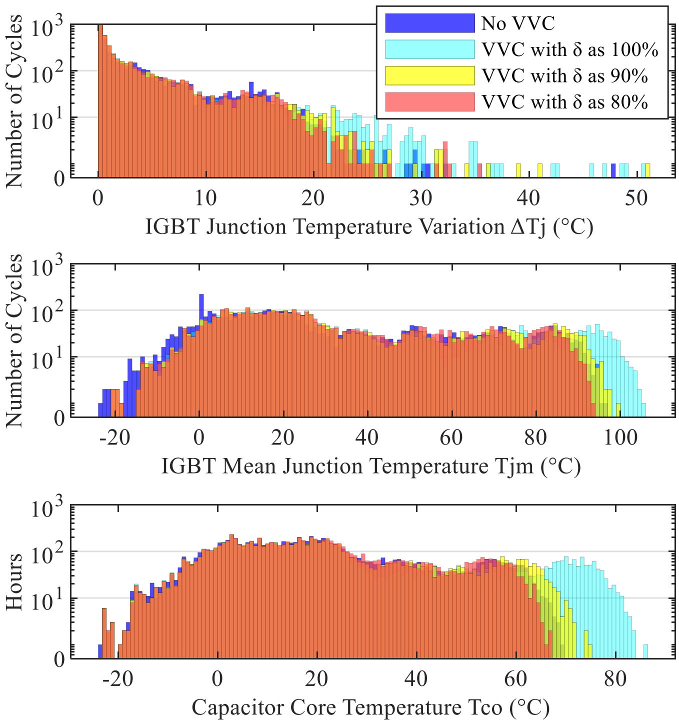

Figure 3.8 Thermal analysis results of IGBT junction temperature and DC-link capacitor core temperature at PV 5.

From this figure, the IGBT junction temperature variation and mean values, as well as the capacitor core temperature, are all increased, due to the VVC implementation. However, with the application of the proposed restriction factor δ, the circumstances for device operations at high temperatures are significantly reduced. Moreover, a smaller δ demonstrates more efficient temperature reduction performance. Thus, the regulated inverter apparent power with the restriction factor can lead to reduced IGBT and DC-link capacitor temperature, such that their lifetimes are supposed to increase.

3.4.4 Lifetime Estimation of Inverters

The obtained Rainflow counting results can then be used in (3.7)-(3.9) to calculate the lifetime of the IGBT module. For the DC-link capacitor, the core temperature profile can be directly incorporated in (3.13) and the Miner's rule is applied to estimate its lifetime. Figure 3.9 demonstrates the lifetimes of the IGBT modules and DC-link capacitors of selected inverters.

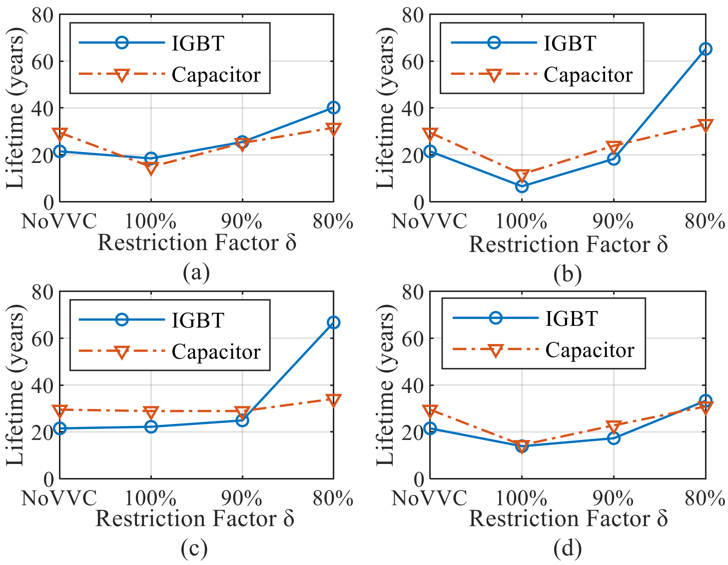

Figure 3.9 Lifetimes of IGBT module and DC-link capacitor with different δ values for (a) PV 2; (b) PV 5; (c) PV 8; (d) PV 12.

From Figure 3.9, without the VVC function, due to the identical mission profiles of solar irradiance and ambient temperature, the IGBT lifetime at all the PVs is calculated as 21.5 years, and the capacitor lifetime is 29.5 years. The application of the proposed restriction factor δ can effectively prevent the lifetime degradation caused by the inverter use for VVC. Furthermore, the lifetime of IGBT module can be significantly increased when applying a much lower δ. This is because the PV curtailment works to guarantee a much lower and stable junction temperature, but it may lead to huge curtailment power loss.

The minimum and the average lifetime of all the IGBT modules and capacitors, as well as the one-year energy loss are given in Table 3-II. Compared to no VVC, the lifetime results of the VVC without the reliability constraints (i.e., δ = 100%) are significantly reduced, especially for the minimum lifetime, though the total energy loss is also decreased. With the reliability constraints applied, as the restriction factor δ decreases, both the minimum and the average lifetimes increase, as a technical benefit. However, the total energy loss increases considerably when δ is set as 80%, leading to bad economic efforts.

Thus, the proposed PV inverter reliability-constrained VVC mothed can efficiently improve both minimum and average lifetimes of the inverters. However, a low restriction factor may seriously impair the VVC performance and the PV power generation efficiency. To this point, the restriction factor is expected to be effectively designed and validated via simulations. For this test system, it is suggested as 90% to make a fair trade-off between the inverter lifetime and the total energy loss.

Table 3-II Lifetime and Energy Loss Results of PV Inverter Reliability Constrained VVC with Different Values of Restriction Factor

Restriction Factor δ		Minimum Lifetime (years) at PV No.		Average Lifetime (years) of All PVs		One-Year Energy Loss (MWh)		
		IGBT Module	DC-Link Capacitor	IGBT Module	DC-Link Capacitor	Network Loss	PV Curtailment	Total Loss
No VVC		21.5 (All)	29.5 (All)	21.5	29.5	772.13	0	772.13
VVC	100%	6.6 (PV 5)	6.2 (PV 11)	19.1	15.9	549.8	0.37	550.17
	90%	16.4 (PV 6)	9.3 (PV 11)	44.9	22.5	562.96	18.26	581.22
	80%	33.3 (PV 12)	12.1 (PV 11)	163.3	28.9	548.6	269.49	818.09

3.4.5 Sensitivity Analysis on Weighting Factors

In this subchapter, the impacts of different weighting factors on simulation results are analysed. A Pareto front is obtained by simulations with different values of w_1 and w_2 in (3.50), as shown in Figure 3.10 (a). Furthermore, the sensitivity of the average IGBT/capacitor lifetime towards the weighting factor w_1 is analysed and presented in Figure 3.10 (b). Note that the restriction factor applied in this subchapter is 90%.

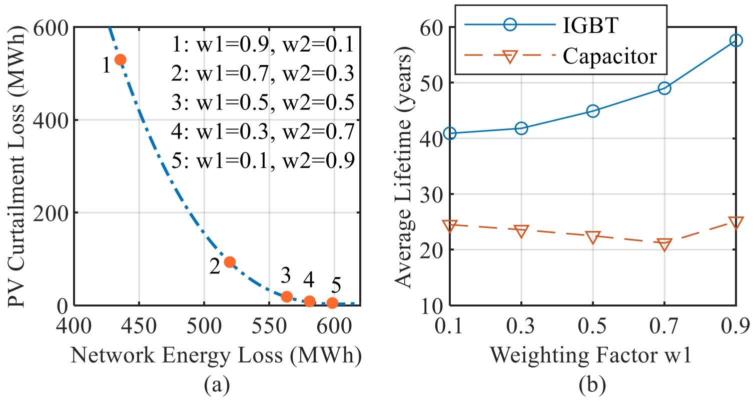

Figure 3.10 Sensitivity analysis of weighting factors. (a) Pareto front. (b) Average IGBT/capacitor lifetime.

In Figure 3.10 (a), a Pareto front is drawn with the five solution points of different weighting factors. It is worth noting that the solution point 3 with both w_1 and w_2 as 0.5 has the least total energy loss of 581.22 MWh, which suggests this pair of the weighting factors for minimising the energy loss. From Figure 3.10 (b), it can be seen that as w_1 increases, the average lifetime of the IGBT modules tends to rise. However, for DC-link capacitors, the average lifetime decreases slightly until w_1 reaches 0.7 and then increases.

3.4.6 Validation on the 69-bus Distribution Network

In this subchapter, a 69-bus distribution network is used to further validate the proposed VVC method for large systems. The network topology is given in Figure 3.11, and the network parameters can be found in [108]. In this test system, 18 buses marked with red in Figure 3.11 have PVs, and each of them contains 120 individual PV systems and has a total power generation capacity of 600 kW. Other aspects of the test system including the inverter oversizing rate, voltage limits, device models and parameters, uncertainty profiles, etc. are consistent with those in the 33-bus test system in Chapter 3.4.1.

With the proposed PV inverter reliability-constrained VVC optimisation model, as well as the whole inverter reliability analysis procedure, the inverter lifetimes with the different restriction factors can be calculated. The lifetime results of PV inverters at selected buses are demonstrated in Figure 3.12. Moreover, the simulation results including the minimum and the average lifetime of IGBTs and capacitors, as well as the energy loss, are summarised in Table 3-III.

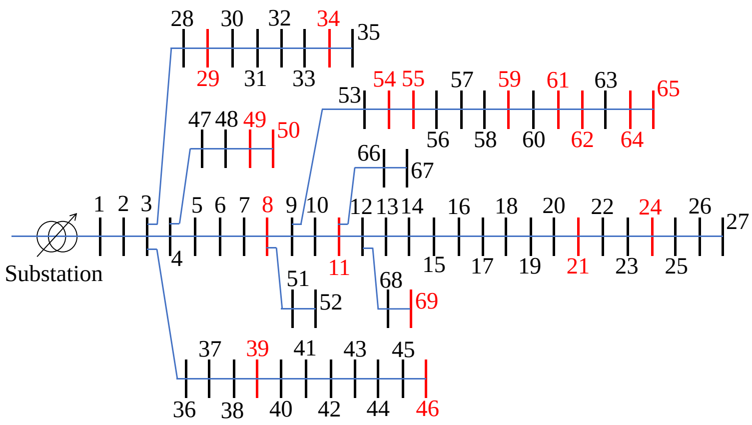

Figure 3.11 Network topology of the 69-bus test system.

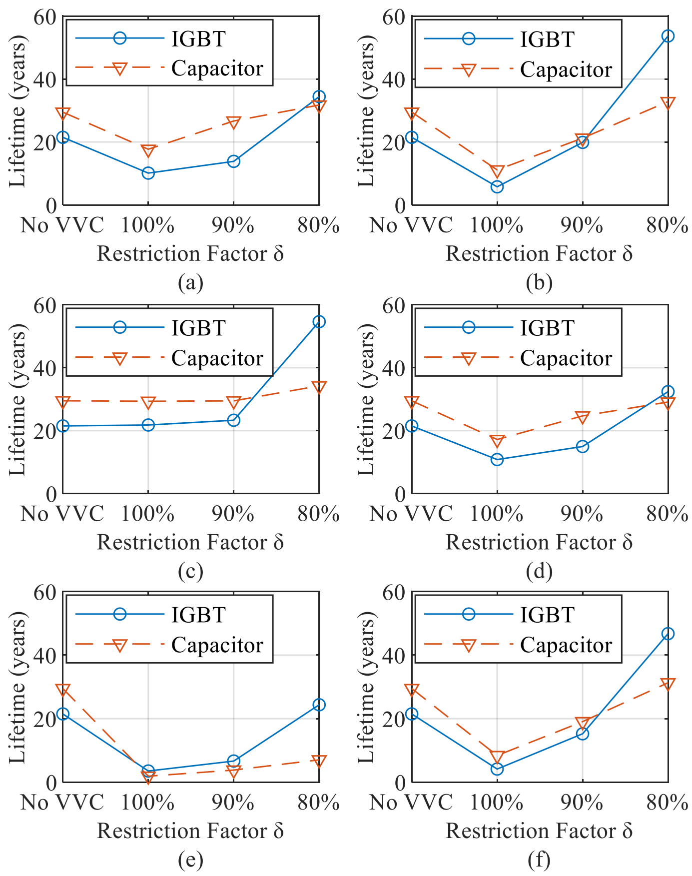

Figure 3.12 Lifetimes of IGBTs and DC-link capacitors for PVs at Buses No. (a) 11; (b) 24; (c) 34; (d) 49; (e) 61; (f) 65.

Figure 3.12 clearly demonstrates the efficiency of the proposed PV inverter reliability-constrained VVC method for inverter lifetime enhancement. When the PV inverters are used for

VVC without restrictions, i.e., δ=100%, the lifetimes of the IGBTs and DC-link capacitors are significantly reduced compared to the no-VVC case. With the application of the proposed restriction factor and reliability constraints, the inverter lifetime degradation is efficiently alleviated, and a lower restriction factor demonstrates higher efficiency in lifetime enhancement.

It is worth noting in Figure 3.12 (c) that PV inverters at Bus 34 present minor lifetime changes between the 100% case and the no-VVC one, because the loads along the corresponding feeder are relatively small and the connected PV inverters are much less utilised for reactive power compensation. Similar results can also be found for PV inverters at Buses 29, 39 and 46.

Table 3-III Lifetime and Energy Loss Results of PV Inverter Reliability Constrained VVC with Different Values of Restriction Factor (69-Bus System)

<table>
<tr><th colspan="2" rowspan="2">Restriction Factor δ</th><th colspan="2">Minimum Lifetime (years) at Bus No.</th><th colspan="2">Average Lifetime (years) of All PVs</th><th colspan="3">One-Year Energy Loss (MWh)</th></tr>
<tr><th>IGBT Module</th><th>DC-Link Capacitor</th><th>IGBT Module</th><th>DC-Link Capacitor</th><th>Network Loss</th><th>PV Curtailment</th><th>Total Loss</th></tr>
<tr><td colspan="2">No VVC</td><td>21.5 (All)</td><td>29.5 (All)</td><td>21.5</td><td>29.5</td><td>989.7</td><td>0</td><td>989.7</td></tr>
<tr><td rowspan="3">VVC</td><td>100%</td><td>3.5 (Bus 61)</td><td>1.9 (Bus 61)</td><td>12.8</td><td>18.7</td><td>871.95</td><td>7.74</td><td>879.69</td></tr>
<tr><td>90%</td><td>5.3 (Bus 62)</td><td>3.8 (Bus 61)</td><td>16.7</td><td>23.4</td><td>864.26</td><td>30.95</td><td>895.21</td></tr>
<tr><td>80%</td><td>24.4 (Bus 61)</td><td>7 (Bus 61)</td><td>42.8</td><td>29.2</td><td>766.24</td><td>479.06</td><td>1245.3</td></tr>
</table>

The summarised results in Table 3-III further demonstrate that as δ decreases, both minimum and average lifetimes of IGBTs and DC-link capacitors tend to rise, as a technical benefit. However, a low δ, e.g., 80% can lead to serious PV curtailment and considerably increased total energy loss, impairing the economic efficiency. Furthermore, it can be seen that the minimum lifetime is much smaller than that in Table 3-II, and always occurs at Buses 61 and 62. The reason is that for the heavy-load buses, especially Bus 61 which has much larger active and reactive loads than the other buses in the test system, remarkably high reactive power compensation from the nearby inverters is required. This leads to constantly high inverter apparent power output and component temperature, and thus significantly reduced lifetime. Therefore, the reliability of the PV inverters for VVC can be affected by the network topology, as well as the PV locations and loads.

3.5 Conclusion

The existing inverter-based VVC methods have not considered the PV inverter reliability issue, while significant lifetime degradation can be found when the inverters are utilised for VVC functions. To enhance the inverter reliability and keep high VVC performance, this chapter proposes a PV inverter reliability-constrained VVC optimisation method for distribution networks. Based on the inverter reliability models and the analysis method, inverter reliability constraints are developed with a restriction factor for inverter apparent power regulation and a PV curtailment scheme. With the reliability constraints, a multi-objective reliability-constrained VVC optimisation model is formulated, which aims to minimise both network power loss and PV curtailed power, while enhancing the inverter lifetime. Simulations are carried out on two distribution networks, and the simulation results verify the effectiveness of the proposed inverter reliability constraints and VVC method. The proposed VVC method can not only achieve high performance in the reduction of network power loss and PV curtailed power, but also efficiently improve the PV inverter lifetime.

Chapter 4 PV INVERTER RELIABILITY CONSTRAINED VOLT/VAR CONTROL WITH POWER SMOOTHING VIA A CONVEX-CONCAVE PROGRAMMING METHOD

In Chapter 3, a PV inverter reliability constrained VVC method with inverter apparent power restriction is proposed. This method can realise efficient inverter reliability enhancement via successfully limiting the maximum inverter apparent power output in VVC functions. However, a potential drawback of this method is that it may compromise the inverter apparent power output capability with a low restriction factor, leading to large PV generation curtailment and impaired economic benefits. To this end, considering the significant impact of power device junction temperature variation on inverter reliability analysed in Chapter 1, this chapter proposes a PV inverter reliability-constrained (PiReCon-) VVC method with inverter apparent power smoothing to enhance the inverter reliability in VVC functions. Firstly, a flexible inverter power smoothing scheme with inverter var support and PV curtailment is proposed, and new reliability constraints are developed with a power smoothing factor to efficiently constrict the variation of inverter apparent power output. Secondly, a new VVC optimisation model is proposed with the developed reliability constraints in which a non-convex quadratic-equality constraint is introduced. Thirdly, this chapter develops a penalty convex-concave programming method to effectively tackle the non-convexity issue of the proposed VVC optimisation model. The proposed PiReCon-VVC method is tested on a 33-bus distribution network, and simulation results verify the high efficiency of the proposed VVC method in both minimising the network power losses and enhancing the PV inverter reliability.

4.0 Nomenclature

A. Sets and Indices

B	Set of network branches.
$j,\ k,\ l$	Index of network buses.

$J(k)$	Set of parent buses of bus k.
K	Set of network buses.
$L(k)$	Set of child buses of bus k.
n	Iteration index of convex-concave procedure.
SC, sc	Set and index of uncertainty scenarios.
T, t	Set and index of operating time intervals.

B. Parameters

1) PV Inverter Parameters

i_P	Inverter output sinusoidal current amplitude (A).
P^{loss}	IGBT power loss (W).
T_a	Ambient temperature (K).
T_j, T_c, T_h	IGBT junction, case and heatsink temperature (K).
V_{AC}	AC voltage RMS value (V).
V_{DC}	Applied DC-link voltage (V).
Z_{th}	IGBT thermal impedance (K/W).

2) Network Parameters

I_{jk}^{cap}	Current capacity of the branch line from bus j to bus k (A).
$P^{net,loss}$	Network power loss on branch lines (W).
$P^{curt,loss}$	Power loss on PV curtailment (W).
r_{jk}, x_{jk}	Resistance/Reactance of the branch line from bus j to bus k (Ω).
S_k^{cap}	Inverter apparent power capacity at bus k (VA).
$\underline{V}_k, \overline{V}_k$	Lower and upper limits of voltage at bus k (p.u.).
ξ	Smoothing factor for inverter apparent power.

3) CCP Parameters

GAP	Gap of CCP iteration.
s	Slack variable for guaranteeing a feasible region.

σ	Penalty factor.
σ^{max}	Upper bound of penalty factor.
ε	Predefined tolerance for CCP convergence.
μ	Penalty factor growth rate.
ξ	Smoothing factor for inverter apparent power.

C. Variables

$i_{jk,t}$	Square value of current of the branch line from bus j to bus k at time t (A,A^2).
$P_{jk,t}$,$Q_{jk,t}$	Active/Reactive power through the branch line from bus j to bus k at time t (W,var).
$P_{k,t}^{L}$, $Q_{k,t}^{L}$	Uncertain active/reactive load at bus k at time t (W,var).
$P_{k,t}^{inv}$, $Q_{k,t}^{inv}$	Scheduled inverter active/reactive power output at bus k at time t (W,var).
$P_{k,t}^{PV,a}$	Actual PV active power output at bus k at time t (W).
$P_{k,t}^{PV,c}$	PV curtailed active power at bus k at time t (W).
$P_{k,t}^{PV,m}$	Uncertain PV MPPT power generation at bus k at time t (W).
$S_{k,t}$	Inverter apparent power output at bus k at time t (VA).
$v_{k,t}$	Square value of voltage of bus k at time t(p.u.).
$x^{(n)}$	Solution point at n th iteration of CCP.
ρ	Occurrence probability of uncertainty scenarios.

4.1 Introduction

4.1.1 Motivation

Proliferation of distributed photovoltaic (PV) systems allows and promotes the development of active distribution networks (ADNs), which are highly promising to deal with the increasing PV penetration and improve power system security and stability [18] [109]. Besides, ADNs have great potentials in exploiting benefits of PVs and enhancing network hosting capacity [110] [111].

However, the intermittency and volatility of PV power generation brings challenges to the system operation, posing huge threats on network voltage control. It is indicated in [112] [113] that the increasing penetration of PVs leads to dramatic voltage violations due to the intermittent nature of PV power. Moreover, high PV penetration in ADNs may incur heavy voltage rise during peak generation hours, impairing power quality.

More importantly, concerns on ADN reliability have been rising, which depends heavily on the reliability of related controllable devices [114]. It is becoming apparent that the network operation and maintenance costs have been increasing due to the degradation of associated devices such as inverters. In the report [78], CIGRE working group C6.11 highlights the R&D needs for reliability of advanced devices required for ADNs, which is considered as a crucial issue for sustainable and reliable ADN operation. Moreover, the work [115] considers the inverter lifetime reduction as a crucial cost index for the ADN operation. In this regard, the reliability of PV inverters is expected to be taken into account in ADN operation.

4.1.2 Literature Review

In a highly PV-penetrated ADN, PV inverters, which are fast-response power electronic devices, can be utilised to provide volt/var control (VVC) functions [43]. The IEEE 1547.8 working group has also advocated the use of PV inverters for providing VVC functions in ADNs.

In recent years, advanced inverter-based VVC methods for ADNs have been developed. Ref. [50] and [53] developed distributed control methods, considering PV curtailment and unbalanced network, respectively. The work [49] developed a two-stage method for PV inverter dispatch, and [52] proposed a three-stage scheme coordinating various VVC devices.

The inverter-based VVC methods for ADNs are highly promising. However, there is an industrially practical concern, i.e., the reliability of PV inverters. Reliable operation of PV inverters is critical for both PV power generation and reliable VVC functionality, highlighting the importance of PV inverter reliability in VVC-featured ADNs. However, PV inverters contain delicate power electronic switching components, and their lifetime is highly susceptible to their working conditions. Ref. [62] points out that the PV inverter is the most vulnerable subsystem in a PV unit, due to its complex physical structure and varying operating status. The work [67] identifies tremendous lifetime degradation when a PV inverter is used for reactive power compensation outside feed-in hours. Moreover, in [116], the reliability of PV inverter is assessed when a centralised VVC method is applied, and potential impacts of VVC on inverter lifetime are analysed. To this end, it is essential to systematically consider the PV inverter reliability in VVC methods. However, in the existing VVC works, the PV inverter reliability has not been investigated.

To consider inverter reliability in VVC, it is important to understand the inverter failure mechanism and figure out how to efficiently incorporate inverter reliability into VVC optimisation models. Power electronic devices are one of the most critical components inside inverters and their lifetime is a predominant factor for inverter reliability [117]. Moreover, lifetime of power devices is critically affected by their thermal loading, i.e., the cycling of junction temperature [67] [118]. In a recent work [79], the PV inverter reliability is considered in a VVC model, with constricting the upper bound of inverter power output to reduce the junction temperature. However, this method may lead to compromised inverter power capability and thus undesirable PV generation curtailment. Besides, this work does not consider junction temperature variation, which is another significant contributor to inverter failure.

The serious impact of junction temperature variation on power device lifetime has been extensively verified by literature [70] [119] [120] and device manufacturers [89] [121], and the power device reliability can be effectively improved via reducing its junction temperature variation [122] [123] [124]. Therefore, effective regulation of junction temperature variation in VVC methods can be highly beneficial to enhancing PV inverter reliability.

It is revealed in [116] that the power device junction temperature is positively correlated to the inverter output current which is proportional to its apparent power output. This implies that effective smoothing of inverter apparent power output may contribute to the reduction of junction temperature variation and hence the lengthening of inverter lifetime. Power ramp rate control methods in [113] and [125] can limit PV power generation variations, efficiently mitigating the impacts of PV power intermittency on power system operation. However, these methods mainly focus on the local PV active power control to address the intermittency issues, and they do not help smooth the inverter apparent power output in the centralised VVC methods under steady-state operating conditions. The smoothing of inverter apparent power output in VVC for reliability enhancement has never been reported in literature, leaving a research gap.

Additionally, calculation of inverter apparent power output involves a quadratic equation of the active and reactive power, which leads to non-convexity of the VVC optimisation problem. Convex programming methods such as second-order cone programming (SOCP) [81] can be used to address the non-convex quadratic optimisation problems. However, these methods are not universal for use, and only applicable under certain conditions [82]. Furthermore, these methods may have low accuracy on relaxation of original equality constraints [126]. To this end, it is imperative to develop a practicable and efficient solution method to address the intractable non-convex VVC optimisation problems with the quadratic power equality constraint.

4.1.3 Contributions

In regards of the above unsolved issues, this chapter proposes a PV inverter reliability constrained (PiReCon-) VVC method considering inverter power smoothing. This method is formulated as an optimisation model with development of new inverter reliability constraints, which aims to minimise network power losses and improve PV inverter lifetime.

Main contributions of this chapter are summarised as follows.

1) An inverter power smoothing scheme with high control flexibility is developed, which utilises a power smoothing factor to constrict variation of inverter apparent power output. Accordingly, new inverter reliability constraints for power smoothing are proposed.

2) A PiReCon-VVC method for ADNs is proposed with the power smoothing scheme and formulated as an optimisation problem with system-wide information. It is the first time to address junction temperature variation in a central VVC method to enhance inverter reliability.

3) A penalty convex-concave procedure (CCP) programming method is developed to solve the non-convex optimisation problem with high computing efficiency.

4.1.4 Chapter Organisation

The remainder of this chapter is organised as follows. Chapter 4.2 addresses the impact of inverter apparent power variation on inverter reliability. A PV inverter reliability constrained VVC model with a proposed power smoothing scheme is developed in Chapter 4.3. Chapter 4.4 develops a penalty CCP programming method to solve the proposed non-convex VVC model. In

Chapter 4.5, implementation of the proposed VVC method is discussed. Simulations are carried out in Chapter 4.6 and conclusions are drawn in Chapter 4.7.

4.2 Impact of Inverter Power Variation on Reliability

Electrical and mechanical characteristics of PV inverters determine that their reliability is highly relevant to the component temperature, especially junction temperature of power devices such as insulated gate bipolar transistors (IGBTs). In [116], it is indicated that, given the PWM modulation pattern and ambient temperature, the IGBT junction temperature is strictly increasing with the inverter output current. The inverter output current amplitude i_P can be calculated by the following equations.

$$S = \sqrt{(P^{inv})^2 + (Q^{inv})^2} \tag{4.1}$$

$$i_P = \sqrt{2}S/V_{AC} \tag{4.2}$$

In (4.1), S is the inverter apparent power calculated by the inverter active power P^{inv} and reactive power Q^{inv}. Besides, V_{AC} is the root mean square (RMS) value of inverter AC voltage. Considering (4.2), the inverter apparent power output can have direct impacts on the inverter output current, further affecting component temperature and thus inverter reliability and lifetime. The assessment method of inverter reliability is demonstrated in Figure 4.1 and key formulas are given as well.

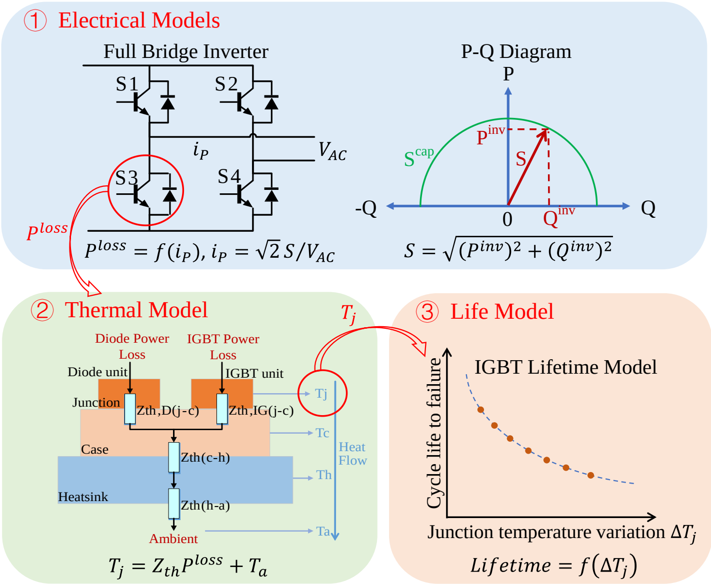

Figure 4.1 PV inverter reliability analysis process.

In Figure 4.1, firstly, the electrical models present how the inverter power outputs (including S, P^{inv} and Q^{inv}) affect the inverter output current i_P and the IGBT power loss P^{loss}. Assuming a constant V_{AC}, a given IGBT module and a specific PWM modulation pattern, the IGBT power loss P^{loss} depends on the inverter apparent power S only.

Then, based on the thermal model of the IGBT module, the IGBT junction temperature T_j can be derived from its power loss P^{loss}, with the thermal impedance Z_{th} and the ambient temperature T_a.

Last, in the life model, the IGBT lifetime dependency on its junction temperature variation is given. A decreased lifetime can be found with an increasing junction temperature variation ΔT_j.

The above assessment method implies that, the variation of inverter apparent power output, which leads to the variation of IGBT junction temperature, can severely affect the inverter lifetime. More detailed quantitative relationships regarding the inverter reliability analysis under the inverter-based VVC function can be found in [116].

Apparently, effective limitation of inverter apparent power variation can benefit the inverter reliability in VVC methods.

4.3 PV Inverter Reliability Constrained VVC with Power Smoothing

In this subchapter, by introducing new reliability constraints with a power smoothing factor to constrict inverter apparent power outputs, the proposed method can not only minimise power losses, but also guarantee enhanced inverter lifetime.

4.3.1 Inverter Reliability Constraints

It is implied by the inverter reliability analysis that, by effectively stabilising the component temperature inside the inverters, the inverter reliability can be significantly improved.

However, it is hard to directly incorporate variables of component temperature or lifetime into an optimisation model. That is because the relationships among the inverter apparent power, the component temperature and the inverter lifetime involve complex non-linear models or high-dimensional terms. On the other hand, a logic-based algorithm, e.g., the Rainflow counting method [69], is required to interpret component temperature profiles for lifetime estimation, and this method is completely intractable for mathematical programming optimisation.

Alternatively, based on the impact of inverter apparent power variation on its reliability indicated in Chapter 4.2, this chapter proposes new inverter reliability constraints to directly constrict the inverter apparent power variation, which is achieved by efficiently smoothing its apparent power output. The inverter reliability constraints are proposed as follows.

$$\left|S_{k,t} - S_{k,t-1}\right| \leq \xi \cdot S_k^{cap} \tag{4.3}$$

$$S_{k,t} = \sqrt{\left(P_{k,t}^{inv}\right)^2 + \left(Q_{k,t}^{inv}\right)^2} \tag{4.4}$$

Here, k is the index of network buses, and t is the index of inverter operation time slots. $S_{k,t}$, $P_{k,t}^{inv}$ and $Q_{k,t}^{inv}$ represent the dynamic inverter apparent, active and reactive power outputs, respectively. S_k^{cap} is the inverter apparent power capacity.

This chapter proposes a power smoothing factor (in percentage) as ξ and it is used in (4.3) to limit the variation of inverter apparent power within a proportion of the inverter capacity. The power smoothing factor ξ can be set as different values to reflect different expectations of inverter apparent power variation. A higher ξ indicates that the inverter apparent power is allowed to vary in a wider range, which may impair the inverter reliability. On the contrary, a lower ξ means more efforts in keeping the inverter apparent power in a narrow range, so that the inverter reliability can be improved. However, a lower ξ may affect the PV power generation and inverter var capability, reducing the efficiency of power generation and VVC.

It is worth noting that the proposed power smoothing factor is used for limiting the inverter apparent power setpoint change between adjacent VVC operation time slots. In addition, this factor can be used as a parameter in a central VVC optimisation model which considers steady-state operating conditions.

With this power smoothing factor ξ, the new inverter reliability constraints are applicable in a VVC method to enhance the inverter lifetime to an expected level. The efficiency of the proposed inverter reliability constraints, as well as the selection of the power smoothing factor, will be discussed in case study. Moreover, it is noted that, the expectations on the inverter lifetime, PV power generation and VVC performance (highly depending on the network setting and inverter capacity), as well as the computing efficiency are the main factors affecting the selection of this power smoothing factor ξ.

4.3.2 Inverter Power Smoothing

To fulfill the inverter reliability constraints in practice, an inverter power smoothing scheme is applied. On one hand, in a VVC method, the inverters can inject or absorb reactive power to reduce the variation of the inverter apparent power output. On the other hand, the inverters can be controlled to curtail the PV active power generation to a specific level when necessary [127]. With the VVC reactive power output and PV active power curtailment, the inverter apparent power smoothing can be implemented with high flexibility, so that the inverter apparent power output can be efficiently limited with the power smoothing factor ξ. The mechanism of the inverter apparent power smoothing scheme is demonstrated in Figure 4.2.

Compared with the conventional methods that locally control active power to achieve renewable generation smoothing, the proposed power smoothing scheme considers a centralised VVC method that takes into account the system-wide information to control both active and reactive power, thus smoothing the inverter apparent power output. Moreover, the proposed scheme aims to enhance the PV inverter reliability by smoothing the apparent power output.

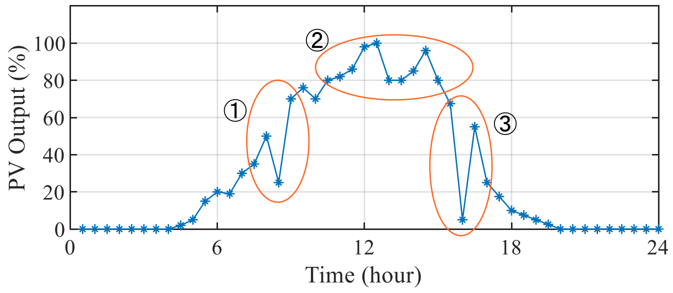

(a)

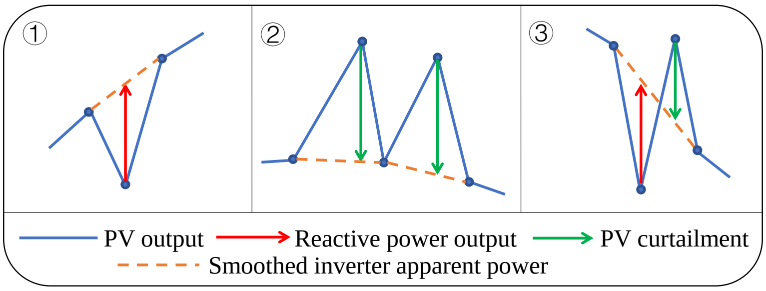

(b)

Figure 4.2 PV inverter apparent power smoothing mechanism: (a) 24-hour PV power generation profile. (b) Inverter apparent power smoothing.

Note that, as a kind of power loss sacrificed for the smoothed inverter apparent power output, the curtailed PV active power generation is supposed to be minimised in the VVC method.

4.3.3 PV Inverter Reliability Constrained VVC Model

4.3.3.1 Objective Function

In this chapter, a PiReCon-VVC optimisation model is proposed to minimise the sum of network power loss $P^{net,loss}$ and curtailed PV power generation $P^{curt,loss}$, as below.

$$\min_{P_{k,t}^{inv},Q_{k,t}^{inv}} \left(P^{net,loss} + P^{curt,loss}\right) \tag{4.5}$$

$$P^{net,loss} = \sum_{t\in T} \sum_{j,k\in B} r_{jk} i_{jk,t}\,, \forall jk,t \tag{4.6}$$

$$P^{curt,loss} = \sum_{t\in T} \sum_{k\in K} P_{k,t}^{PV,c}\,, \forall k,t \tag{4.7}$$

Here, r_{jk} and i_{jk} denote the line resistance and the square of the branch current from bus j to bus k, respectively. $P_{k,t}^{PV,c}$ denotes the curtailed PV active power generation. T, B and K are the sets of inverter operation time slots, network branches and network buses, respectively. The inverter active and reactive power outputs $P_{k,t}^{inv}$ and $Q_{k,t}^{inv}$ are the control variables in the proposed VVC model. It is worth noting that the network power loss and the curtailed PV power generation may have different weightings when interpreted with business models.

4.3.3.2 Inverter Reliability Constraints with Power Smoothing

The proposed inverter reliability constraints with power smoothing are formulated as follows.

$$\left(S_{k,t}\right)^2 = \left(P_{k,t}^{inv}\right)^2 + \left(Q_{k,t}^{inv}\right)^2, \forall k,t \tag{4.8}$$

$$-\xi \cdot S_k^{cap} \leq S_{k,t} - S_{k,t-1} \leq \xi \cdot S_k^{cap}, \forall k,t \tag{4.9}$$

$$0 \leq S_{k,t} \leq S_k^{cap}, \forall k,t \tag{4.10}$$

$$0 \leq P_{k,t}^{inv} \leq P_{k,t}^{PV,m}, \forall k,t \tag{4.11}$$

$$P_{k,t}^{PV,c} = P_{k,t}^{PV,m} - P_{k,t}^{inv}, \forall k,t \tag{4.12}$$

Here, the relationship of inverter power outputs is given as (4.8), and the dynamic inverter apparent power output is smoothed with the proposed power smoothing factor ξ in (4.9). Constraint (4.10) provides the allowed range of the inverter apparent power output. The PV curtailment function is presented in (4.11) and (4.12), where $P_{k,t}^{PV,m}$ denotes the PV power generation in the maximum power point tracking (MPPT) mode, and it can be curtailed to $P_{k,t}^{inv}$ to facilitate power smoothing.

4.3.3.3 Network Operating Constraints

The branch flow model with second-order conic relaxation is used as the network operating constraints and given below.

$$P_{k,t}^{inv} - P_{k,t}^{L} = \sum_{l \in L(k)} P_{kl,t} - \sum_{j \in J(k)} \left(P_{jk,t} - r_{jk} i_{jk,t}\right), \forall k,t \tag{4.13}$$

$$Q_{k,t}^{inv} - Q_{k,t}^{L} = \sum_{l \in L(k)} Q_{kl,t} - \sum_{j \in J(k)} \left(Q_{jk,t} - x_{jk} i_{jk,t}\right), \forall k,t \tag{4.14}$$

$$v_{k,t} = v_{j,t} - 2\left(r_{jk} P_{jk,t} + x_{jk} Q_{jk,t}\right) + \left(r_{jk}^2 + x_{jk}^2\right) i_{jk,t}, \forall jk,t \tag{4.15}$$

$$\left\| \begin{matrix} 2P_{jk,t} \\ 2Q_{jk,t} \\ i_{jk,t} - v_{j,t} \end{matrix} \right\|_2 \leq i_{jk,t} + v_{j,t}, \forall jk, t \tag{4.16}$$

Herein, j, k and l are the indices of network buses, $J(k)$ and $L(k)$ are the sets of the parent and child buses of bus k, respectively. Besides, P_{jk} and Q_{jk} denote the branch active and reactive power from bus j to bus k, while r_{jk} and x_{jk} indicate the line resistance and reactance of the branch, respectively. Moreover, P_k^L, Q_k^L and v_k are the active load, the reactive load and the square of the voltage at bus k, respectively.

Constraint (4.16) is a second-order conic relaxed model for the original branch flow model, and the detailed relaxation method can be found in [128]. This branch flow model with second-order conic relaxation, i.e., (4.13)-(4.16), is highly efficient and has been widely used in the inverter-based VVC optimisation problems.

Along with the power flow calculation, the bus voltage and the branch current are limited within the upper/lower bounds and the line capacity, respectively. The corresponding network operating constraints are formulated as follows.

$$\left(\underline{V}_k\right)^2 \leq v_{k,t} \leq \left(\overline{V}_k\right)^2, \forall k, t \tag{4.17}$$

$$0 \leq i_{jk,t} \leq \left(I_{jk}^{cap}\right)^2, \forall jk, t \tag{4.18}$$

Thus, a PiReCon-VVC optimisation model is formulated by (4.5)-(4.18). It is noted that as a part of the inverter reliability constraints, (4.8) makes the optimisation model non-convex and intractable to solve. Therefore, convexification of (4.8) is the key point to solve the proposed optimisation problem and a solution method is developed in Chapter 4.4.

4.3.3.4 Stochastic Optimisation Model

The proposed VVC optimisation model contains uncertainty variables including $P_{k,t}^{PV,m}$, $P_{k,t}^L$, and $Q_{k,t}^L$. In this chapter, a scenario-based stochastic optimisation approach [42] is applied to address the uncertainty problem.

Firstly, Monte Carlo Sampling (MCS) is applied to generate large amounts of scenarios of

$P_{k,t}^{PV,m}$, $P_{k,t}^{L}$, and $Q_{k,t}^{L}$, based on the probability distribution functions (PDFs) which can characterise their realisation probability distributions. Then, to improve computing efficiency, a scenario reduction method [104] is applied to reduce the original scenarios into a small number of representative scenarios, each of which has its own assigned occurrence probability.

With the representative scenarios and their occurrence probabilities, the objective function of the proposed optimisation model (4.5) can be rewritten as follows.

$$\underset{P_{k,t}^{inv},Q_{k,t}^{inv}}{\text{Min}} \sum_{sc\in SC}\left\{\rho_{sc} \times f\left[\left(P_{k,t}^{inv}, Q_{k,t}^{inv}\right), \lambda\left(P_{k,t,sc}^{PV,m}, P_{k,t,sc}^{L}, Q_{k,t,sc}^{L}\right)\right]\right\} \tag{4.19}$$

Here, sc is the index of representative scenarios in the scenario set SC. ρ_{sc} denotes the occurrence probability of scenario sc. f represents the objective function with the control variables $\left(P_{k,t}^{inv}, Q_{k,t}^{inv}\right)$ and the uncertainty realisation indicated by λ.

It is worth noting that the proposed PV curtailment constraint (4.11) limits the control variable $P_{k,t}^{inv}$ within the uncertainty variable $P_{k,t,sc}^{PV,m}$. Thus, the optimised $P_{k,t}^{inv}$ is always confined by the scenario that has the lowest PV MPPT power output, regardless of $P_{k,t,sc}^{PV,m}$ in the other representative scenarios. This is obviously unreasonable. To this point, an ancillary variable $P_{k,t,sc}^{PV,a}$, which indicates the actual PV active power output under scenario sc, is introduced and it has the following expression.

$$P_{k,t,sc}^{PV,a} = \begin{cases} P_{k,t,sc}^{PV,m}, & if\ P_{k,t,sc}^{PV,m} < P_{k,t}^{inv} \\ P_{k,t}^{inv}, & if\ P_{k,t,sc}^{PV,m} \geq P_{k,t}^{inv} \end{cases} \tag{4.20}$$

Eq. (4.20) indicates that given an optimised decision $P_{k,t}^{inv}$, if the PV MPPT output is lower than this decision, actual PV output $P_{k,t,sc}^{PV,a}$ will be $P_{k,t,sc}^{PV,m}$; otherwise, it will be curtailed to $P_{k,t}^{inv}$.

Since minimising the PV curtailment in the objective function is equivalent to maximising the actual PV output $P_{k,t,sc}^{PV,a}$, (4.20) can be reformulated into the following inequalities.

$$0 \leq P_{k,t,sc}^{PV,a} \leq P_{k,t,sc}^{PV,m} \tag{4.21}$$

$$0 \leq P_{k,t,sc}^{PV,a} \leq P_{k,t}^{inv} \tag{4.22}$$

Thus, the curtailed PV power is calculated as follows,

$$P_{k,t,sc}^{PV,c} = P_{k,t,sc}^{PV,m} - P_{k,t,sc}^{PV,a} \tag{4.23}$$

4.4 Penalty Convex-Concave Procedure Programming Method

The proposed inverter reliability constraint (4.8) in the quadratic-equality form causes non-convexity for the developed optimisation problem. In this subchapter, a penalty CCP programming method is developed to solve the non-convex problem.

4.4.1 Basis of Convex-Concave Procedure

The CCP is an efficient heuristic method which can be used to solve the difference of convex (DoC) programming problems [129]. A DoC programming problem can be presented in the following form.

$$\underset{x}{\text{Min}}\, f_0(x) - g_0(x) \tag{4.24}$$

$$\text{s.t.} \quad f_i(x) - g_i(x) \leq 0,\ \forall i \tag{4.25}$$

Here, $x\ (\in \mathbf{R}^m)$ indicates a vector of optimisation variables, $f_i: \mathbf{R}^m \to \mathbf{R}$ and $g_i: \mathbf{R}^m \to \mathbf{R}$ are convex functions. To solve the problem, the CCP replaces the concave term $-g_i(x)$ with a convex upper bound, and the original DoC programming problem can be reformulated into the following convex problem.

$$\underset{x}{\text{Min}}\, f_0(x) - \hat{g}_0\left(x; x^{(n)}\right) \tag{4.26}$$

$$\text{s.t.} \quad \hat{g}_i\left(x; x^{(n)}\right) = g_i\left(x^{(n)}\right) + \nabla g_i\left(x^{(n)}\right)^T \left(x - x^{(n)}\right) \quad \forall i \tag{4.27}$$

$$f_i(x) - \hat{g}_i\left(x; x^{(n)}\right) \leq 0 \quad \forall i \tag{4.28}$$

Here, n is the iteration index for the CCP. $\hat{g}_i\left(x; x^{(n)}\right)$ is the linearised function of $g_i(x)$ at a current solution point $x^{(n)}$. With this linear approximation, the problem (4.26)-(4.28) is convex and can be efficiently solved by common solvers. In the CCP, this convex problem is iteratively solved and the solution of the nth iteration is set as $x^{(n+1)}$ for linear approximation in the following iteration. The problem is kept being updated with the new solution and solved until the termination criterion is satisfied. One widely used termination criterion is that the improvement in reduction of the objective value, formulated as the gap below, is no more than a tolerance ε.

$$GAP\left(x^{(n+1)}\right) = f_0\left(x^{(n)}\right) - g_0\left(x^{(n)}\right) - \left(f_0\left(x^{(n+1)}\right) - g_0\left(x^{(n+1)}\right)\right) \leq \varepsilon \tag{4.29}$$

4.4.2 Penalty CCP for PiReCon-VVC Model

As the proposed quadratic equality constraint (4.8) can be reformulated into two quadratic inequality constraints that contain DoC problems, the CCP is applied to solve the proposed PiReCon-VVC problem. In this chapter, a penalty CCP method is further developed, which can recover a feasible solution and guarantee efficient convergence regarding the non-convex optimisation problem. The principle of this developed penalty CCP method is illustrated in Figure 4.3, and the convexification of the proposed model is introduced as follows. Note that in this subchapter, simplified notations P, Q and S are used to represent $P_{k,t}^{inv}$, $Q_{k,t}^{inv}$ and $S_{k,t}$, respectively.

Firstly, equality constraint (4.8) can be replaced with the following two inequalities.

$$P^2 + Q^2 \leq S^2, \forall k, t \tag{4.30}$$

$$P^2 + Q^2 \geq S^2, \forall k, t \tag{4.31}$$

In fact, (4.30) is an SOCP constraint and can be directly transformed into the following second-order cone form.

$$\left\| \begin{matrix} P \\ Q \end{matrix} \right\|_2 \leq S, \forall k, t \tag{4.32}$$

For (4.31), following convex quadratic functions are defined.

$$f(S) = S^2, \forall k, t \tag{4.33}$$

$$g(P,Q) = P^2 + Q^2, \forall k,t \quad (4.34)$$

Thus, in line with (4.25), constraint (4.31) is reformulated into a DoC constraint as below.

$$f(S) - g(P,Q) \le 0, \forall k,t \quad (4.35)$$

Secondly, the CCP forms a linearised function of $g(P,Q)$ as below, by creating a tangent plane at a current solution point $\left(P^{(n)}, Q^{(n)}\right)$, as shown in Figure 4.3 (a).

$$\hat{g}\left(P,Q;P^{(n)},Q^{(n)}\right) = 2P^{(n)}P - \left(P^{(n)}\right)^2 + 2Q^{(n)}Q - \left(Q^{(n)}\right)^2, \forall k,t \quad (4.36)$$

Then, like (4.28), constraint (4.35) can be relaxed as below.

$$f(S) \le \hat{g}\left(P,Q;P^{(n)},Q^{(n)}\right), \forall k,t \quad (4.37)$$

Thus, based on the above, the optimisation model with constraints (4.32) and (4.37) instead of (4.8) is now convex. However, as indicated in Figure 4.3 (a), due to the convexity of $g(P,Q)$, the created tangent plane, presented by the right side of (4.37), is always lower than $g(P,Q)$ except the solution point $\left(P^{(n)}, Q^{(n)}\right)$. In other words, despite the initial point, there is no feasible solution satisfying both (4.32) and (4.37), making the CCP stagnant at the first iteration. In this regard, based on the work [130], a slack variable, as well as a penalty mechanism are incorporated in the CCP, forming a penalty CCP method. These terms are added to objective function (4.5) and constraint (4.37) as below.

$$\mathrm{Min}\left(P^{net,loss} + P^{curt,loss} + \sigma^{(n)} \textstyle\sum_{t\in T} \sum_{k\in K} s_{k,t}\right) \quad (4.38)$$

$$f(S) \le \hat{g}\left(P,Q;P^{(n)},Q^{(n)}\right) + s_{k,t}, \forall k,t \quad (4.39)$$

Here, s is the slack variable introduced to guarantee a feasible region and it is minimised in the objective function. Moreover, σ is a penalty factor applied on s, which is supposed to be increased during iterations to improve convergence. The mechanism of the penalty CCP with slack variable is demonstrated in Figure 4.3 (b).

Then, constraint (4.39) can be reformulated into a second-order cone form as (4.40), where $Z_{k,t}$ is presented in (4.41).

$$\left\| \frac{2S}{1 - Z_{k,t}} \right\|_2 \leq 1 + Z_{k,t}, \forall k, t \tag{4.40}$$

$$Z_{k,t} = \hat{g}\left(P, Q; P^{(n)}, Q^{(n)}\right) + s_{k,t}, \forall k, t \tag{4.41}$$

Finally, with the penalty CCP, the non-convex PiReCon-VVC problem is convexified by replacing the original equality constraint (4.8) with constraints (4.32), (4.36), (4.40) and (4.41). Also, the original objective function (4.5) is modified by adding a penalty term as (4.38).

As the penalty CCP aims to guarantee the strict equality of (4.8), in line with [126] and [131], the termination criterion is set as below. Herein, ε is a pre-specified tolerance, and N_T and N_K denote the numbers of involved operation time slots and network buses, respectively.

$$GAP = \frac{1}{N_T N_K} \sum_{t \in T} \sum_{k \in K} \left| \left(S_{k,t}{}^{(n)} \right)^2 - \left(P_{k,t}^{inv}{}^{(n)} \right)^2 - \left(Q_{k,t}^{inv}{}^{(n)} \right)^2 \right| \leq \varepsilon \tag{4.42}$$

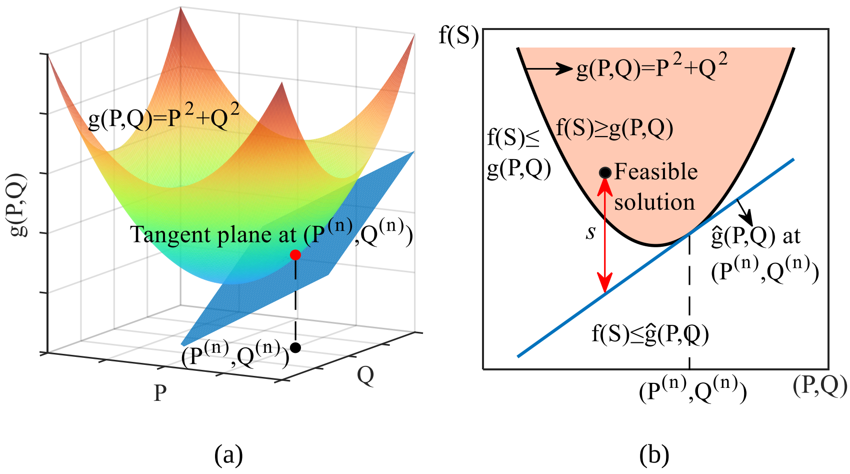

Figure 4.3 Illustration of penalty CCP: (a) Linear approximation with tangent plane; (b) Two-dimension projection.

The penalty CCP is also presented below as Algorithm 4.1.

Algorithm 4.1: Penalty Convex-Concave Procedure

---

1. Given an initial point $x^{(0)}$, an initial penalty factor $\sigma^{(0)} > 0$, a penalty growth rate $\mu > 1$, and a penalty factor upper bound σ^{max}. Let the iteration index $n = 0$.

2. Form a linear approximation of $g_i(x)$ at the point $x^{(n)}$, as below:

$$\hat{g}_i\left(x; x^{(n)}\right) = g_i\left(x^{(n)}\right) + \nabla g_i\left(x^{(n)}\right)^T \left(x - x^{(n)}\right) \quad \forall i$$

---

3. Solve the following penalised problem:

$$\min_x \{f_0(x) - \hat{g}_0(x; x^{(n)}) + \sigma^{(n)} \sum_i s_i\}$$

$$s.t.\ f_i(x) - \hat{g}_i(x; x^{(n)}) \le s_i,\ \forall i$$

$$s_i \ge 0,\ \forall i;$$

and obtain the optimal solution as $x^{(n+1)}$.

4. Evaluate the termination criterion at $x^{(n+1)}$, if $GAP(x^{(n+1)}) \le \varepsilon$, terminate the process and report the optimal solution $x^{(n+1)}$; otherwise, update penalty factor $\sigma^{(n+1)} = \min(\mu\sigma^{(n)}, \sigma^{max})$, update iteration $n = n + 1$, and go to step 2.

4.5 Implementation of PiReCon-VVC Method

Finally, this chapter formulates a scenario-based stochastic optimisation model of the PiReCon-VVC method. In addition, a full implementation procedure of the PiReCon-VVC method is introduced to ensure enhanced inverter reliability.

4.5.1 Stochastic Convex Optimisation Model of PiReCon-VVC

A stochastic optimisation model of the PiReCon-VVC method is formulated as below.

$$\underset{P_{k,t}^{inv}, Q_{k,t}^{inv}}{\text{Min}} \{\sum_{sc \in SC} \rho_{sc} (P_{sc}^{net,loss} + P_{sc}^{curt,loss}) + \sigma^{(n)} \sum_{t \in T} \sum_{k \in K} s_{k,t}\} \tag{4.43}$$

s.t.

$$\text{(4.6), (4.7), (4.13)-(4.18), (4.21)-(4.23)},\ \forall k, t, sc \tag{4.44}$$

$$\left\| \begin{matrix} P_{k,t}^{inv} \\ Q_{k,t}^{inv} \end{matrix} \right\|_2 \le S_{k,t}, \forall k, t \tag{4.45}$$

$$Z_{k,t} = 2P_{k,t}^{inv(n)} P_{k,t}^{inv} - \left(P_{k,t}^{inv(n)}\right)^2 + 2Q_{k,t}^{inv(n)} Q_{k,t}^{inv} - \left(Q_{k,t}^{inv(n)}\right)^2 + s_{k,t}, \forall k, t \tag{4.46}$$

$$\left\| \begin{matrix} 2S_{k,t} \\ 1 - Z_{k,t} \end{matrix} \right\|_2 \le 1 + Z_{k,t}, \forall k, t \tag{4.47}$$

$$s_{k,t} \ge 0, \forall k, t \tag{4.48}$$

$$-\xi \cdot S_k^{cap} \le S_{k,t} - S_{k,t-1} \le \xi \cdot S_k^{cap}, \forall k, t \tag{4.49}$$

$$0 \leq S_{k,t} \leq S_k^{cap}, \forall k, t \tag{4.50}$$

$$\left\{\left(P_{k,t,sc}^{PV,m}, P_{k,t,sc}^{L}, Q_{k,t,sc}^{L}\right), \rho_{sc}\right\} \in \Psi \tag{4.51}$$

Constraint (4.44) indicates that the corresponding constraints are modified for each bus, each time slot and each scenario. Constraints (4.45)-(4.50) are the proposed inverter reliability constraints with apparent power smoothing. Herein, the non-convexity of the original model with (4.8) is tackled by the developed penalty CCP with constraints (4.45)-(4.48) and the penalty term in objective function (4.43). Moreover, the uncertain PV MPPT power outputs and loads are modeled as representative uncertainty scenarios in a set Ψ as (4.51).

This optimisation model is solved iteratively via the developed penalty CCP until converging on the termination criterion.

4.5.2 Implementation of PiReCon-VVC

The proposed PiReCon-VVC method with the inverter power smoothing scheme is implemented via a central dispatch manner. The implementation process can be described by the following three key steps. Firstly, the proposed PiReCon-VVC optimisation problem is formulated with the inverter reliability constraints and system-wide information. Secondly, the optimisation problem is solved, and the optimal setpoint decisions of inverter var output and PV curtailment over a dispatch interval are obtained. Thirdly, the signals of optimal setpoint decisions are sent to the inverters in the distribution network, and the inverters change the apparent power outputs to the optimised setpoints. By doing so, both central VVC and inverter power smoothing can be done simultaneously.

To guarantee long-term efficient inverter power smoothing, this chapter applies a rolling-horizon based implementation scheme. First, given an optimisation horizon that covers a fixed number of operation time slots, the proposed PiReCon-VVC method is applied to obtain the optimal inverter setpoint decisions. Then, with the proceeding of each operation time slot, new optimisation horizons are formed and the proposed method continues to be applied. The optimised inverter apparent power output at the first time slot of current optimisation horizon is used as the initial apparent power (i.e., $S_{k,0}$ in (4.49)) of the next horizon, thus guaranteeing long-term consistent power smoothing. This implementation scheme is demonstrated in Figure 4.4.

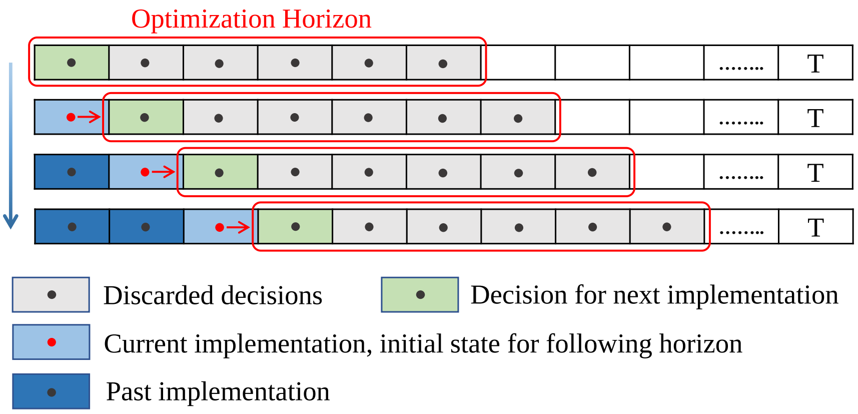

Figure 4.4 Rolling horizon-based implementation scheme.

With the rolling-horizon based implementation, the proposed PiReCon-VVC method can be implemented in practice as illustrated in Figure 4.5.

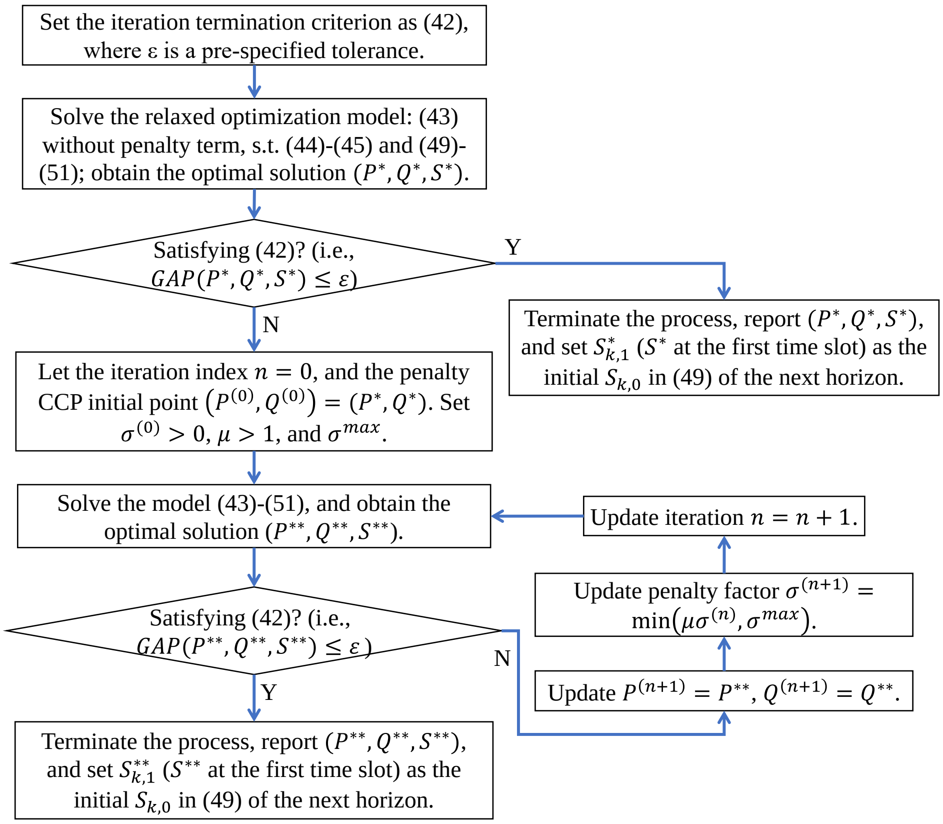

Figure 4.5 Implementation procedure of PiReCon-VVC method for each horizon.

4.6 Case Study

4.6.1 Test System Description

In this chapter, a modified 33-bus distribution network is used to verify the proposed PiReCon-VVC method, and the network parameters can be found in [91]. In this network, PVs are installed at 12 buses. The network topology and the PV locations are demonstrated in Figure 4.6. Each PV is the aggregation of 100 individual PV systems with a total power capacity of 500 kW. The total PV power capacity is about 160% of the peak loads, presenting a high PV penetration case. Besides, the associated inverter capacity of individual systems is oversized by 10% to 5.5 kVA to allow more var compensation. It is noted that the optimal allocation (placement and size) of PV systems, considering practical factors such as location availability, solar irradiance strength, capital cost, connection points and network operating limits, is out of this chapter's scope. More information of PV allocation can be found in [132].

The root bus voltage is set as 1 p.u., and the allowed range of bus voltages is [0.95, 1.05] p.u. In this chapter, the length of inverter operation time slot t is set as one hour, and the optimisation horizon is set as 6 hours. Moreover, the proposed PiReCon-VVC method is implemented for one year for PV inverter reliability analysis.

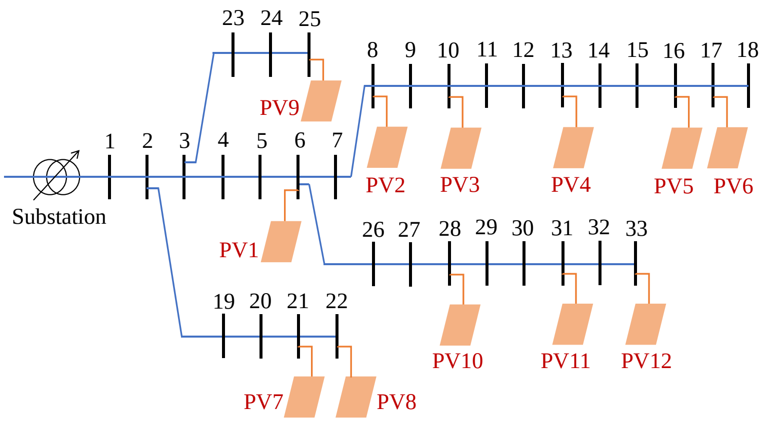

Figure 4.6 Network topology of test system.

In this chapter, the PV inverter reliability is assessed via lifetime evaluation of the IGBT modules, and the detailed lifetime evaluation method as well as the device parameters can be found in [79]. Besides, the one-year hourly real-time temperature records in Chicago from December 2016 to November 2017 [95] are used as the ambient temperature data for inverter reliability analysis. It is assumed that the solar irradiance and ambient temperature are the same across the whole test system, resulting in no geographic impacts on PV inverter reliability. It is noted that the reliability models used for inverter lifetime evaluation are mature models with the hardware validation in power electronics.

For the stochastic programming, Monte Carlo Sampling (MCS) is used to generate 2000 initial uncertainty realisation scenarios of PV power generation and loads. Gaussian distribution is applied to characterise the uncertainty realisations with the historical PV real-time profiles from [107] and the one-year typical load profiles from IEEE Reliability Test System-1996 [94]. Then, a backward scenario reduction method [104] is utilised to reduce the initial scenarios into 20 representative scenarios with their assigned occurrence probabilities. The 20 representative scenarios form the scenario set Ψ in (4.51).

Regarding the penalty CCP, the convergence tolerance $\varepsilon = 10^{-7}$ in (4.42), and the penalty parameters $\sigma^{(0)} = 0.1$, $\mu = 2$, $\sigma^{max} = 100$ in Algorithm 4.1.

It is worth noting that other test systems or parameter settings (PV location and size, operation time length, network operating limits, etc.) can also be used without affecting the effectiveness of the proposed VVC method.

Numerical simulations are carried out on a 64-bit PC with 3.20-GHz CPU and 16-GB RAM on the MATLAB platform. The proposed optimisation problem, which is a CCP-based convex problem, is iteratively solved by GUROBI solver [85].

4.6.2 VVC Optimisation Result

In this test, simulations are conducted with different settings of the power smoothing factor ξ, to verify the performance of the proposed PiReCon-VVC method.

By solving the PiReCon-VVC model (4.43)-(4.51), the inverter active and reactive power outputs of all the PVs are optimised. Figure 4.7 demonstrates the one-year inverter reactive power outputs of PV 4, with ξ as 100% and 20% respectively. ξ as 100% means that the VVC is fully performed without the inverter power smoothing constraints, i.e., the full-VVC case. Note that the positive values of reactive power mean power injection to the network, while negative ones mean absorption.

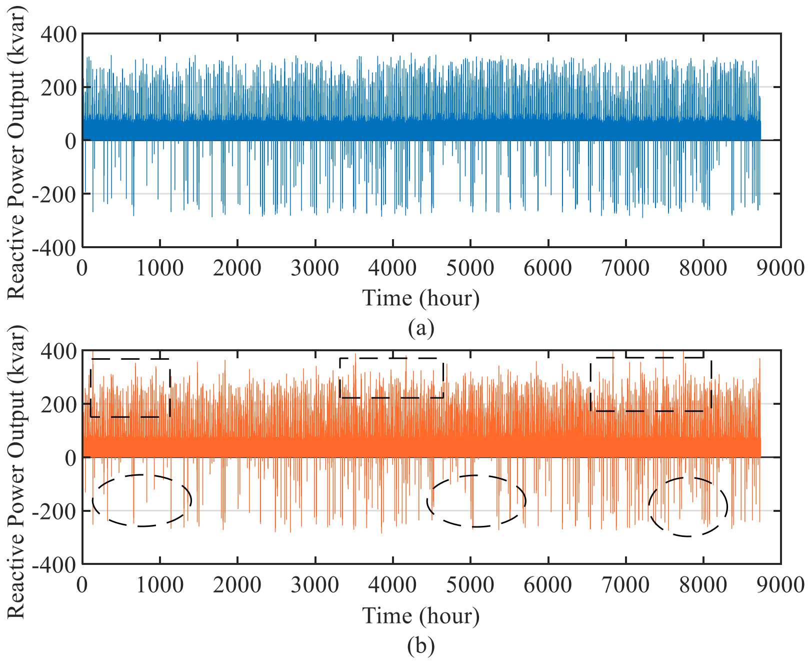

Figure 4.7 One-year reactive power outputs of PV 4: (a) Full VVC (ξ=100%); (b) PiReCon-VVC with ξ=20%.

Compared to the full-VVC case in Figure 4.7 (a), the PV inverters with PiReCon-VVC in Figure 4.7 (b) are utilised to provide some additional reactive power injection for power smoothing, as indicated in the rectangles, and this usually happens during the valleys of inverter apparent power. On the other hand, the inverter reactive power absorption is reduced, as shown in the circles. This is because the reactive power absorption in the VVC usually occurs when the PV power generation is high, leading to the peaks of inverter apparent power. Thus, the less reactive power absorption associated with PV curtailment can effectively reduce the inverter apparent power peaks. This verifies the effectiveness of the proposed PiReCon-VVC method for inverter apparent power smoothing.

Additionally, the one-day inverter apparent power profiles of PV 4 with different ξ values, compared with the no-VVC case, are shown in Figure 4.8.

It can be seen from Figure 4.8 that prompt var compensation is provided when the PV active power outputs are low, while the PV outputs during PV generation peaks are curtailed. Therefore, the inverter apparent power output is efficiently smoothed by the proposed PiReCon-VVC method. Moreover, the inverter apparent power profile with ξ as 20% is smoother than that with 30%, and this verifies the effectiveness of the proposed power smoothing factor.

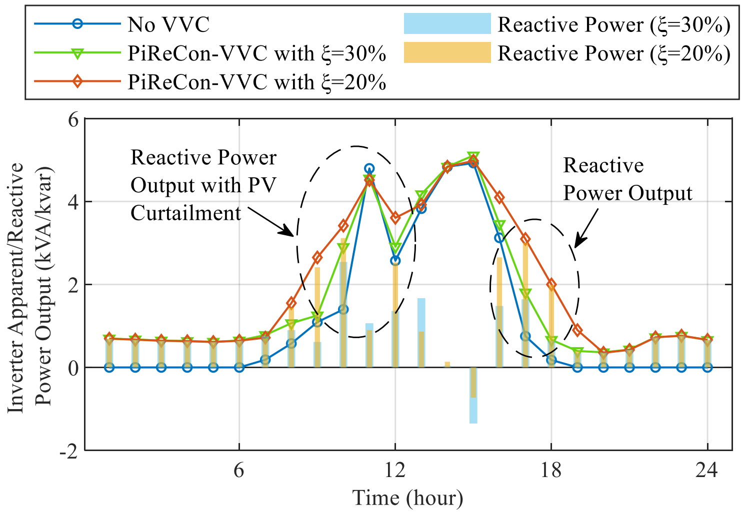

Figure 4.8 Inverter apparent/reactive power profiles of PV 4 (on Day 16).

4.6.3 Inverter Reliability Analysis Result

With the optimised inverter power outputs and calculated power loss, the IGBT junction temperature can be obtained from its thermal model. Then, a Rainflow counting technique [69] is applied to transfer the IGBT junction temperature profile into a number of regulated thermal cycles. Each cycle has its own value of junction temperature variation ΔT_j, which is a key factor for inverter lifetime evaluation. Figure 4.9 illustrates the Rainflow counting results of ΔT_j at PV 4 under different cases.

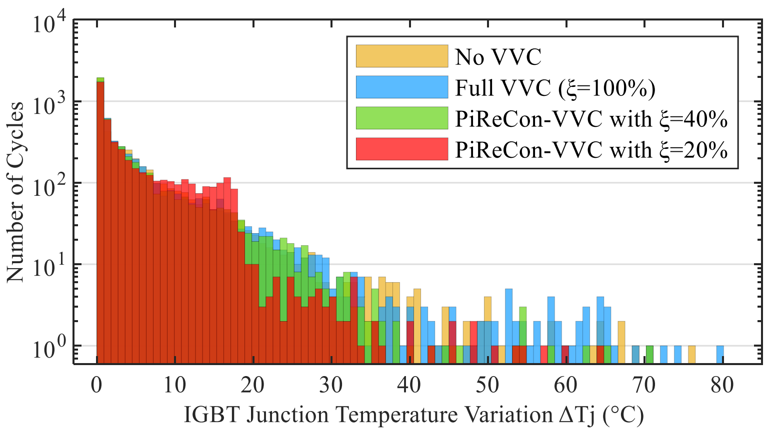

Figure 4.9 IGBT thermal analysis results of inverters at PV 4.

Compared to the no-VVC case, the IGBT junction temperature variation under the full-VVC case is increased due to the additional use of PV inverters for var compensation. However, with the PiReCon-VVC method, the temperature variation is effectively reduced by the proposed inverter reliability constraints for power smoothing. Besides, a lower power smoothing factor can achieve better performance in reduction of the junction temperature variation.

The inverter lifetime evaluation is then conducted based on the IGBT life model [116]. The inverter lifetimes with different ξ values at selected PVs are demonstrated in Figure 4.10.

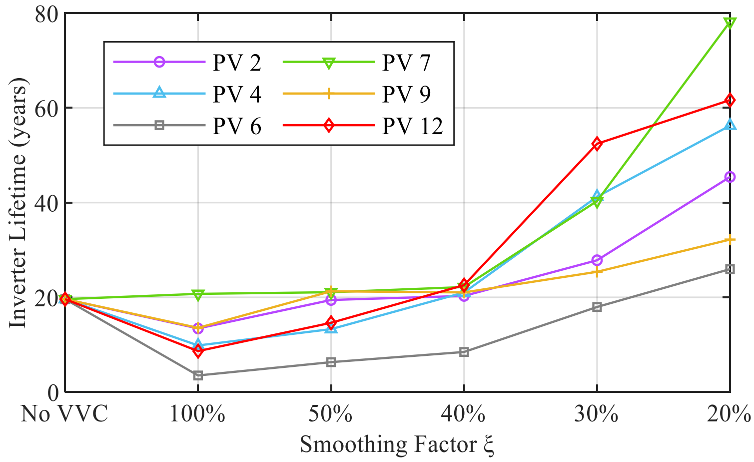

Figure 4.10 Inverter lifetimes based on IGBT lifetime evaluation with different ξ values at selected PVs.

In this figure, due to the same PV output profile and ambient temperature, the inverter lifetimes without VVC at all the PVs are calculated as the same 19.6 years. Under the full-VVC case (ξ=100%), almost all the inverter lifetimes are reduced, due to the severer junction temperature variation caused by the inverter use for VVC. When applying the proposed PiReCon-VVC method with inverter power smoothing, the inverter lifetime reduction can be efficiently mitigated. Especially when the power smoothing factor ξ approaches 30%, the inverter lifetimes are significantly enhanced, which can be even higher than those under the no-VVC case.

For the different locations, the impacts of the full VVC method (ξ=100%) on the inverter lifetimes are quite different. The PVs at the ends of long feeders, such as PVs 6 and 12, tend to have short lifetimes, due to the more VVC efforts for bus voltage regulation. In comparison, the inverter lifetime of PV 7 which is at a short feeder with a light load is not seriously impacted by the full VVC method, and its lifetime can be increased when ξ is set to be a low percentage, such as 30%.

4.6.4 Validation of Computing Efficiency

In this chapter, the proposed PiReCon-VVC method is implemented for one year. In each optimisation horizon, the PiReCon-VVC optimisation problem is iteratively solved by the developed penalty CCP until convergence. Via simulations, the convergence of the penalty CCP is validated, i.e., the gap can be always reduced into the specified tolerance. Figure 4.11 visualises the convergence process of the penalty CCP with different power smoothing factors for one optimisation horizon.

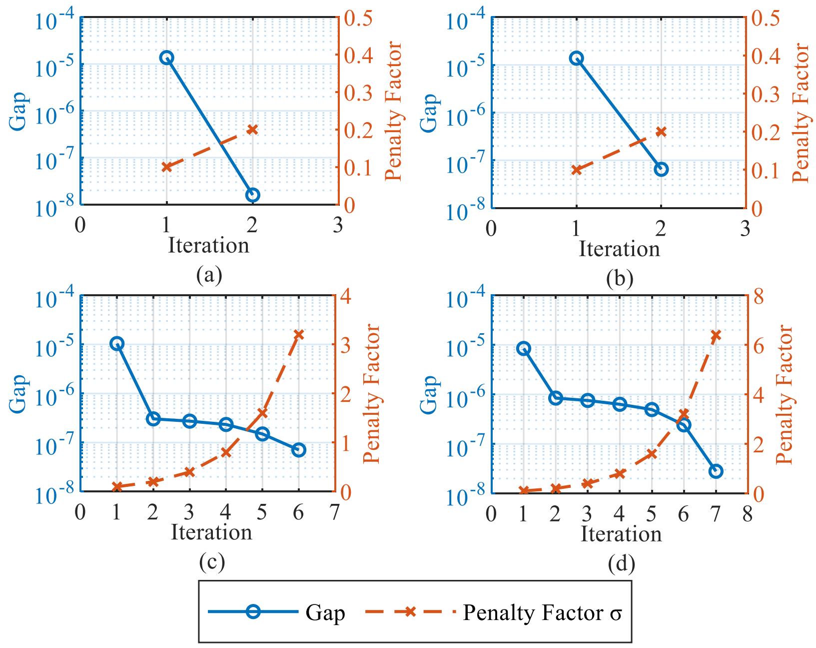

Figure 4.11 Convergence process of penalty CCP with power smoothing factor ξ as: (a) 50%; (b) 40%; (c) 30%; (d) 20%.

Figure 4.11 demonstrates that the penalty CCP can quickly converge at the stopping criterion when ξ is set as 50% and 40%, and for ξ at or below 30%, it takes more iterations for the penalty CCP to converge.

Besides, the average iterations and solving time of all the optimisation horizons for each ξ value are calculated and presented in Table 4-I. It is clearly demonstrated that, the lower ξ causes the more CCP iterations. Furthermore, the average solving time increases obviously when ξ decreases from 40% to 20%. Thus, it can be inferred that a ξ lower than 20% requires exhausting computing efforts. Regarding the one-hour operation interval, all the solving time is fully compatible for practical online use.

Table 4-I Computing Efficiency Results

Power Smoothing Factor ξ	Average Iterations	Average Solving Time (s)
50%	1.09	19.3
40%	1.44	18.5
30%	2.22	21.2
20%	3.51	48.3

4.6.5 Comparison with Conventional Solution Methods

In this subchapter, the use of the developed penalty CCP method is justified by comparison with other conventional solution methods.

Firstly, compared to the conventional CCP method, the motivation of the developed penalty CCP method is justified with the solution success rate which represents the ratio of the horizons where a solution can be obtained to the total horizons. The comparison results are shown in Table 4-II.

Table 4-II Solution Success Rate Comparison

Power Smoothing Factor ξ	Solution Success Rate	
	Conventional CCP	Penalty CCP
50%	83%	100%
40%	80%	100%
30%	23%	100%
20%	7%	100%

Due to the limitations explained in Chapter 4.4.2, the conventional CCP method cannot solve all the problems and it has a significantly reduced solution success rate with the decrease of the power smoothing factor. In comparison, the penalty CCP method with the slack variable can always guarantee a solution for all the horizons.

Then, the average solving time and the average gap (given by (4.42)) are compared among the developed penalty CCP method, the spatial branching algorithm [133], and the off-the-shelf Interior Point Optimiser (IPOPT). The spatial branching algorithm, which is also used in the latest version (v. 9.1.2) of the advanced GUROBI solver, as well as the IPOPT, are widely used for solving the non-convex quadratically constrained optimisation problems. The comparison results are shown in Table 4-III.

Table 4-III Comparison Between Penalty CCP and Conventional Solution Methods

Power Smoothing Factor ξ	Average Solving Time (s)			Average Gap		
	Spatial Branching	IPOPT	Penalty CCP	Spatial Branching	IPOPT	Penalty CCP
50%	66.5	24.6	19.3	4.87×10^{-7}	1.78×10^{-5}	1.80×10^{-8}
40%	64.8	30.3	18.5	5.08×10^{-7}	1.44×10^{-5}	2.21×10^{-8}
30%	56.8	29.5	21.2	5.30×10^{-7}	1.26×10^{-5}	2.93×10^{-8}
20%	59.6	36.8	48.3	4.40×10^{-7}	1.12×10^{-5}	3.54×10^{-8}

In regards of the average solving time, the penalty CCP has a better performance than the other two solution methods when ξ is no less than 30%. With ξ as 20%, the IPOPT has less solving time than the penalty CCP method. However, the average gaps of the IPOPT are much larger than those of the developed penalty CCP method. Thus, the comparison results verify the high computing efficiency of the developed penalty CCP method in solving the non-convex quadratically constrained optimisation problems.

4.6.6 Trade-off between Lifetime and Energy Loss

The minimum and average inverter lifetimes of all PVs, as well as the one-year energy losses are compared in Table 4-IV for different values of the power smoothing factor ξ. To achieve efficient sensitivity analysis on ξ, the candidate setting values of ξ are extended by using a smaller step size of 5%, between 40% and 20%. Additionally, 80% is also used to test the performance with a large power smoothing factor. Note that the value of ξ as 100% means the full-VVC case without any power smoothing constraint.

Compared to the no-VVC case, the full VVC method significantly reduces the network energy loss, but the excessive use of PV inverters for var compensation leads to the heavily shortened inverter lifetime. On the other hand, the proposed PiReCon-VVC method provides high efficiency in inverter lifetime enhancement. Especially when the power smoothing factor ξ equals to 35% or lower, both inverter minimum and average lifetimes increase remarkably. However, as ξ decreases, both the network energy loss and the PV curtailment energy loss tend to rise, leading to compromised economic benefits.

Table 4-IV Inverter Lifetime and Energy Loss Results

Power Smoothing Factor ξ		Minimum Lifetime (at PV No.) (years)	Average Lifetime of All PVs (years)	One-Year Energy Loss (MWh)		
				Network Loss	PV Curtailment	Total Loss
No VVC		19.6 (All)	19.6	769.82	0	769.82
VVC	100% (Full VVC)	3.5 (PV 6)	14.5	518.21	0	518.21
	80%	4.3 (PV 6)	15.1	519.82	0	519.82
	50%	6.3 (PV 6)	19.5	525.18	0.84	526.02
	40%	8.5 (PV 6)	22.4	528.94	2.03	530.97
	35%	13.1 (PV 5)	26.1	533.47	5.7	539.17
	30%	16.7 (PV 5)	36.3	536.53	12.13	548.66
	25%	17.8 (PV 5)	40.6	548.44	23.51	571.95
	20%	15.5 (PV 10)	43.5	552.36	43.07	595.43

Based on the above analysis as well as the computing efficiency results in Table 4-I, it is concluded that with the decreasing ξ, the proposed PiReCon-VVC method can efficiently enhance the PV inverter lifetime at a cost of the increased energy losses and the affected computing efficiency. To this end, it is expected to select a proper power smoothing factor for making a trade-off decision. For this test system. it is suggested to set ξ as 30% or 35%, which can make a fair trade-off among inverter reliability enhancement, system energy loss reduction and guarantee of computing efficiency.

Alternatively, quantitative selection criteria of the power smoothing factor can be set according to the user requirements. For example, if PV owners require the inverters to have a minimum lifetime of 10 years, then the power smoothing factor should be set as 35%, which meets the lifetime requirement while having the lowest energy loss and the highest computing efficiency.

4.7 Conclusion

Considering the importance of PV inverter reliability in VVC-featured ADNs, this chapter proposes a PiReCon-VVC method with inverter power smoothing under uncertainties. Based on the inverter reliability analysis, new reliability constraints are proposed with a power smoothing factor to constrict the inverter apparent power variation and a PV curtailment scheme to facilitate the power smoothing. Then, with the proposed reliability constraints, a scenario-based stochastic VVC optimisation model is formed to minimise the power losses. Moreover, a CCP programming method is developed to solve the proposed non-convex PiReCon-VVC optimisation problem.

Via the comprehensive case study, the simulation results verify that the proposed PiReCon-VVC method can efficiently minimise the power losses, while guaranteeing or even enhancing the PV inverter reliability. Besides, the developed CCP method is validated with high computing efficiency.

Chapter 5 A PARETO FRONT ANALYSIS METHOD FOR PV INVERTER BASED VOLT/VAR CONTROL CONSIDERING INVERTER LIFETIME

In Chapters 3 and 4, new PV inverter based VVC optimisation models with developed reliability constraints using a restriction factor and a smoothing factor for inverter apparent power regulation are proposed. In this chapter, a novel multi-objective PV inverter based VVC optimisation model which incorporates inverter apparent power into the objective function is proposed, and a Pareto front analysis method is developed for the proposed model to maintain satisfactory inverter lifetime. Firstly, the reliability of PV inverters is analysed via lifetime evaluation of the critical components inside inverters, and the long-term impact of VVC operation on PV inverter reliability is identified. Secondly, a multi-objective PV inverter based VVC optimisation model is proposed with a weighting factor to balance the minimisations of both inverter apparent power output and network power loss. Thirdly, a Pareto front analysis method is developed to visualise the impacts of the weighting factor on VVC performance and inverter reliability, so that a proper weighting factor can be determined to realise minimised network power loss with expected inverter lifetime. The effectiveness of the proposed VVC optimisation model and the Pareto front analysis method is verified in case study.

5.0 Nomenclature

A. Sets and Indices

B	Set of network branches.
i	Index of IGBT thermal cycles.
j, k, l	Index of network buses.
$J(k)$	Set of parent buses of bus k.
K	Set of network buses.
$L(k)$	Set of child buses of bus k.

n Index of capacitor ripple current frequencies.

$SC,\ sc$ Set and index of uncertainty scenarios.

$T,\ t$ Set and index of operating time intervals.

B. Parameters

1) DC-Link Capacitor Parameters

$ESR(f_n)$ Equivalent series resistance under frequency f_n (Ω).

f_{sw} Switching frequency (Hz).

H_b Base lifetime (hours).

I_{RP} RMS value of capacitor's ripple current (A).

i_P Inverter output sinusoidal current amplitude (A).

P_{CA}^{loss} DC-link capacitor power loss (W).

T_a Ambient temperature (K).

$T_{co},\ T_c$ Capacitor core and case temperature (K).

T_m Maximum rated core temperature of capacitor (K).

V_{AC} AC voltage RMS value (V).

V_{DC} Applied DC-link voltage (V).

V_{DCr} Rated DC voltage of capacitor (V).

$Z_{th(co-c)}$ Capacitor thermal impedance from core to case (K/W).

$Z_{th(c-a)}$ Capacitor thermal impedance from case to ambient (K/W).

2) Network Parameters

I_{jk}^{cap} Current capacity of the branch line from bus j to bus k (A).

$P^{net,loss}$ Network power loss on the branch lines (W).

$r_{jk},\ x_{jk}$ Resistance/Reactance of the branch line from bus j to bus k (Ω).

S_k^{cap} Inverter apparent power capacity at bus k (VA).

$\underline{V}_k,\ \overline{V}_k$ Lower and upper limits of voltage at bus k (p.u.).

Φ Normalisation process for two objectives by using Utopian and Nadir points.

θ	Weighting factor step size for sensitivity analysis.
ω	Weighting factor for the multi-objective VVC model.
ω_A	Weighting factor satisfying average inverter lifetime threshold.
ω_M	Weighting factor satisfying minimum inverter lifetime threshold.

C. Variables

$I_{jk,t}$, $i_{jk,t}$	Current and its square value of the branch line from bus j to bus k at time t (A,A^2).
$P_{jk,t}$,$Q_{jk,t}$	Active/Reactive power through the branch line from bus j to bus k at time t (W,var).
$P_{k,t}^{L}$, $Q_{k,t}^{L}$	Uncertain active/reactive load at bus k at time t (W,var).
$P_{k,t}^{PV}$	Uncertain PV active power output at bus k at time t (W).
$Q_{k,t}^{inv}$	Inverter reactive power output at bus k at time t (var).
$S_{k,t}$	Inverter apparent power output at bus k at time t (VA).
$S_{k,t}^{sl}$	Slack variable indicating maximum allowed inverter apparent power output at bus k at time t (VA).
$V_{k,t}$, $v_{k,t}$	Voltage and its square value of bus k at time t(p.u.).
ρ	Occurrence probability of uncertainty scenarios.

5.1 Introduction

5.1.1 Background and Motivation

Penetration of photovoltaics (PVs) in distribution networks has been growing dramatically in recent years. The number of rooftop PV installations in Australia had reached 3 million by November 2021 [2]. The rapid uptake of solar energy contributes to a clean, sustainable and affordable energy future. However, the increasing PV penetration has brought serious technical challenges, especially voltage rises and fluctuations. Study in [13] points out that the high PV penetration in distribution networks can cause undesired reverse power flow and over-voltage, and thus impaired power quality for customers.

On the other hand, PV inverters have great potential in providing flexible and responsive volt/var control (VVC), which is highly promising for the distribution networks [43]. Using PV inverters to support reactive power has been advocated by the IEEE 1547.8 working group [47]. In Australia which has the very high rooftop PV penetration, the AS/NZS 4777.2 standard [15] has also specified that PV inverters should be able to automatically inject and absorb reactive power based on a droop curve when there is voltage excursion.

However, the vulnerable nature of the key components inside a PV inverter, such as the DC-link capacitor, has posed a critical concern to the inverter operational reliability, especially when the inverter based VVC is applied. Ref. [62] indicates that the inverter is the most fragile subsystem in a PV system due to vulnerability and complexity of the power electronic components. In addition, the work [116] verifies the remarkably negative impact of the VVC function on PV inverter lifetime. As the operational reliability of PV inverter is essential for both reliable VVC support and sustainable PV energy utilisation, it is imperative to consider the inverter lifetime when developing PV inverter based VVC methods.

5.1.2 Literature Review

In literature, various advanced PV inverter based VVC methods are developed to address the voltage issues caused by high PV penetration. The work [60] develops a multi-objective adaptive VVC model for minimising both network power loss and voltage deviation, while ref. [50] further proposes a distributed online VVC method. In [49], a two-stage VVC method, which firstly selects partial PV inverters to provide VVC and then dispatches optimal reactive power, is developed. Furthermore, ref. [52] develops a three-stage robust VVC method which coordinates multiple VVC devices from both central and local control perspectives. The work [134] proposes an event-driven predictive approach for real-time VVC optimisation associated with a two-level local adaptive voltage droop control algorithm. The work [135] presents a multistage coordination method of VVC and conservation voltage reduction, by incorporating inverters and soft open points. A VVC method coordinating different phases with unbalanced PV integration is proposed in [53]. Recently, the work [136] proposes a hierarchically coordinated inverter based VVC method considering distribution network voltage stability. However, in the above literature, the PV inverter operational reliability is not investigated or considered in the VVC optimisation models.

The vulnerable nature of PV inverters, as well as the seriously negative impacts of VVC on the inverter lifetime, highlight the significance of considering PV inverter operational reliability in the VVC development. To this aim, it is needed to understand inverter failure mechanism and effectively incorporate it into VVC modelling for a purpose of enhancing inverter operational reliability.

It is verified in the literature that the operational reliability of a PV inverter is determined by the lifetime of power electronic components inside the inverter, such as power devices and capacitors [65]. For the power devices, e.g., insulated gate bipolar transistors (IGBTs), the junction temperature cycling can have critical impacts on their lifetime, and efficient restriction on junction temperature variation can contribute to enhancing the power device reliability [137]. On the other hand, studies [118] and [138] indicate that the DC-link capacitor, which is parallel with the inverter DC input to arrest current and voltage harmonics, usually has the shorter lifetime than the power devices due to its harsh working conditions and high susceptibility. Thus, the DC-link capacitor most likely determines an inverter operational reliability and maintenance frequency. It is verified in [139] that the DC-link capacitor lifetime is mainly affected by its thermal loading, i.e., core temperature, and its lifetime dependency on core temperature can be effectively presented by the capacitor lifetime model [73] [74]. To enlarge the capacitor lifetime, it is expected to control the core temperature. Moreover, ref. [140] provides a thermal model which calculates the core temperature of a capacitor based on the power loss dissipated on it. Therefore, the reliability models of the DC-link capacitor, including the lifetime, thermal, and power loss models, are crucial for analysing the inverter operational reliability.

It would be sensible to consider the DC-link capacitor reliability models in VVC optimisation problems, such that the inverter operational reliability can be ensured. However, it is remarkably challenging that these reliability models contain non-convex or high-dimensional terms, making the VVC optimisation problems unsolvable. Thus, it is imperative to develop an approach which can efficiently consider and address the DC-link capacitor reliability models in VVC modelling.

The capacitor lifetime model implies that effective reduction of the core temperature can improve the DC-link capacitor lifetime, thus benefiting the inverter operational reliability. Reducing the core temperature for improving the capacitor reliability for a single inverter has been discussed in [141] [142] without considering network operating conditions. Moreover, the recent work [79] develops a reliability constraint to restrict the inverter apparent power output for a VVC optimisation model. This work considers system-wide information of the network and efficiently limits the core temperature for enhancing the inverter operational reliability. However, this VVC optimisation model requires PV power generation curtailment to fulfill the reliability constraint, leading to compromised end-user benefits. Thus, potential methods of incorporating the core temperature reduction into VVC modelling remain to be further investigated.

5.1.3 Contributions

Considering the above issues, this chapter proposes a multi-objective PV inverter based VVC optimisation model and a Pareto front analysis method to minimise the network power loss while achieving expected inverter lifetime.

This chapter demonstrates three main contributions as below.

1) The PV inverter operational reliability is analysed based on lifetime evaluation of the DC-link capacitor. Then, the long-term impact of VVC on the inverter operational reliability is identified as an indirect correlation between inverter apparent power output and DC-link capacitor lifetime.

2) A multi-objective PV inverter based VVC optimisation model with a weighting factor is proposed to simultaneously minimise both the network power loss and inverter apparent power output. This work is the first in the literature to address inverter operational reliability in the objective function of a VVC optimisation model. Then, a stochastic optimisation method with second-order conic programming (SOCP) is used to obtain a solution under uncertainties.

3) A Pareto front analysis method is proposed to select a proper value for the weighting factor, through a numerical simulation of long-term VVC optimisation. With the selected weighting factor, the proposed VVC optimisation model can achieve efficient network power loss reduction with expected inverter lifetime.

5.1.4 Chapter Organisation

The remainder of this chapter is organised as below. Chapter 5.2 presents the PV inverter reliability analysis method considering DC-link capacitor lifetime. Chapter 5.3 investigates the long-term impact of VVC functions on PV inverter lifetime. In Chapter 5.4, a multi-objective PV inverter based VVC optimisation model with apparent power minimisation is formulated. Chapter 5.5 develops a Pareto front analysis method for the selection of a proper weighting factor in the objective function. Case study and conclusion are given in Chapters 5.6 and 5.7, respectively.

5.2 PV Inverter Reliability Analysis Considering DC-Link Capacitor Lifetime

5.2.1 Topology of PV Inverter

PV inverters are critical power electronic devices for DC-to-AC power conversion as well as supporting the power grid with VVC functions. This chapter applies a typical single-phase two-stage PV inverter for the provision of the VVC function, and the detailed information for this type of inverter, as well as its topology and schematic diagram, can be found in Chapter 3.2.1. This type of inverter is commonly used in small-size distributed PV systems such as rooftop PVs, which are compatible with being aggregated as a large inverter fleet to provide VVC functions for the power grid [52].

5.2.2 Reliability Analysis Models of DC-Link Capacitor

Power devices and the DC-link capacitor are usually the two most fragile components inside a PV inverter, and their lifetimes are two critical factors for inverter reliability assessment [65]. In fact, the lifetimes of power devices and DC-link capacitors are highly dependent on their types and models. In Chapter 3, an IGBT and an aluminum electrolytic capacitor are used as the power device and DC-link capacitor for inverter reliability analysis, and the simulation results verified that the lifetime of the aluminum electrolytic capacitor is lower than the IGBT when used for the VVC function. This chapter applies an aluminum electrolytic capacitor and it is assumed that the inverter operational reliability is determined by the lifetime of the DC-link capacitor [143].

The PV inverter operational reliability can be assessed according to the lifetime evaluation of the DC-link capacitor, via the following steps. Firstly, based on the inverter operating conditions, the capacitor power loss model is applied to obtain the power loss on the capacitor. Secondly, with the obtained power loss, the capacitor thermal model is used to calculate the capacitor core temperature. Thirdly, the capacitor lifetime can be evaluated by utilising the lifetime model which describes the dependency of the capacitor lifetime on its core temperature.

Based on Chapter 3.2.4, detailed reliability analysis models of the DC-link capacitor are presented as below.

$$P_{CA}^{loss} = \sum_{n} \{[I_{RP}(f_n)]^2 \cdot ESR(f_n)\} \tag{5.1}$$

$$I_{RP}(f_1) = \frac{V_{AC} i_P}{2V_{DC}} \tag{5.2}$$

$$T_{co} = Z_{th(co-c)} P_{CA}^{loss} + T_c \tag{5.3}$$

$$T_c = Z_{th(c-a)} P_{CA}^{loss} + T_a \tag{5.4}$$

$$H_f = H_b \cdot \left(4.3 - 3.3 \frac{V_{DC}}{V_{DCr}}\right) \cdot 2^{((T_m - T_{co})/10)} \tag{5.5}$$

$$C_{LF} = \sum_{t \in T} \frac{h_t}{H_{f,t}} \tag{5.6}$$

$$LF = \frac{T}{C_{LF}} \tag{5.7}$$

Eq. (5.1) and (5.2) indicate the capacitor power loss model, where P_{CA}^{loss} is the capacitor power loss, n denotes the index of the frequency of capacitor's current harmonics., $I_{RP}(f_n)$ denotes the root mean square (RMS) value of capacitor's ripple current under frequency f_n, and $ESR(f_n)$ denotes the capacitor ESR value. i_P represents the amplitude of inverter output current. V_{AC} and V_{DC} are the AC output voltage (RMS value) and the applied DC-link voltage of the inverter, respectively. Thus, the power loss of a capacitor is the accumulated power loss with different ripple currents over the entire frequency range. For a single-phase PV inverter, the second harmonic frequency and the PWM switching frequency are the two main components of the DC-side ripple current frequencies [101]. Thus, this chapter assumes that the capacitor's power loss is only affected by the ripple currents at these two frequency levels. The calculation of the ripple current under the PWM switching frequency is determined by various modulation schemes, the details of which can be found in [102]. Moreover, the ESR values under different frequency levels are usually provided by the device manufacturer.

Eq. (5.3) and (5.4) are the capacitor thermal model. Here, T_{co} and T_c denote the capacitor core temperature and case temperature, respectively, and T_a is the ambient temperature. $Z_{th(co-c)}$ and $Z_{th(c-a)}$ are the thermal impedance from the capacitor core to the case, and from the case to the ambient, respectively. The power loss caused by the ripple current dissipates from the capacitor core to the case, and then to the ambient. The thermal model of a typical aluminum electrolytic capacitor is illustrated in Figure 5.1(a). Using the Foster RC thermal model, the total thermal impedance can be calculated by thermal capacitances C_{th} and thermal resistances R_{th}, as shown in Figure 5.1(b). It is noted that the thermal capacitances C_{th} are used to reflect the thermal transients within seconds, while the thermal resistances R_{th} are mainly considered for steady-state thermal analysis with a longer time interval [72].

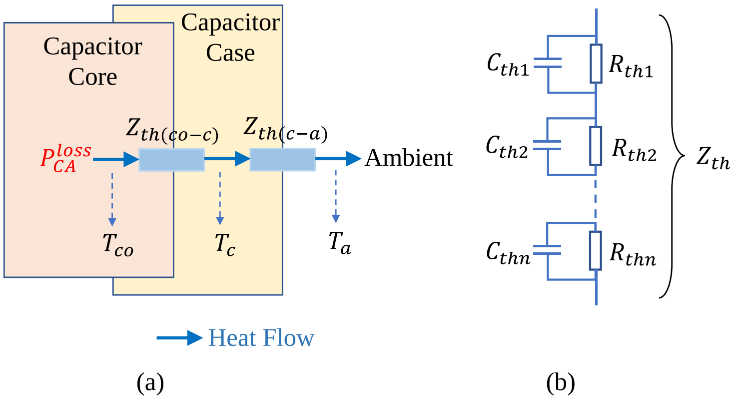

Figure 5.1 Capacitor thermal model: (a) heat flow of an electrolytic capacitor. (b) Foster RC thermal model.

Eq. (5.5)-(5.7) present the capacitor lifetime models. Here, H_f (calculated in hours) represents the capacitor's lifetime under a specific thermal/voltage stress level of T_{co} and V_{DC}. V_{DCr} and T_m are the rated DC-link voltage and the maximum core temperature of the capacitor, respectively. H_b is the capacitor's base lifetime. C_{LF} is the accumulated capacitor lifetime consumption over a specific operating timescale T, t is the index of inverter operating time slot within T, and h_t is the time (in hours) accumulated under the thermal/voltage stress level of T_{co} and V_{DC} through t. $H_{f,t}$ is the calculated lifetime (in hours) of the capacitor under this stress level, by (5.5). Note that the unit of capacitor lifetime LF is consistent with that of T. For example, if the adopted timescale is T years, the calculated DC-link capacitor lifetime is LF

years.

Based on the reliability models (5.1)-(5.7), the following insights can be drawn.

- Given a specific PWM modulation pattern, the capacitor power loss is in a positive correlation with the inverter output current.
- Under a given ambient temperature, the capacitor core temperature is in a strictly linear correlation with the capacitor power loss.
- Given a constant DC-link voltage, the capacitor's lifetime is in a negative correlation with the capacitor core temperature.

5.3 Long-Term Impact of VVC on Inverter Operational Reliability

Based on the insights above, it can be inferred that an increased PV inverter output current i_P can cause increased ripple current and power loss on the DC-link capacitor, leading to raised capacitor core temperature and thus reduced capacitor lifetime. Therefore, an indirect correlation can be identified between the PV inverter output current and its operational reliability.

The impact of VVC on inverter output current has been analysed in Chapter 3.2.5. Based on the analysis, the models detailing the relationship between VVC and inverter output current are presented below.

$$i_P = \frac{\sqrt{2}P^{PV}}{V_{AC}} \tag{5.8}$$

$$S = \sqrt{(P^{PV})^2 + (Q^{inv})^2} \tag{5.9}$$

$$i_P = \frac{\sqrt{2}S}{V_{AC}} \tag{5.10}$$

Eq. (5.8) calculates the inverter output current amplitude i_P without VVC functions, where P^{PV} denotes the PV active power outputs and V_{AC} is the inverter AC output voltage (RMS value) which can be regarded as constant. Eq. (5.9) and (5.10) calculate the i_P when a VVC function is applied on the inverter to provide an additional reactive power Q^{inv}, where S denotes the inverter apparent power output.

Comparing (5.10) with (5.8), it can be concluded that the VVC function can lead to increased PV inverter output current by increasing its apparent power output with var compensation. The long-term impact of the VVC function on the operational reliability of PV inverters is clearly illustrated in Figure 5.2.

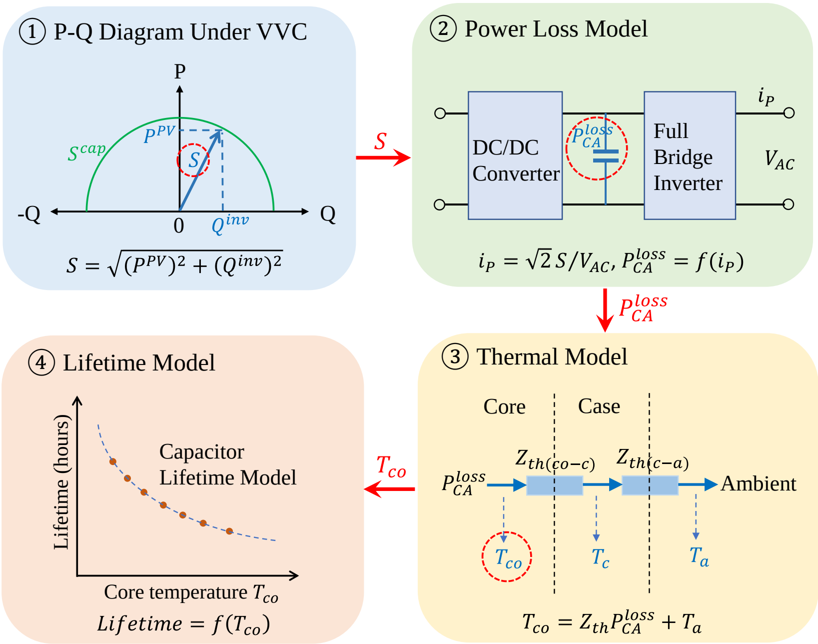

Figure 5.2 Long-term impact of the VVC function on PV inverter reliability considering DC-link capacitor lifetime.

It is seen that using PV inverters for VVC can raise the inverter apparent power output S and the DC-link capacitor power loss P_{CA}^{loss}. Further, the capacitor core temperature T_{co} is increased, and the capacitor lifetime is reduced due to the negative correlation. Thus, the inverter operational reliability is impaired.

Given the relationship between inverter apparent power output and its operational reliability, this chapter proposes to minimise the inverter apparent power output as an additional objective in a PV inverter based VVC optimisation model.

5.4 Multi-Objective VVC Optimisation

According to the VVC's impact on PV inverter reliability, this chapter proposes a multi-objective inverter based VVC optimisation model, incorporating the inverter apparent power S into the objective function. This model aims to guarantee the VVC performance in network power loss reduction and the operational reliability of the associated inverters.

The proposed model is formulated and solved via the following main steps. First, minimisation of S is involved in the optimisation model to enhance the PV inverter operational reliability. Second, a multi-objective PV inverter based VVC optimisation model is developed. Then, this chapter applies a second order conic programming (SOCP) method to reformulate the developed optimisation model into a solvable convex model. Last, a solution method based on scenario-based stochastic optimisation is applied to address the uncertainty issues of the PV power outputs and loads.

5.4.1 Minimisation of Inverter Apparent Power

To make sure the apparent power outputs of all the PV inverters in the network are efficiently minimised, this chapter introduces a slack variable S^{sl} which indicates the maximum allowed inverter apparent power output. A minimisation problem of the inverter apparent power with a corresponding constraint is proposed as follows.

$$\min_{Q_{k,t}^{inv}} \sum_{k,t} S_{k,t}^{sl} \tag{5.11}$$

$$\sqrt{\left(P_{k,t}^{PV}\right)^2 + \left(Q_{k,t}^{inv}\right)^2} \leq S_{k,t}^{sl} \leq S_k^{cap}, \forall k, t \tag{5.12}$$

Here, k and t denote the indices of the network buses and VVC operating time slots, respectively. $P_{k,t}^{PV}$ is the PV active power output at bus k during time slot t and $Q_{k,t}^{inv}$ denotes the inverter reactive power output at bus k during time slot t. S_k^{cap} denotes the capacity of inverter apparent power at bus k.

This chapter assumes that the PV inverters work in the MPPT mode, and no PV power curtailment is required for the proposed VVC optimisation model.

The proposed model (5.11)-(5.12) with the use of slack variable $S_{k,t}^{sl}$ can efficiently minimise the inverter apparent power output level across the network.

5.4.2 Multi-Objective VVC Optimisation Model

The aim of this chapter is to simultaneously minimise the network power loss and the inverter apparent power outputs, which can reduce utilities' operational costs and ensure the inverter operational reliability. The minimisation of the inverter apparent power outputs naturally reduces the inverter var outputs, affecting the VVC capability in network power loss reduction. Thus, these two minimisation objectives are conflicting. In this chapter, a classic weighted sum algorithm [60] is applied, which can convert the original multi-objective function into an equivalent single-objective function with a weighting factor.

With the weighted sum algorithm, a multi-objective VVC optimisation model is formulated as follows.

$$\min_{Q_{k,t}^{inv}} \left[(1-\omega) \cdot \Phi\left(P^{net,loss}\right) + \omega \cdot \Phi\left(\sum_{k,t} S_{k,t}^{sl} \right) \right] \tag{5.13}$$

s.t.

$$P^{net,loss} = \sum_{t \in T} \sum_{jk \in B} r_{jk} I_{jk,t}^2 \tag{5.14}$$

$$P_{k,t}^{PV} - P_{k,t}^{L} = \sum_{l \in L(k)} P_{kl,t} - \sum_{j \in J(k)} (P_{jk,t} - r_{jk} I_{jk,t}^2), \forall k, t \tag{5.15}$$

$$Q_{k,t}^{inv} - Q_{k,t}^{L} = \sum_{l \in L(k)} Q_{kl,t} - \sum_{j \in J(k)} (Q_{jk,t} - x_{jk} I_{jk,t}^2), \forall k, t \tag{5.16}$$

$$V_{k,t}^2 = V_{j,t}^2 - 2\left(r_{jk} P_{jk,t} + x_{jk} Q_{jk,t}\right) + (r_{jk}^2 + x_{jk}^2) I_{jk,t}^2, \forall jk, t \tag{5.17}$$

$$I_{jk,t}^2 = \frac{P_{jk,t}^2 + Q_{jk,t}^2}{V_{j,t}^2}, \forall jk, t \tag{5.18}$$

$$\underline{V}_k \le V_{k,t} \le \overline{V}_k, \forall k, t \tag{5.19}$$

$$0 \le I_{jk,t} \le I_{jk}^{cap}, \forall jk, t \tag{5.20}$$

$$\sqrt{\left(P_{k,t}^{PV}\right)^2 + \left(Q_{k,t}^{inv}\right)^2} \le S_{k,t}^{sl} \le S_{k}^{cap}, \forall k, t \tag{5.21}$$

In the objective function (5.13), due to the different scales between the network power loss and the inverter apparent power, Φ, which indicates a normalisation process, is introduced to normalise the two objectives by utilising the Utopian and Nadir points. Detailed normalisation process can be found in [60]. Besides, ω is the applied weighting factor that trades-off between the inverter apparent power output and the network power loss. $Q_{k,t}^{inv}$ is the control variable of the proposed optimisation model.

The network power loss is calculated by (5.14). Equations (5.15)-(5.18) present the well-established branch flow model for distribution networks. Here, j, k and l denote the network bus indices, and $J(k)$ and $L(k)$ denote the set of the parent buses and child buses of bus k, respectively. P_{jk}, Q_{jk} and I_{jk} are the active power, reactive power, and current flowing through the branch from bus j to bus k, respectively. $r_{jk}$and x_{jk} are the corresponding line resistance and line reactance of the branch. Furthermore, P_k^L, Q_k^L and V_k are the active load, reactive load and voltage at bus k, respectively. Constraints (5.19) and (5.20) indicate the allowed range of the bus voltage and the branch current, respectively. Constraint (5.21) is the proposed constraint for apparent power minimisation.

It is worth noting that the VVC optimisation model with $\omega = 0$ means the conventional VVC for the network power loss reduction only, while $\omega = 1$ refers to the VVC function for inverter apparent power reduction only.

5.4.3 Second-Order Conic Programming Method

The developed optimisation model (5.13)-(5.21) presents a non-convex quadratic optimisation problem that is hard to be solved by common off-the-shelf solvers. In this chapter, an SOCP method [128] is applied to reformulate the non-convex branch flow model (5.15)-(5.18) into the following convex model.

$$P_{k,t}^{PV} - P_{k,t}^{L} = \sum_{l \in L(k)} P_{kl,t} - \sum_{j \in J(k)} (P_{jk,t} - r_{jk} i_{jk,t}), \forall k, t \tag{5.22}$$

$$Q_{k,t}^{inv} - Q_{k,t}^{L} = \sum_{l \in L(k)} Q_{kl,t} - \sum_{j \in J(k)} (Q_{jk,t} - x_{jk} i_{jk,t}), \forall k, t \tag{5.23}$$

$$v_{k,t} = v_{j,t} - 2\left(r_{jk} P_{jk,t} + x_{jk} Q_{jk,t}\right) + (r_{jk}^2 + x_{jk}^2) i_{jk,t}, \forall jk, t \tag{5.24}$$

$$\left\| \begin{matrix} 2P_{jk,t} \\ 2Q_{jk,t} \\ i_{jk,t} - v_{j,t} \end{matrix} \right\|_2 \leq i_{jk,t} + v_{j,t}, \forall jk, t \tag{5.25}$$

Here, new variables $i_{jk,t}$ and $v_{k,t}$ indicate the square values of the branch current from bus j to bus k, and the voltage at bus k, respectively. Constraint (5.25) is an SOCP relaxation model for the original equality (5.18), and the relaxation can achieve high computing efficiency with proved exactness for the VVC with the network power loss minimisation. Detailed relaxation method and proof of exactness can be found in [128].

With $i_{jk,t}$ and $v_{k,t}$, constraints (5.14), (5.19) and (5.20) can be rewritten as follows.

$$P^{net,loss} = \sum_{t \in T} \sum_{jk \in B} r_{jk} i_{jk,t} \tag{5.26}$$

$$\left(\underline{V}_k\right)^2 \leq v_{k,t} \leq \left(\overline{V}_k\right)^2, \forall k, t \tag{5.27}$$

$$0 \leq i_{jk,t} \leq \left(I_{jk}^{cap}\right)^2, \forall jk, t \tag{5.28}$$

Moreover, (5.21) can be rewritten into the following convex models, where (5.29) is a second-order conic constraint.

$$\left\| \begin{matrix} P_{k,t}^{PV} \\ Q_{k,t}^{inv} \end{matrix} \right\|_2 \leq S_{k,t}^{sl}, \forall k, t \tag{5.29}$$

$$S_{k,t}^{sl} \leq S_k^{cap}, \forall k, t \tag{5.30}$$

Thus, the multi-objective function (5.13) subject to the constraints (5.22)-(5.30) is now a convex SOCP problem that can be solved efficiently by common off-the-shelf solvers.

5.4.4 Scenario-Based Stochastic Optimisation Method

The developed VVC optimisation model has uncertainty variables, i.e., the PV power outputs $P_{k,t}^{PV}$ and the active and reactive loads $P_{k,t}^{L}$ and $Q_{k,t}^{L}$. This chapter applies a scenario-based stochastic optimisation method to address the uncertainty issue.

For a scenario-based stochastic optimisation problem, its objective function can be expressed as below [42].

$$\min_x \sum_{sc \in SC} \left(\rho_{sc} \cdot f(x, \lambda_{sc})\right) \tag{5.31}$$

Here, sc and SC are the index and set of uncertainty scenarios respectively, and ρ_{sc} is the occurrence probability of scenario sc. λ_{sc} indicates the realisation of the uncertainty variables in scenario sc, and $f(x, \lambda_{sc})$ is the corresponding objective function with λ_{sc} and the control variable x.

In this chapter, the uncertainty scenarios are generated via the following three key steps. Firstly, probability distribution functions (PDFs) are adopted to characterise the realisation probability distributions of the uncertainty variables $P_{k,t}^{PV}$, $P_{k,t}^{L}$, and $Q_{k,t}^{L}$. Secondly, Monte Carlo Sampling (MCS) is used based on the probability distributions to generate a large number of uncertainty scenarios of $P_{k,t}^{PV}$, $P_{k,t}^{L}$, and $Q_{k,t}^{L}$. Thirdly, a scenario reduction method is applied to reduce the originally generated scenarios into a properly scaled representative scenarios with assigned occurrence probabilities. These refined representative scenarios can then be put into the optimisation model to consider and address the uncertainties.

Thus, a multi-objective stochastic optimisation problem that is still convex can be formulated as follows.

$$\min_{Q_{k,t}^{inv}} \sum_{sc \in SC} \left\{ \rho_{sc} \left[(1-\omega) \cdot \Phi\left(P^{net,loss}\right) + \omega \cdot \Phi\left(\sum_{k,t} S_{k,t}^{sl} \right) \right] \right\} \tag{5.32}$$

$$\text{s.t.} \qquad \text{(5.22)-(5.30)}, \ \forall k, t, sc \tag{5.33}$$

$$\left\{ \left(P_{k,t,sc}^{PV}, P_{k,t,sc}^{L}, Q_{k,t,sc}^{L}\right), \rho_{sc} \right\} \in \Psi, \forall k, t, sc \tag{5.34}$$

where Ψ denotes a set of representative uncertainty scenarios.

5.5 Pareto Front Analysis for Inverter Lifetime

In this chapter, the operational reliability of PV inverters is evaluated by lifetime estimation of DC-link capacitors through reliability models given in Chapter 5.2. For practical implementation, the inverter lifetime is expected to be over a satisfying level. In the proposed multi-objective optimisation model given in Chapter 5.4, the weighting factor ω can determine the performance of network power loss reduction and inverter reliability enhancement. However, the indirect correlation between inverter apparent power output and inverter lifetime brings difficulty to setting the weighting factor in the proposed model. To tackle this problem, this chapter further proposes a Pareto front analysis method with a numerical simulation of long-term VVC optimisation to provide useful instruction of setting the weighting factor. Via this method, the weighting factor can be set with a proper value to achieve efficient VVC with expected inverter lifetime.

5.5.1 Pareto Front Analysis Method

A Pareto front analysis method is proposed as follows.

Firstly, solving the optimisation problem (5.32)-(5.34), numerical simulations are conducted to obtain the solutions with different values of the weighting factor over a long-term period. By using the capacitor reliability models given in Chapter 5.2, the inverter lifetime with different weighting factor values can be obtained, and the minimum/average lifetime values of all the inverters in the network can be calculated as well. With the results of the minimum/average inverter lifetimes and the network energy loss reduction, a Pareto front of the two conflicting dimensions can be formed. It is noted that, the minimisation of the network power loss and the inverter apparent power in the original problem is equivalent to maximising the total network energy loss reduction and the inverter lifetime, so the Pareto front is expected to be in the form of a maximisation problem.

Then, a threshold for the minimum inverter lifetime is required by the PV owners. On the pareto front, the solution, which is just over the threshold and with the largest energy loss reduction, is identified and the weighting factor value ω_M is obtained. Similarly, another threshold for the average inverter lifetime is given for a purpose of guaranteeing the inverter operational reliability across the network, and the corresponding weighting factor value ω_A is obtained. These values can achieve efficient VVC performance in long-term network power loss reduction while satisfying corresponding inverter lifetime requirements.

Finally, the larger of ω_M and ω_A can be suggested as the weighting factor in the proposed multi-objective optimisation model (5.32)-(5.34), to fulfill the PV owner and network requirements of both minimum and average inverter lifetimes.

The above proposed Pareto front analysis method is demonstrated in Figure 5.3. Importantly, the effectiveness of this method is further validated in Chapter 5.6 – Case Study.

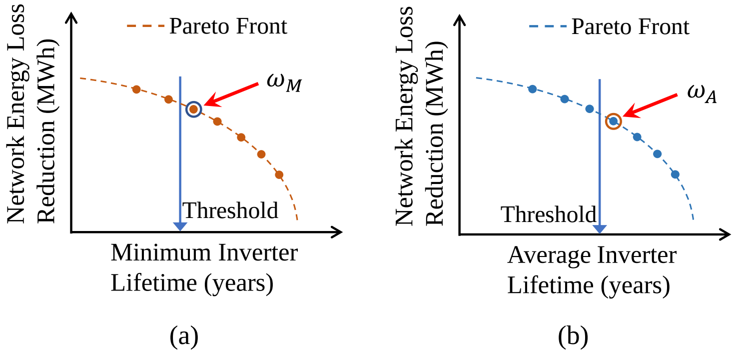

Figure 5.3 Pareto front analysis method: (a) minimum inverter lifetime; (b) average inverter lifetime.

5.5.2 Weighting Factor Setting Procedure

With a proper value set as the weighting factor, the proposed VVC optimisation model with the Pareto front analysis method can effectively minimise the network power loss while achieving expected inverter lifetime.

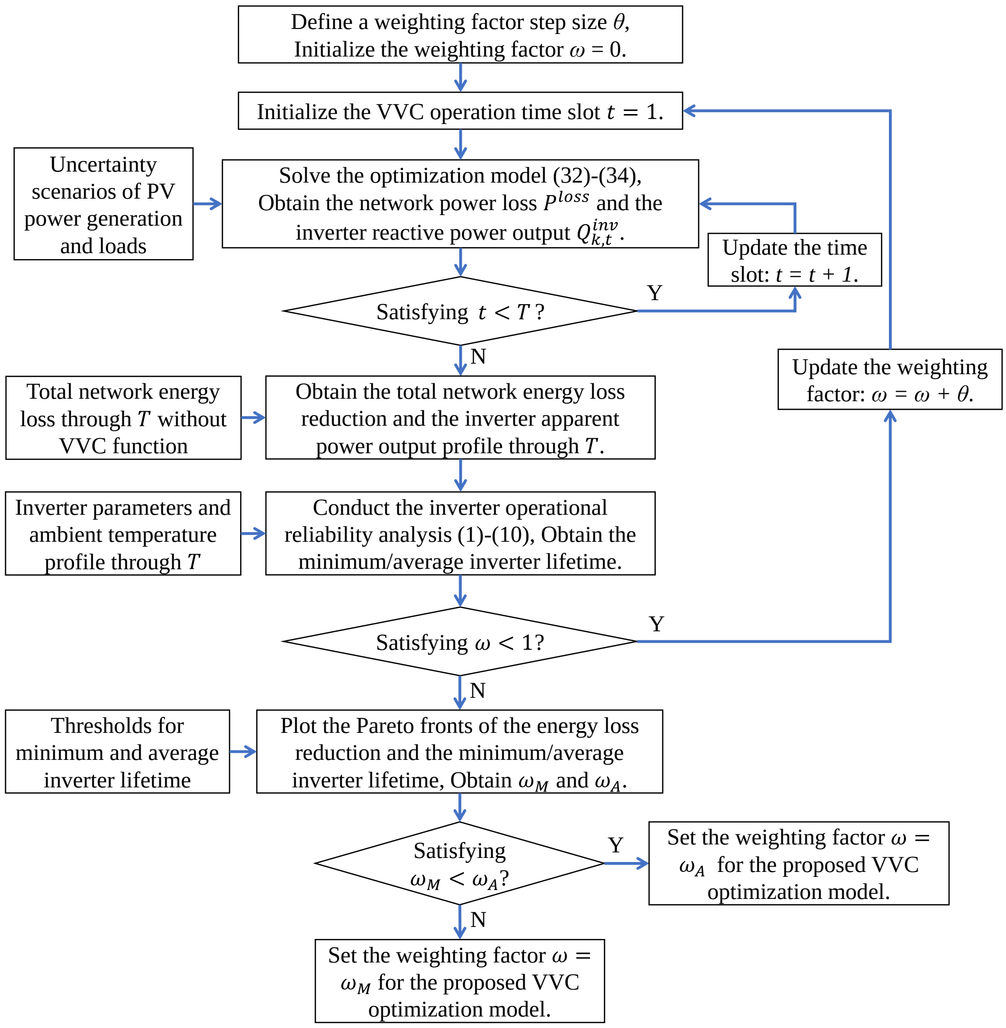

Figure 5.4 Procedure of setting the weighting factor.

Combining numerical simulations, PV inverter operational reliability analysis and Pareto front analysis, the detailed procedure for setting the weighting factor for the proposed VVC optimisation method is demonstrated in Figure 5.4.

5.6 Case Study

5.6.1 Test System Description

In this chapter, a modified 33-bus distribution network is adopted to verify the developed VVC optimisation model, and the network parameters can be found in [91]. In the network, 12 aggregated PV systems are installed, and each one is an aggregation of 100 individual 5 kW PV systems. Moreover, associated PV inverters of individual PVs are all oversized to 5.5 kVA (by 10%) to allow more reactive power support [58]. Figure 5.5 demonstrates the network topology and the PV locations.

In this chapter, the allowed limits of bus voltage are set as 0.95 p.u. and 1.05 p.u., and the voltage of the root bus is set as 1 p.u. The length of the VVC operating time slot t is one hour. For accurate evaluation of inverter lifetime, the proposed VVC optimisation is carried out for one year. It is worth noting that, the inverter state over each VVC operating time slot is assumed to be steady, to effectively analyse the impact of long-term hourly VVC operation on inverter reliability.

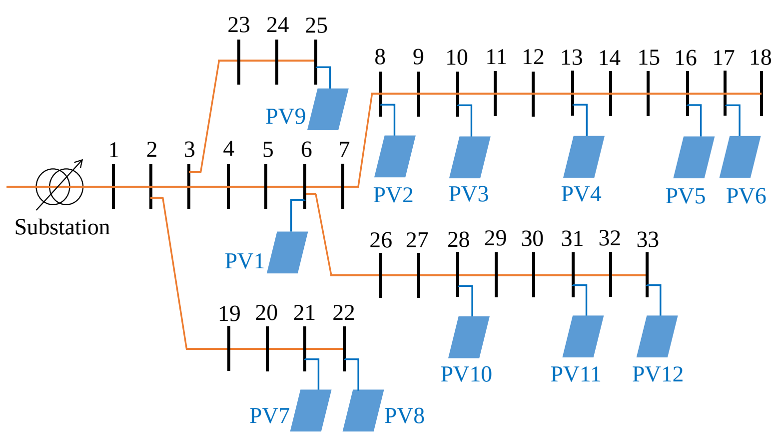

Figure 5.5 Network topology of test system.

The inverter operational reliability is analysed via the lifetime estimation approach of the DC-link capacitor. This case study applies a 450 V/105 °C aluminum electrolytic capacitor to validate the developed model, and Table 5-I demonstrates the capacitor's parameters for reliability analysis. The applied DC-link voltage V_{DC} is 450 V, and the PWM switching frequency is 20 kHz. The ambient temperature data used in (5.4) are from the annual hourly-step temperature records of Chicago from December 2016 to November 2017 [95]. This chapter assumes that the solar irradiance and the ambient temperature are identical across the entire distribution network, eliminating geographically environmental impacts on inverter operational reliability.

Table 5-I Parameter of DC-Link Capacitor

V_{DCr}	450V	$R_{th(co-a)}$	3.73K/W
ESR(100Hz)	52.1mΩ	H_b	2000h
ESR(20kHz)	35.6mΩ	T_m	105°C

As for stochastic optimisation, firstly, 2000 initial scenarios representing the uncertainties of PV power outputs and loads are created by using the MCS with a Gaussian distribution based PDF. The applied PV power output profile for the MCS is from [107], and the load profile is from the IEEE Reliability Test System (RTS) - 1996 [94]. Then, this chapter adopts a backward scenario reduction method which is given by [104] to reduce the initially generated scenarios into 20 representative scenarios, and each representative scenario is assigned with a certain occurrence probability. These 20 representative scenarios with associated occurrence probabilities compose the uncertainty set Ψ in (5.34). In addition, the step size of the weighting factor ω is set as 0.1.

It is worth noting that other parameters can also be used without affecting the effectiveness of the proposed model.

The simulations are carried out on a 64-bit PC with 3.20-GHz CPU and 16-GB RAM on the MATLAB platform. The proposed VVC optimisation problem is solved by the GUROBI solver [85].

5.6.2 VVC Optimisation Results

Solving the formulated VVC optimisation problem (5.32)-(5.34), the inverter reactive power outputs $Q_{k,t}^{inv}$, under different cases of ω, can be optimised. Figure 5.6 presents the annual inverter reactive power output profiles at PV 10, with ω as 0, 0.4, and 0.8. It is noted that the positive reactive power outputs represent power injection to the grid, while the negative values mean power absorption.

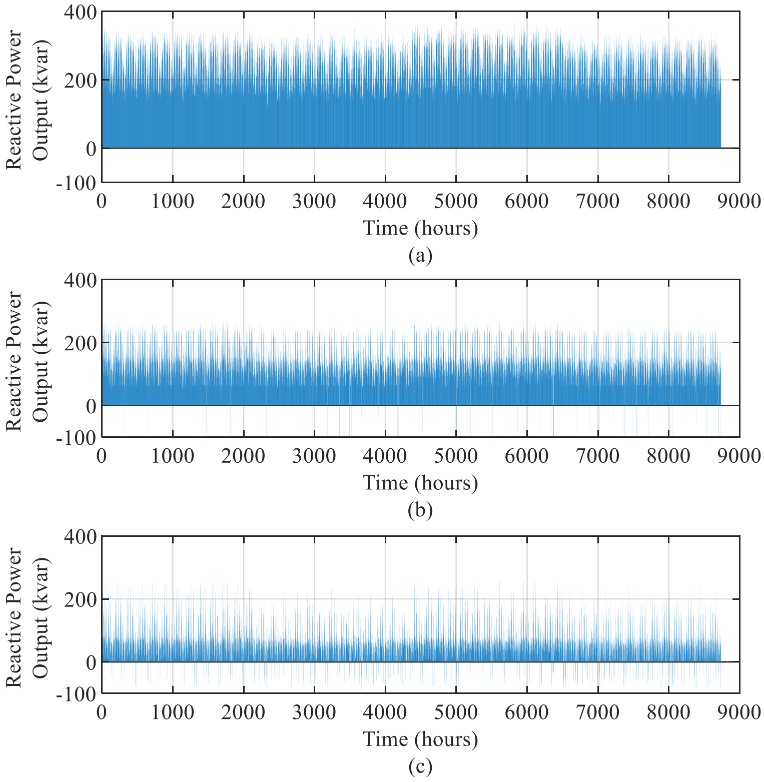

Figure 5.6 One-year inverter reactive power output profile at PV 10 with ω as: (a) 0; (b) 0.4; (c) 0.8.

Compared to the case of ω as 0 (i.e., the conventional VVC for the network power loss reduction only), the proposed multi-objective VVC optimisation model can efficiently reduce the inverter reactive power output. Besides, a higher value of ω can lead to a better performance in reactive power reduction.

Moreover, taking one day as an example, the daily inverter apparent power output profiles at PV 10, under the different cases of ω, are presented in Figure 5.7.

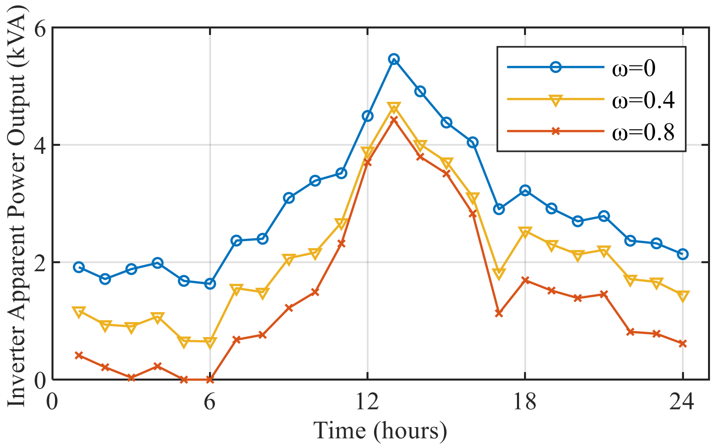

Figure 5.7 Daily inverter apparent power output at PV 10 (on Day 1).

It is obvious in Figure 5.7 that the inverter apparent power output is effectively reduced by the proposed VVC optimisation model. Similarly, a higher ω can lead to a more significant reduction in the inverter apparent power output.

5.6.3 Inverter Operational Reliability Analysis Results

5.6.3.1 Thermal Analysis Results

With the obtained optimisation results, i.e., the inverter apparent power outputs, firstly, the inverter thermal analysis is conducted. The power loss model (5.1) and the thermal model (5.3)-(5.4) of the DC-link capacitor are used to calculate the capacitor core temperature. In this chapter, it is assumed that the active power used for inverter current phasing adjustment is negligible, and only the inverter reactive power contributes to the DC-link capacitor's power loss during PV non-feed-in hours at night.

Figure 5.8 demonstrates the analysis results of the inverter DC-link capacitor core temperature at PV 10, under the cases of ω as 0.1 and 0.9. In this figure, the Y-axis represents the hours accumulated for different groups of capacitor core temperature, for the one-year simulation. These hours are further used for the lifetime evaluation of DC-link capacity with Eq. (5.6) and (5.7).

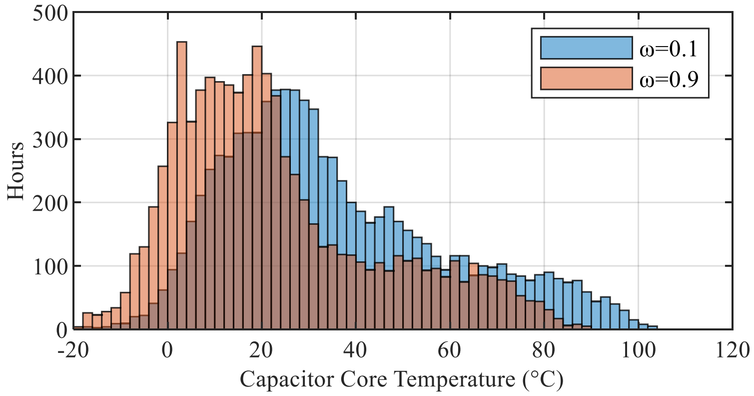

Figure 5.8 Thermal analysis for inverter DC-link capacitor of PV 10.

Obviously, the different values of ω can lead to the different DC-link capacitor thermal states. The capacitor core temperature level with ω as 0.9 is much lower than that with ω as 0.1, which indicates the effective use of a large ω in enhancing the inverter operational reliability.

5.6.3.2 Lifetime Results

Secondly, the analysis results of the capacitor core temperature are used in the lifetime model (5.5)-(5.7) to calculate the DC-link capacitor lifetime as the inverter lifetime. The calculated inverter lifetime of each PV in the network with the different values of ω, as well as the lifetime under the no-VVC case, are demonstrated in Figure 5.9.

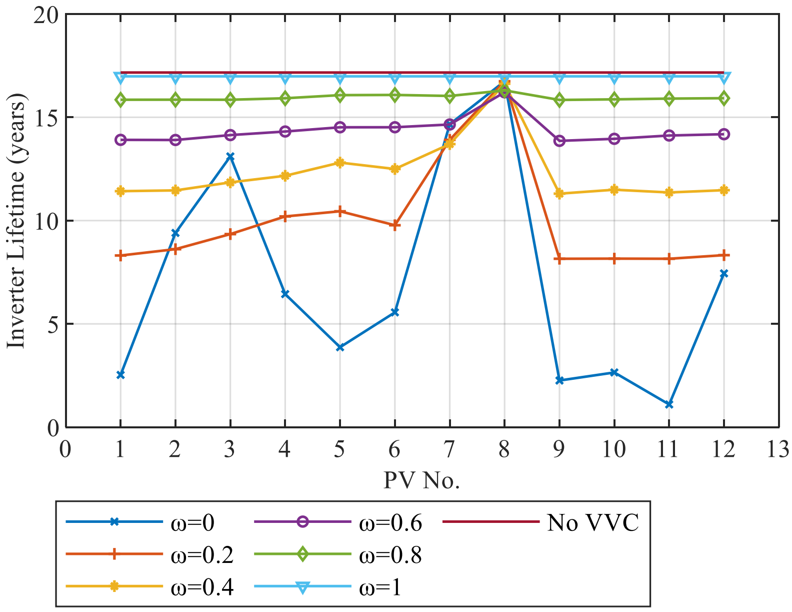

Figure 5.9 Inverter lifetimes of all PVs.

For the no-VVC case, the inverter lifetime of each PV is obtained as the same 17.2 years, due to the identical PV power generation and ambient temperature profiles. For the conventional VVC case, i.e., the case with ω as 0, due to the unregulated inverter var compensation, the inverter lifetimes of all the PVs are reduced. Especially, the inverter lifetimes of PVs 1, 5, 9, 10 and 11 are even lower than 5 years.

In addition, the proposed VVC optimisation model for minimising the inverter apparent power output can effectively improve the inverter lifetime. Moreover, with the increase of ω, the inverter lifetimes increase as well, approaching the lifetimes of the no-VVC case as ω increases to 1.

Moreover, the minimum/average inverter lifetimes of all the PVs in the network, under the different values of ω, are presented in Figure 5.10.

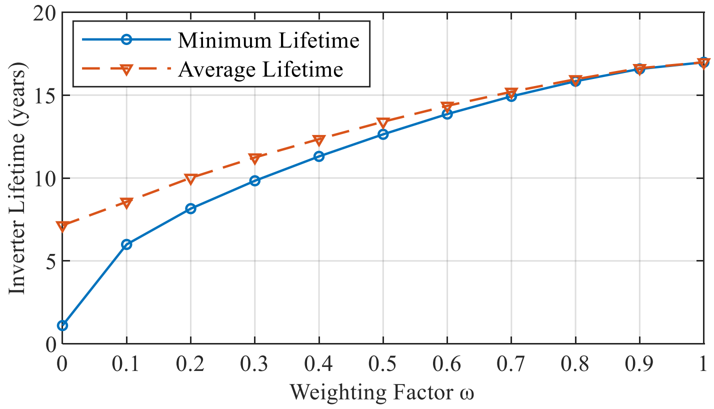

Figure 5.10 Minimum and average inverter lifetimes of PVs in the network.

It is demonstrated that both the minimum and the average inverter lifetimes of all the PVs benefit from the proposed VVC optimisation model, compared to the conventional VVC case with ω as 0. Besides, an increased ω can lead to the larger minimum and average inverter lifetimes.

5.6.4 Settling of Weighting Factor

In this case study, the thresholds for the minimum and average inverter lifetime are set as 8 and 12 years, respectively. According to Chapter 5.5, the Pareto front analysis method is carried out. Numerical simulations of one-year VVC optimisation with different values of ω are conducted, then the results of the total network energy loss reduction and the minimum/average inverter lifetime are obtained. With these results, two Pareto fronts are plotted as shown in Figure 5.11. It is noted that the network energy loss reduction is calculated from the annual network energy loss under the no-VVC case, i.e., 770.3 MWh.

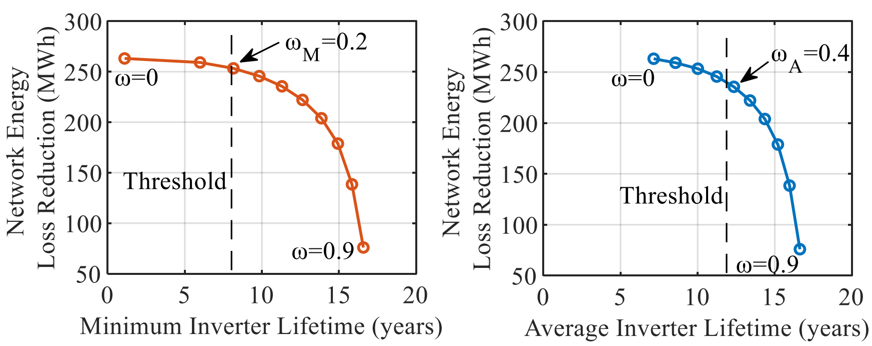

(a) (b)

Figure 5.11 Pareto front analysis results: (a) minimum inverter lifetime; (b) average inverter lifetime.

The Pareto front in Figure 5.11 (a) demonstrates the relationship between the total network energy loss reduction and the minimum inverter lifetime. With the threshold for the minimum inverter lifetime, i.e., 8 years, the weighting factor ω_M is obtained as 0.2.

On the other hand, Figure 5.11 (b) shows the Pareto front for the total network energy loss reduction and the average inverter lifetime. With the threshold for the average inverter lifetime, i.e., 12 years, the weighting factor ω_A is obtained as 0.4.

Finally, by comparing ω_M and ω_A, the larger one, i.e., ω_A, should be adopted to fulfill both thresholds. Therefore, the weighting factor ω should be set as 0.4 and used in the proposed PV inverter based VVC optimisation model, to achieve the most efficient network power loss reduction while achieving the expected inverter lifetime.

5.7 Conclusion

This chapter proposes a multi-objective PV inverter based VVC optimisation model and a Pareto front analysis method, which can minimise network power loss while achieving expected inverter lifetime. Firstly, the inverter operational reliability is analysed via lifetime estimation of the vulnerable DC-link capacitor. Secondly, the long-term impact of VVC on the inverter operational reliability is identified, and it is expected to minimise the inverter apparent power output for enhancing reliability. Thirdly, a multi-objective PV inverter based VVC optimisation model is formulated. This model is convexified by an SOCP method and the PV and load uncertainties are addressed by utilising a scenario-based stochastic optimisation method. Lastly, a Pareto front analysis method is proposed to select a proper value of the weighting factor, thus keeping satisfying inverter lifetime. The case study verifies that the proposed PV inverter based VVC optimisation model can efficiently reduce the network power loss while achieving the expected inverter lifetime.

Chapter 6 CONCLUSION AND FUTURE WORK

Significant challenges brought by the proliferation of DPVs highlights the importance of a quick transitioning from traditional distribution networks to active distribution networks. In active distribution networks, PV inverters of DPV systems have potential to be utilised to provide VVC functions for fast and flexible voltage regulation. This PV inverter based VVC method has been proved to be a highly efficient voltage control measure for future PV-penetrated distribution networks.

However, considering real-world application of PV inverter based VVC, a very practical concern arises, i.e., PV inverter reliability. Despite the vulnerable nature of PV inverters and their dynamic working conditions, additional utilisation for reactive power support may further degrade the inverter reliability, leading to much shortened inverter lifetime, potential hazard to electricity safety, and impaired economic benefits. This research takes the initiative to investigate how the VVC function can affect the PV inverter reliability. Based on the analysis results, advanced PV inverter based VVC methods considering inverter reliability enhancement are proposed to effectively address the inverter reliability concern in VVC methods.

The major contributions of this research are briefly summarised as follows.

1) Develop a complete PV inverter reliability assessment approach to evaluate the lifetime of PV inverters when used for the VVC function.
2) Develop new VVC constraints modelling PV inverter reliability, which utilise a proposed restriction factor to limit the amplitude of inverter apparent power output.
3) Propose a multi-objective PV inverter reliability constrained VVC optimisation model with the developed VVC constraints for power limitation and a PV curtailment scheme.
4) Develop a scenario-based stochastic optimisation method to address the uncertainties of PV power generation and loads.
5) Propose an inverter power smoothing scheme with high control flexibility, which uses

reactive power output from VVC and PV curtailment to smooth the inverter apparent power output.

6) Develop new inverter reliability constraints for power smoothing via utilising a proposed smoothing factor to constrict the variation of inverter apparent power.

7) Propose a PV inverter reliability constrained VVC optimisation model with the developed apparent power smoothing scheme for inverter reliability enhancement.

8) Develop a penalty convex-concave procedure programming method to tackle the non-convexity issue of the proposed VVC optimisation model with power smoothing.

9) Propose a multi-objective PV inverter based VVC optimisation model with a weighting factor to simultaneously minimise both the network power loss and inverter apparent power output.

10) Develop a Pareto front analysis method for selection of a proper weighting factor, to realise the most efficient network power loss reduction with expected inverter lifetime.

The proposed models, methodologies, and solution algorithms are successfully demonstrated via a number of simulations, and comparisons are carried out with existing literature where applicable. The simulation results have verified the high efficiency of the proposed models, methodologies, and solution algorithms.

The above research outputs have potential to be extended to cover a broader spectrum of VVC strategies considering device reliability. Some potential directions of future work are provided below.

1) This research focuses on PV inverter based VVC methods. Other power electronic converters providing VVC functions can be considered, such as battery converters and wind turbine inverters.

2) Economic modelling and risk constraints can be applied in the proposed PV inverter reliability constrained VVC model to interpret the costs of network power loss, PV curtailment, and inverter lifetime degradation.

3) Other VVC control schemes such as localised VVC and distributed VVC, as well as other

optimisation methodologies such as robust optimisation and interval optimisation, can be incorporated into the proposed models.

4) Instead of sensitivity analysis, direct optimisation of the proposed restriction factor in Chapter 3, smoothing factor in Chapter 4, and weighting factor in Chapter 5 can be studied so that an optimum result of energy loss and inverter lifetime can be achieved.

5) Actual implementation of the proposed VVC methods such as controller design, communication setting, and inverter coordination scheme can be further investigated. Moreover, hardware experiments can be included in future research to further validate the proposed VVC optimisation model and inverter reliability analysis process.

6) In this research, PV system sizes and locations in the network are fixed. In fact, optimal PV system planning in the distribution network for VVC while considering PV inverter reliability can be investigated.

BIBLIOGRAPHY

[1] "Renewable Capacity Statistics 2022," The International Renewable Energy Agency, Abu Dhabi, 2022.

[2] "Solar PV and batteries," Department of Climate Change, Energy, the Environment and Water, Australian Government, [Online]. Available: https://www.energy.gov.au/households/solar-pv-and-batteries. [Accessed July 2022].

[3] "Clean Energy Australia Report 2022," Clean Energy Council, Melbourne, 2022.

[4] N. Vazquez, S. S. Yu, T. K. Chau, T. Fernando and H. H. -C. Iu, "A Fully Decentralized Adaptive Droop Optimization Strategy for Power Loss Minimization in Microgrids With PV-BESS," *IEEE Trans. Energy Convers.,* vol. 34, no. 1, pp. 385-395, March 2019.

[5] U. R. Nair, M. Sandelic, A. Sangwongwanich, T. Dragičević, R. Costa-Castelló and F. Blaabjerg, "An Analysis of Multi Objective Energy Scheduling in PV-BESS System Under Prediction Uncertainty," *IEEE Trans. Energy Convers.,* vol. 36, no. 3, pp. 2276-2286, Sept. 2021.

[6] R. H. Lasseter, Z. Chen and D. Pattabiraman, "Grid-Forming Inverters: A Critical Asset for the Power Grid," *IEEE Journal of Emerging and Selected Topics in Power Electronics,* vol. 8, no. 2, pp. 925-935, June 2020.

[7] Y. Yang, F. Blaabjerg and H. Wang, "Low-Voltage Ride-Through of Single-Phase Transformerless Photovoltaic Inverters," *IEEE Trans. Ind. Appl.,* vol. 50, no. 3, pp. 1942-1952, May-June 2014.

[8] S. Weckx, C. Gonzalez and J. Driesen, "Combined Central and Local Active and Reactive Power Control of PV Inverters," *IEEE Trans. Sustain. Energy,* vol. 5, no. 3, pp. 776-784, July 2014.

[9] T. H. A. T. MP, "Record 3 million rooftop solar energy installations," November 2021. [Online]. Available: https://www.minister.industry.gov.au/ministers/taylor/media-releases/record-3-million-rooftop-solar-energy-installations. [Accessed July 2022].

[10] "HOW MUCH CAN YOU SAVE WITH SOLAR PANELS," Renew Energy, [Online]. Available: https://www.renewenergy.com.au/how-much-can-you-save-with-solar-panels/. [Accessed August 2022].

[11] M. J. E. Alam, K. M. Muttaqi and D. Sutanto, "A Novel Approach for Ramp-Rate Control of Solar PV Using Energy Storage to Mitigate Output Fluctuations Caused by Cloud Passing," *IEEE Trans. Energy Convers.,* vol. 29, no. 2, pp. 507-518, June 2014.

[12] P. D. F. Ferreira, P. M. S. Carvalho, L. A. F. M. Ferreira and M. D. Ilic, "Distributed Energy Resources Integration Challenges in Low-Voltage Networks: Voltage Control Limitations and Risk of Cascading," *IEEE Trans. Sustain. Energy,* vol. 4, no. 1, pp. 82-88, Jan. 2013.

[13] R. A. Shayani and M. A. G. d. Oliveira, “Photovoltaic Generation Penetration Limits in Radial Distribution Systems,” *IEEE Trans. Power Syst.,* vol. 26, no. 3, pp. 1625-1631, Aug. 2011.

[14] W. Chen, J. Qiu and Q. Chai, “Customized Critical Peak Rebate Pricing Mechanism for Virtual Power Plants,” *IEEE Trans. Sustain. Energy,* vol. 12, no. 4, pp. 2169-2183, Oct. 2021.

[15] “AS/NZS 4777.2:2020 - Grid connection of energy systems via inverters, Part 2: Inverter requirements,” Standard Australia, 2020. [Online]. Available: https://www.standards.org.au/standards-catalogue/sa-snz/other/el-042/as-slash-nzs--4777-dot-2-colon-2020. [Accessed July 2022].

[16] Q. Chai, C. Zhang, Z. Dong and W. Chen, “Optimal Daily Scheduling of Distributed Battery Energy Storage Systems Considering Battery Degradation Cost,” in *2021 IEEE Power & Energy Society General Meeting (PESGM)*, Washington, D.C., 2021.

[17] “Access, pricing and incentive arrangements for DER,” Australian Energy Market Commission, Sydney, 2021.

[18] C. D’Adamo, S. Jupe and C. Abbey, “Global survey on planning and operation of active distribution networks—Update of CIGRE C6.11 working group activities,” *Proc. Int. Conf. Exhib. Elect. Distrib.,* 2009.

[19] “Dynamic Export Limits Requirement,” Energy & Mining, Government of South Australia, [Online]. Available: https://www.energymining.sa.gov.au/industry/modern-energy/solar-batteries-and-smarter-homes/regulatory-changes-for-smarter-homes/dynamic-export-limits-requirement. [Accessed July 2022].

[20] “Emergency Solar Management,” Government of Western Australia, [Online]. Available: https://www.wa.gov.au/organisation/energy-policy-wa/emergency-solar-management. [Accessed July 2022].

[21] B. Wang, C. Zhang, Z. Y. Dong and X. Li, “Improving Hosting Capacity of Unbalanced Distribution Networks via Robust Allocation of Battery Energy Storage Systems,” *IEEE Trans. Power Syst.,* vol. 36, no. 3, pp. 2174-2185, May 2021.

[22] B. Wang, C. Zhang and Z. Y. Dong, “Interval Optimization Based Coordination of Demand Response and Battery Energy Storage System Considering SOC Management in a Microgrid,” *IEEE Trans. Sustain. Energy,* vol. 11, no. 4, pp. 2922-2931, Oct. 2020.

[23] F. Capitanescu, L. F. Ochoa, H. Margossian and N. D. Hatziargyriou, “Assessing the Potential of Network Reconfiguration to Improve Distributed Generation Hosting Capacity in Active Distribution Systems,” *IEEE Trans. Power Syst.,* vol. 30, no. 1, pp. 346-356, Jan. 2015.

[24] D. Koraki and K. Strunz, “Wind and Solar Power Integration in Electricity Markets and Distribution Networks Through Service-Centric Virtual Power Plants,” *IEEE Trans. Power Syst.,* vol. 33, no. 1, pp. 473-485, Jan. 2018.

[25] W. Chen, J. Qiu, J. Zhao, Q. Chai and Z. Y. Dong, “Customized Rebate Pricing Mechanism for Virtual Power Plants Using a Hierarchical Game and Reinforcement Learning Approach,” *IEEE Trans. Smart Grid,* Early Access, 2022.

[26] Q. Zhao, Y. Shen and M. Li, “Control and Bidding Strategy for Virtual Power Plants With Renewable Generation and Inelastic Demand in Electricity Markets,” *IEEE Trans. Sustain. Energy,* vol. 7, no. 2, pp. 562-575, April 2016.

[27] A. Baringo, L. Baringo and J. M. Arroyo, “Day-Ahead Self-Scheduling of a Virtual Power Plant in Energy and Reserve Electricity Markets Under Uncertainty,” *IEEE Trans. Power Syst.,* vol. 34, no. 3, pp. 1881-1894, May 2019.

[28] W. Chen, J. Qiu, J. Zhao, Q. Chai and Z. Y. Dong, “Bargaining Game-Based Profit Allocation of Virtual Power Plant in Frequency Regulation Market Considering Battery Cycle Life,” *IEEE Trans. Smart Grid,* vol. 12, no. 4, pp. 2913-2928, July 2021.

[29] S. Alyami, Y. Wang, C. Wang, J. Zhao and B. Zhao, “Adaptive Real Power Capping Method for Fair Overvoltage Regulation of Distribution Networks With High Penetration of PV Systems,” *IEEE Trans. Smart Grid,* vol. 5, no. 6, pp. 2729-2738, Nov. 2014.

[30] “Solar energy - A new solar connection option,” SA Power Networks, 2021. [Online]. Available: https://www.sapowernetworks.com.au/future-energy/solar/. [Accessed July 2022].

[31] T. Niknam, M. Zare and J. Aghaei, “Scenario-Based Multiobjective Volt/Var Control in Distribution Networks Including Renewable Energy Sources,” *IEEE Trans. Power Del.,* vol. 27, no. 4, pp. 2004-2019, Oct. 2012.

[32] M. E. Elkhatib, R. El-Shatshat and M. M. A. Salama, “Novel coordinated voltage control for smart distribution networks with DG,” *IEEE Trans. Smart Grid,* vol. 2, no. 4, p. 598–605, Dec. 2011.

[33] N. Daratha, B. Das and J. Sharma, “Coordination Between OLTC and SVC for Voltage Regulation in Unbalanced Distribution System Distributed Generation,” *IEEE Trans. Power Syst.,* vol. 29, no. 1, pp. 289-299, Jan. 2014.

[34] X. Liu, A. Aichhorn, L. Liu and H. Li, “Coordinated Control of Distributed Energy Storage System With Tap Changer Transformers for Voltage Rise Mitigation Under High Photovoltaic Penetration,” *IEEE Trans. Smart Grid,* vol. 3, no. 2, pp. 897-906, June 2012.

[35] S. Karagiannopoulos, P. Aristidou and G. Hug, “A Centralised Control Method for Tackling Unbalances in Active Distribution Grids,” in *2018 Power Systems Computation Conference (PSCC)*, Dublin, 2018.

[36] A. Jafari, H. G. Ganjehlou, T. Khalili, B. Mohammadi-Ivatloo, A. Bidram and P. Siano, “A Two-Loop Hybrid Method for Optimal Placement and Scheduling of Switched Capacitors in Distribution Networks,” *IEEE Access,* vol. 8, pp. 38892-38906, 2020.

[37] Y. Xu, Z. Y. Dong, K. P. Wong, E. Liu and B. Yue, “Optimal Capacitor Placement to Distribution Transformers for Power Loss Reduction in Radial Distribution Systems,” *IEEE Trans. Power Syst.,* vol. 28, no. 4, pp. 4072-4079, Nov. 2013.

[38] H. Khani, M. Moallem, S. Sadri and M. Dolatshahi, “A New Method for Online Determination of the Location of Switched Capacitor Banks in Distribution Systems,” *IEEE Trans. Power Del.,* vol. 26, no. 1, pp. 341-351, Jan. 2011.

[39] M. Chamana and B. H. Chowdhury, “Optimal Voltage Regulation of Distribution Networks With Cascaded Voltage Regulators in the Presence of High PV Penetration,” *IEEE Trans. Sustain. Energy,* vol. 9, no. 3, pp. 1427-1436, July 2018.

[40] Y. Xu, Z. Y. Dong, R. Zhang and D. J. Hill, “Multi-Timescale Coordinated Voltage/Var Control of High Renewable-Penetrated Distribution Systems,” *IEEE Trans. Power Syst.,* vol. 32, no. 6, pp. 4398-4408, Nov. 2017.

[41] K. Turitsyn, P. Šulc, S. Backhaus and M. Chertkov, “Distributed control of reactive power flow in a radial distribution circuit with high photovoltaic penetration,” in *IEEE PES Gen. Meeting*, Minneapolis, 2010.

[42] C. Zhang and Y. Xu, “Hierarchically-Coordinated Voltage/VAR Control of Distribution Networks Using PV Inverters,” *IEEE Trans. Smart Grid.,* vol. 11, no. 4, pp. 2942-2953, July 2020.

[43] K. Turitsyn, P. Sulc, S. Backhaus and M. Chertkov, “Options for Control of Reactive Power by Distributed Photovoltaic Generators,” *Proc. IEEE,* vol. 99, no. 6, pp. 1063-1073, June 2011.

[44] P. Jahangiri and D. C. Aliprantis, “Distributed Volt/VAr Control by PV Inverters,” *IEEE Trans. Power Syst.,* vol. 28, no. 3, pp. 3429-3439, Aug. 2013.

[45] F. Ding, A. Nagarajan, S. Chakraborty and M. Baggu, “Photovoltaic Impact Assessment of Smart Inverter Volt-VAR Control on Distribution System Conservation Voltage Reduction and Power Quality,” National Renewable Energy Laboratory, Denver, 2016.

[46] Y. Zhang, Y. Xu, H. Yang and Z. Dong, “Voltage regulation-oriented co-planning of distributed generation and battery storage in active distribution networks,” *Int. J. Elec. Power and Energy Syst.,* vol. 105, pp. 79-88, Feb. 2019.

[47] “IEEE Standard for Interconnection and Interoperability of Distributed Energy Resources with Associated Electric Power Systems Interfaces,” IEEE 1547, 2018. [Online]. Available: https://standards.ieee.org/ieee/1547/5915/. [Accessed July 2022].

[48] “Standard Language Protocols for Photovoltaic and Storage Grid Integration,” EPRI, 2010. [Online]. Available: https://www.epri.com/research/products/1020906. [Accessed July 2022].

[49] T. Ding, C. Li, Y. Yang, J. Jiang, Z. Bie and F. Blaabjerg, “A Two-Stage Robust Optimization for Centralized-Optimal Dispatch of Photovoltaic Inverters in Active Distribution Networks,” *IEEE Trans. Sustain. Energy,* vol. 8, no. 2, pp. 744-754, April 2017.

[50] J. Li, Z. Xu, J. Zhao and C. Zhang, “Distributed Online Voltage Control in Active Distribution Networks Considering PV Curtailment,” *IEEE Trans. Ind. Informat.,* vol. 15, no. 10, pp. 5519-5530, Oct. 2019.

[51] R. A. Jabr, “Robust Volt/VAr Control With Photovoltaics,” *IEEE Trans. Power Syst.,* vol. 34, no. 3, pp. 2401-2408, May 2019.

[52] C. Zhang, Y. Xu, Z. Dong and J. Ravishankar, “Three-Stage Robust Inverter-Based Voltage/Var Control for Distribution Networks With High-Level PV,” *IEEE Trans. Smart Grid.,* vol. 10, no. 1, pp. 782-793, Jan. 2019.

[53] L. Wang, R. Yan, F. Bai, T. Saha and K. Wang, "A Distributed Inter-Phase Coordination Algorithm for Voltage Control With Unbalanced PV Integration in LV Systems," *IEEE Trans. Sustain. Energy,* vol. 11, no. 4, pp. 2687-2697, Oct. 2020.

[54] Y. Long and D. S. Kirschen, "Bi-level Volt/VAR Optimization in Distribution Networks with Smart PV Inverters," *IEEE Trans. Power Syst.,* Early Access, 2022.

[55] Y. Wang, T. Zhao, C. Ju, Y. Xu and P. Wang, "Two-Level Distributed Volt/Var Control Using Aggregated PV Inverters in Distribution Networks," *IEEE Trans. Power Del.,* vol. 35, no. 4, pp. 1844-1855, Aug. 2020.

[56] X. Sun, J. Qiu and J. Zhao, "Optimal Local Volt/Var Control for Photovoltaic Inverters in Active Distribution Networks," *IEEE Trans. Power Syst.,* vol. 36, no. 6, pp. 5756-5766, Nov. 2021.

[57] S. M. N. R. Abadi, A. Attarha, P. Scott and S. Thiébaux, "Affinely Adjustable Robust Volt/Var Control for Distribution Systems With High PV Penetration," *IEEE Trans. on Power Syst.,* vol. 36, no. 4, pp. 3238-3247, July 2021.

[58] H. Liu, C. Zhang, Q. Chai, K. Meng, Q. Guo and Z. Y. Dong, "Robust Regional Coordination of Inverter-Based Volt/Var Control via Multi-Agent Deep Reinforcement Learning," *IEEE Trans. Smart Grid,* vol. 12, no. 6, pp. 5420-5433, Nov. 2021.

[59] R. Xu, C. Zhang, Y. Xu, Z. Dong and R. Zhang, "Multi-Objective Hierarchically-Coordinated Volt/Var Control for Active Distribution Networks With Droop-Controlled PV Inverters," *IEEE Trans. Smart Grid,* vol. 13, no. 2, pp. 998-1011, March 2022.

[60] C. Zhang, Y. Xu, Z. Y. Dong and R. Zhang, "Multi-Objective Adaptive Robust Voltage/VAR Control for High-PV Penetrated Distribution Networks," *IEEE Trans. Smart Grid.,* vol. 11, no. 6, pp. 5288-5300, Nov. 2020.

[61] M. Schmela, "PHOTON: Inverter survey 2012 stats," in *PHOTON's 3rd PV Inverter Conference*, San Francisco, Feb. 2012.

[62] A. Golnas, "PV System Reliability: An Operator's Perspective," *IEEE Journal of Photovoltaics,* vol. 3, no. 1, pp. 416-421, Jan. 2013.

[63] L. M. Moore and H. N. Post, "Five years of operating experience at a large, utility-scale photovoltaic generating plant," *Prog. Photovolt: Res. Appl.,* vol. 16, no. 3, pp. 249-259, 2008.

[64] S. Yang, A. T. Bryant, P. A.Mawby, D. Xiang, L. Ran and P. Tavner, "An industry-based survey of reliability in power electronic converters," *IEEE Trans. Ind. Appl.,* vol. 47, no. 3, pp. 1441-1451, May/Jun. 2011.

[65] A. Sangwongwanich, Y. Yang, D. Sera and F. Blaabjerg, "Mission Profile-Oriented Control for Reliability and Lifetime of Photovoltaic Inverters," *IEEE Trans. Ind. Appl.,* vol. 56, no. 1, pp. 601-610, Jan/Feb. 2020.

[66] Y. Yang, A. Sangwongwanich and F. Blaabjerg, "Design for reliability of power electronics for grid-connected photovoltaic systems," *CPSS Trans. Power Electronics and Applications,* vol. 1, no. 1, pp. 92-103, Dec. 2016.

[67] A. Anurag, Y. Yang and F. Blaabjerg, "Thermal performance and reliability analysis of single-phase PV inverters with reactive power injection outside feed-in operating hours," *IEEE Trans. Emerg. Sel. Topics Power Electron.,* vol. 3, no. 4, pp. 870-880, Dec. 2015.

[68] A. Sangwongwanich, Y. Yang, D. Sera, F. Blaabjerg and D. Zhou, "On the Impacts of PV Array Sizing on the Inverter Reliability and Lifetime," *IEEE Trans. Ind. Appl.,* vol. 54, no. 4, pp. 3656-3667, July-Aug. 2018.

[69] "ASTM E1049-85(2017): Standard Practices for Cycle Counting in Fatigue Analysis," ASTM International, 2017. [Online]. Available: https://www.astm.org/e1049-85r17.html. [Accessed July 2022].

[70] H. Huang and P. A. Mawby, "A Lifetime Estimation Technique for Voltage Source Inverters," *IEEE Trans. Power Electron.,* vol. 28, no. 8, pp. 4113-4119, Aug. 2013.

[71] M. Held, P. Jacob, G. Nicoletti, P. Scacco and M. H. Poech, "Fast power cycling test of IGBT modules in traction application," in *Proc. Int. Conf. Power Electron. Drive Syst.*, Singapore, 1997.

[72] K. Ma, M. Liserre, F. Blaabjerg and T. Kerekes, "Thermal Loading and Lifetime Estimation for Power Device Considering Mission Profiles in Wind Power Converter," *IEEE Trans. Power Electron.,* vol. 30, no. 2, pp. 590-602, Feb. 2015.

[73] H. Wang and F. Blaabjerg, "Reliability of Capacitors for DC-Link Applications in Power Electronic Converters—An Overview," *IEEE Trans. Ind. Appl.,* vol. 50, no. 5, pp. 3569-3578, Sept.-Oct. 2014.

[74] "Aluminum Electrolytic Capacitor Application Guide," Cornell Dubilier, [Online]. Available: https://www.cde.com/resources/technical-papers/AEappGuide.pdf. [Accessed July 2022].

[75] M. Andresen, G. Buticchi and M. Liserre, "Thermal stress analysis and MPPT optimization of photovoltaic systems," *IEEE Trans. Ind. Electron.,* vol. 63, no. 8, pp. 4889-4898, Aug. 2016.

[76] M. Musallam, C. Yin, C. Bailey and M. Johnson, "Mission profile-based reliability design and real-time life consumption estimation in power electronics," *IEEE Trans. Power Electron.,* vol. 30, no. 5, pp. 2601-2613, May 2015.

[77] J. Flicker and S. Gonzalez, "Performance and reliability of PV inverter component and systems due to advanced inverter functionality," in *2015 IEEE 42nd Photovoltaic Specialist Conference (PVSC)*, New Orleans, 2015.

[78] C. D'Adamo and et al., "Development and operation of active distribution networks—Results of CIGRE C6.11 working group," in *Proc. Int. Conf. Exhib. Elect. Distrib.*, 2011.

[79] Q. Chai, C. Zhang, Y. Xu and Z. Y. Dong, "PV Inverter Reliability-Constrained Volt/Var Control of Distribution Networks," *IEEE Trans. Sustain. Energy,* vol. 12, no. 3, pp. 1788-1800, July 2021.

[80] X. Bai, H. Wei, K. Fujisawa and Y. Wang, "Semidefinite programming for optimal power flow problems," *Int. J. Elect. Power Energy Syst.,* vol. 30, no. 6–7, p. 383–392, Jul./Sep. 2008.

[81] R. A. Jabr, "Radial distribution load flow using conic programming," *IEEE Trans. Power Syst.,* vol. 21, no. 3, pp. 1458-1459, Aug. 2006.

[82] Z. Tian and W. Wu, "Recover feasible solutions for SOCP relaxation of optimal power flow problems in mesh networks," *IET Gener. Transm. Distrib.,* vol. 13, no. 7, pp. 1078-1087, Apr. 2019.

[83] J. Due, S. Munk-Nielsen and R. Nielsen, "Lifetime investigation of high power IGBT modules," in *Proc.14th Eur. Conf. Power Electron. Appl.*, Birmingham, 2011.

[84] K. Ma, M. Liserre and F. Blaabjerg, "Reactive Power Influence on the Thermal Cycling of Multi-MW Wind Power Inverter," *IEEE Trans. Ind Appl.,* vol. 49, no. 2, pp. 922-930, March-April 2013.

[85] "GUROBI," [Online]. Available: https://www.gurobi.com/.

[86] P. D. Reigosa, H. Wang, Y. Yang and F. Blaabjerg, "Prediction of Bond Wire Fatigue of IGBTs in a PV Inverter Under a Long-Term Operation," *IEEE Trans. Power Electron.,* vol. 31, no. 10, pp. 7171-7182, Oct. 2016.

[87] R. Moazzami, J. C. Lee and C. Hu, "Temperature acceleration of time-dependent dielectric breakdown," *IEEE Trans. Electron Devices,* vol. 36, no. 11, pp. 2462-2465, Nov. 1989.

[88] R. Bayerer, T. Herrmann, T. Licht, J. Lutz and M. Feller, "Model for Power Cycling lifetime of IGBT Modules - various factors influencing lifetime," in *Proc. Int. Conf. Integr. Power Electron. Syst.*, Nuremberg, 2008.

[89] "AN2019-05: PC and TC Diagrams," Infineon Technologies, Munich, 2021.

[90] M. A. Miner, "Cumulative Damage in Fatigue," *Journal of Applied Mechanics,* vol. 12, no. 3, pp. A159-A164, Sep. 1945.

[91] M. E. Baran and F. F. Wu, "Network Reconfiguration in Distribution Systems for Loss Reduction and Load Balancing," *IEEE Trans. Power Del.,* vol. 4, no. 2, pp. 1401-1407, Apr. 1989.

[92] "Technical Information: F4-75R07W2H3_B51 datasheet," Infineon Technologies AG, Munich, 2014.

[93] J. McPherson, Reliability Physics and Engineering, 3rd ed., Switzerland: Springer Int., 2019.

[94] C. Grigg and et al., "The IEEE Reliability Test System-1996. A report prepared by the Reliability Test System Task Force of the Application of Probability Methods Subcommittee," *IEEE Trans. Power Syst.,* vol. 14, no. 3, pp. 1010-1020, Aug. 1999.

[95] "Historical Hourly Weather Data 2012-2017," Kaggle Dataset, 2017. [Online]. Available: https://www.kaggle.com/datasets/selfishgene/historical-hourly-weather-data. [Accessed July 2019].

[96] T. Ding and et al., "Interval Power Flow Analysis Using Linear Relaxation and Optimality-Based Bounds Tightening (OBBT) Methods," *IEEE Trans. Power Syst.,* vol. 30, no. 1, pp. 177-188, Jan. 2015.

[97] T. Ding, S. Liu, W. Yuan, Z. Bie and B. Zeng, "A Two-Stage Robust Reactive Power Optimization Considering Uncertain Wind Power Integration in Active Distribution Networks," *IEEE Trans. Sustain. Energy,* vol. 7, no. 1, pp. 301-311, Jan. 2016.

[98] A. Singhal, V. Ajjarapu, J. Fuller and J. Hansen, "Real-Time Local Volt/Var Control Under External Disturbances With High PV Penetration," *IEEE Trans. Smart Grid,* vol. 10, no. 4, pp. 3849-3859,

July 2019.

[99] L. Wei, J. McGuire and R. A. Lukaszewski, “Analysis of PWM Frequency Control to Improve the Lifetime of PWM Inverter,” *IEEE Trans. Ind. Appl.,* vol. 47, no. 2, pp. 922-929, March-April 2011.

[100] U. Choi, S. Jørgensen and F. Blaabjerg, “Advanced Accelerated Power Cycling Test for Reliability Investigation of Power Device Modules,” *IEEE Trans. Power Electron.,* vol. 31, no. 12, pp. 8371-8386, Dec. 2016.

[101] X. Pei, W. Zhou and Y. Kang, “Analysis and Calculation of DC-Link Current and Voltage Ripples for Three-Phase Inverter With Unbalanced Load,” *IEEE Trans. Power Electron.,* vol. 30, no. 10, pp. 5401-5412, Oct. 2015.

[102] F. Renken, “The DC-link capacitor current in pulsed single-phase H-bridge inverters,” in *Proc. 2005 European Conference on Power Electronics and Applications*, Dresden, 2005.

[103] T. Khalili, S. Nojavan and K. Zare, “Optimal performance of microgrid in the presence of demand response exchange: A stochastic multi-objective model,” *Computers & Electrical Engineering,* vol. 74, pp. 429-450, Mar. 2019.

[104] L. Wu, M. Shahidehpour and T. Li, “Stochastic Security-Constrained Unit Commitment,” *IEEE Trans. Power Syst.,* vol. 22, no. 2, pp. 800-811, May 2007.

[105] M. Erol-Kantarci and H. T. Mouftah, “Energy-Efficient Information and Communication Infrastructures in the Smart Grid: A Survey on Interactions and Open Issues,” *IEEE Commun. Surveys Tuts.,* vol. 17, no. 1, pp. 179-197, 2015.

[106] H. Li, S. Gong, L. Lai, Z. Han, R. C. Qiu and D. Yang, “Efficient and Secure Wireless Communications for Advanced Metering Infrastructure in Smart Grids,” *IEEE Trans. Smart Grid,* vol. 3, no. 3, pp. 1540-1551, Sept. 2012.

[107] “PVOutput,” [Online]. Available: https://pvoutput.org/.

[108] M. E. Baran and F. F. Wu, “Optimal capacitor placement on radial distribution systems,” *IEEE Trans. Power Del.,* vol. 4, no. 1, pp. 725-734, Jan. 1989.

[109] G. Cao and et al., “Operational Risk Evaluation of Active Distribution Networks Considering Cyber Contingencies,” *IEEE Trans. Ind. Informat.,* vol. 16, no. 6, pp. 3849-3861, June 2020.

[110] F. Capitanescu, L. F. Ochoa, H. Margossian and N. D. Hatziargyriou, “Assessing the Potential of Network Reconfiguration to Improve Distributed Generation Hosting Capacity in Active Distribution Systems,” *IEEE Trans. Power Syst.,* vol. 30, no. 1, pp. 346-356, Jan. 2015.

[111] H. Al-Saadi, R. Zivanovic and S. F. Al-Sarawi, “Probabilistic Hosting Capacity for Active Distribution Networks,” *IEEE Trans. Ind. Informat.,* vol. 13, no. 5, pp. 2519-2532, Oct. 2017.

[112] M. Zeraati, M. E. H. Golshan and J. M. Guerrero, “Distributed Control of Battery Energy Storage Systems for Voltage Regulation in Distribution Networks With High PV Penetration,” *IEEE Trans. Smart Grid,* vol. 9, no. 4, pp. 3582-3593, July 2018.

[113] H. Wen and et al., “Deep Learning Based Multistep Solar Forecasting for PV Ramp-Rate Control

Using Sky Images," *IEEE Trans. Ind. Informat.,* vol. 17, no. 2, pp. 1397-1406, Feb. 2021.

[114] G. Celli, E. Ghiani, F. Pilo and G. G. Soma, "Impact of ICT on the reliability of active distribution networks," CIRED 2012 Workshop: Integration of Renewables into the Distribution Grid, 2012.

[115] C. L. Dewangan, S. Chakrabarti, S. N. Singh and M. Sharma, "A Fair Incentive Scheme for Participation of Smart Inverters in Voltage Control," *IEEE Trans. Ind. Informat.,* vol. 18, no. 1, pp. 656-665, Jan. 2022.

[116] Q. Chai, C. Zhang, Z. Y. Dong and Y. Xu, "Operational reliability assessment of photovoltaic inverters considering voltage/VAR control function," *Electric Power Systems Research,* vol. 190, no. 106706, Jan. 2021.

[117] S. Dusmez, M. Heydarzadeh, M. Nourani and B. Akin, "Remaining Useful Lifetime Estimation for Power MOSFETs Under Thermal Stress With RANSAC Outlier Removal," *IEEE Trans. Ind. Informat.,* vol. 13, no. 3, pp. 1271-1279, June 2017.

[118] H. Wang and et al., "Transitioning to Physics-of-Failure as a Reliability Driver in Power Electronics," *IEEE Trans. Emerg. Sel. Topics Power Electron.,* vol. 2, no. 1, pp. 97-114, March 2014.

[119] H. Wang, M. Liserre and F. Blaabjerg, "Toward Reliable Power Elec-tronics: Challenges, Design Tools, and Opportunities," *IEEE Ind. Electron. Mag.,* vol. 7, no. 2, pp. 17-26, June 2013.

[120] S. Zhao, S. Chen, F. Yang, E. Ugur, B. Akin and H. Wang, "A Composite Failure Precursor for Condition Monitoring and Remaining Useful Life Prediction of Discrete Power Devices," *IEEE Trans. Ind. Informat.,* vol. 17, no. 1, pp. 688-698, Jan. 2021.

[121] "Application Manual Power Semiconductors," Semikron, Nuremberg, May 2015.

[122] M. Andresen, K. Ma, G. Buticchi, J. Falck, F. Blaabjerg and M. Liserre, "Junction Temperature Control for More Reliable Power Electronics," *IEEE Trans. Power Electron.,* vol. 33, no. 1, pp. 765-776, Jan. 2018.

[123] Y. Yang, H. Wang, F. Blaabjerg and T. Kerekes, "A Hybrid Power Control Concept for PV Inverters With Reduced Thermal Loading," *IEEE Trans. Power Electron.,* vol. 29, no. 12, pp. 6271-6275, Dec. 2014.

[124] L. Wei, J. McGuire and R. A. Lukaszewski, "Analysis of PWM Frequency Control to Improve the Lifetime of PWM Inverter," *IEEE Trans. Ind. Appl.,* vol. 47, no. 2, pp. 922-929, March-April 2011.

[125] M. J. E. Alam, K. M. Muttaqi and D. Sutanto, "A Novel Approach for Ramp-Rate Control of Solar PV Using Energy Storage to Mitigate Output Fluctuations Caused by Cloud Passing," *IEEE Trans. Energy Convers.,* vol. 29, no. 2, pp. 507-518, June 2014.

[126] W. Wei, J. Wang, N. Li and S. Mei, "Optimal Power Flow of Radial Networks and Its Variations: A Sequential Convex Optimization Approach," *IEEE Trans. Smart Grid,* vol. 8, no. 6, pp. 2974-2987, Nov. 2017.

[127] X. Su, M. A. S. Masoum and P. J. Wolfs, "Optimal PV Inverter Reactive Power Control and Real Power Curtailment to Improve Performance of Unbalanced Four-Wire LV Distribution Networks,"

IEEE Trans. Sustain. Energy, vol. 5, no. 3, pp. 967-977, July 2014.

[128] M. Farivar and S. H. Low, “Branch Flow Model: Relaxations and Convexification—Part I,” *IEEE Trans. Power Syst.,* vol. 28, no. 3, pp. 2554-2564, Aug. 2013.

[129] A. L. Yuille and A. Rangarajan, “The Concave-Convex Procedure,” *Neural Comput.,* vol. 15, no. 4, pp. 915-936, Apr. 2003.

[130] T. Lipp and S. Boyd, “Variations and extension of the convex-concave procedure,” *Optim. Eng.,* vol. 17, no. 2, pp. 263-287, Jun. 2016.

[131] S. Lu, W. Gu, C. Zhang, K. Meng and Z. Dong, “Hydraulic-Thermal Cooperative Optimization of Integrated Energy Systems: A Convex Optimization Approach,” *IEEE Trans. Smart Grid,* vol. 11, no. 6, pp. 4818-4832, Nov. 2020.

[132] B. Zeng, J. Zhang, X. Yang, J. Wang, J. Dong and Y. Zhang, “Integrated Planning for Transition to Low-Carbon Distribution System With Renewable Energy Generation and Demand Response,” *IEEE Trans. Power Syst.,* vol. 29, no. 3, pp. 1153-1165, May 2014.

[133] M. Locatelli and F. Schoen, “(Global) Optimization: Historical notes and recent developments,” *EURO Journal on Computational Optimization,* vol. 9, no. 100012, 2021.

[134] S. Singh, S. Veda, S. P. Singh, R. Jain and M. Baggu, “Event-Driven Predictive Approach for Real-Time Volt/VAR Control With CVR in Solar PV Rich Active Distribution Network,” *IEEE Trans. Power Syst.,* vol. 36, no. 5, pp. 3849-3864, Sept. 2021.

[135] V. B. Pamshetti, S. Singh, A. K. Thakur and S. P. Singh, “Multistage Coordination Volt/VAR Control With CVR in Active Distribution Network in Presence of Inverter-Based DG Units and Soft Open Points,” *IEEE Trans. Ind. Appl.,* vol. 57, no. 3, pp. 2035-2047, May-June 2021.

[136] C. Zhang, Y. Xu, Y. Wang, Z. Y. Dong and R. Zhang, “Three-Stage Hierarchically-Coordinated Voltage/Var Control Based on PV Inverters Considering Distribution Network Voltage Stability,” *IEEE Trans. Sustain. Energy,* vol. 13, no. 2, pp. 868-881, April 2022.

[137] Q. Chai, C. Zhang, Z. Tong, S. Lu, W. Chen and Z. Y. Dong, “PV Inverter Reliability Constrained Volt/Var Control with Power Smoothing via A Convex-Concave Programming Method,” *IEEE Trans. Ind. Informat.,* 2022, Early Access.

[138] A. Ristow, M. Begovic, A. Pregelj and A. Rohatgi, “Development of a Methodology for Improving Photovoltaic Inverter Reliability,” *IEEE Trans. Ind. Electron.,* vol. 55, no. 7, pp. 2581-2592, July 2008.

[139] D. Zhou, Y. Song, Y. Liu and F. Blaabjerg, “Mission Profile Based Reliability Evaluation of Capacitor Banks in Wind Power Converters,” *IEEE Trans. Power Electron.,* vol. 34, no. 5, pp. 4665-4677, May 2019.

[140] H. Wang, P. Davari, H. Wang, D. Kumar, F. Zare and F. Blaabjerg, “Lifetime Estimation of DC-Link Capacitors in Adjustable Speed Drives Under Grid Voltage Unbalances,” *IEEE Trans. Power Electron.,* vol. 34, no. 5, pp. 4064-4078, May 2019.

[141] Y. -J. Kim, S. -M. Kim and K. -B. Lee, “Improving DC-Link Capacitor Lifetime for Three-Level

Photovoltaic Hybrid Active NPC Inverters in Full Modulation Index Range," *IEEE Trans. Power Electron.,* vol. 36, no. 5, pp. 5250-5261, May 2021.

[142] Z. Qin, H. Wang, F. Blaabjerg and P. C. Loh, "Investigation into the control methods to reduce the DC-link capacitor ripple current in a back-to-back converter," in *IEEE Energy Conversion Congress and Exposition (ECCE)*, 2014.

[143] O. Gandhi, C. D. Rodríguez-Gallegos, N. B. Y. Gorla, M. Bieri, T. Reindl and D. Srinivasan, "Reactive Power Cost From PV Inverters Considering Inverter Lifetime Assessment," *IEEE Trans. Sustain. Energy,* vol. 10, no. 2, pp. 738-747, April 2019.